DEVELOPMENT AND EVALUATION OF A SAFEGUARDS SYSTEM CONCEPT FOR A PEBBLE-FUELED HIGH TEMPERATURE GAS-COOLED REACTOR

A Thesis

by

ERNEST TRAVIS NGURE GITAU

Submitted to the Office of Graduate Studies of
Texas A&M University
in partial fulfillment of the requirements for the degree of

MASTER OF SCIENCE

August 2011

Major Subject: Nuclear Engineering

Development and Evaluation of a Safeguards System Concept for a Pebble-fueled High Temperature Gas-cooled Reactor

Copyright 2011 Ernest Travis Ngure Gitau

DEVELOPMENT AND EVALUATION OF A SAFEGUARDS SYSTEM CONCEPT FOR A PEBBLE-FUELED HIGH TEMPERATURE GAS-COOLED REACTOR

A Thesis

by

ERNEST TRAVIS NGURE GITAU

Submitted to the Office of Graduate Studies of
Texas A&M University
in partial fulfillment of the requirements for the degree of

MASTER OF SCIENCE

Approved by:

Chair of Committee,	William S. Charlton
Committee Members,	Pavel V. Tsvetkov
	Justin T. Yates
Head of Department,	Raymond J. Juzaitis

August 2011

Major Subject: Nuclear Engineering

ABSTRACT

Development and Evaluation of a Safeguards System Concept for a Pebble-fueled High Temperature Gas-cooled Reactor. (August 2011)

Ernest Travis Ngure Gitau, B.S., Missouri University of Science and Technology

Chair of Advisory Committee: Dr. William S. Charlton

Pebble-fueled high temperature gas-cooled reactor (HTGR) technology was first developed by the Federal Republic of Germany in the 1950s. More recently, the design has been embraced by the People's Republic of China and the Republic of South Africa. Unlike light water reactors that generate heat from fuel assemblies comprised of fuel rods, pebble-fueled HTGRs utilize thousands of 60-mm diameter fuel spheres (pebbles) comprised of thousands of TRISO particles.

As this reactor type is deployed across the world, adequate methods for safeguarding the reactor must be developed. Current safeguards methods for the pebble-fueled HTGR focus on extensive, redundant containment and surveillance (C/S) measures or a combination of item-type and bulk-type material safeguards measures to deter and detect the diversion of fuel pebbles. The disadvantages to these approaches are the loss of continuity of knowledge (CoK) when C/S systems fail, or are compromised, and the introduction of material unaccounted for (MUF). Either vulnerability can be exploited by an adversary to divert fuel pebbles from the reactor system.

It was determined that a solution to maintaining CoK is to develop a system to identify each fuel pebble that is inserted and removed from the reactor. Work was performed to develop and evaluate the use of inert microspheres placed in each fuel pebble, whose random placement could be used as a fingerprint to identify the fuel pebble. Ultrasound imaging of 1 mm zirconium oxide microspheres was identified as a possible imaging system and microsphere material for the new safeguards system concept.

The system concept was evaluated, and it was found that a minimum of three microspheres are necessary to create enough random fingerprints for 10,000,000 pebbles. It was also found that, over the lifetime of the reactor, less than 0.01% of fuel pebbles can be expected to have randomly the same microsphere fingerprint. From an MCNP 5.1 model, it was determined that less than fifty microspheres in each pebble will have no impact on the reactivity or temperature coefficient of reactivity of the reactor system. Finally, using an ultrasound system it was found that ultrasound waves can penetrate thin layers of graphite to image the microsphere fingerprint.

DEDICATION

This work dedicated to Gary and Daniel. Countless hours and miles have been spent crisscrossing this country and you can still stand to let me be the one behind the wheel. That is loyalty like no other.

ACKNOWLEDGEMENTS

I would like to thank my advisor, Dr. William Charlton, for providing guidance on this research. Two years ago you took a chance on me, here is hoping it paid off. I would like to extend my appreciation to the Safeguards Systems/Instrumentation Development Research Group that listened week after week to the latest advances and setbacks this research experienced. I would also like to thank Dr. Pavel Tsvetkov and Dr. Justin Yates for serving committee members.

I would like to thank Dr. Rafaella Righetti of the Texas A&M University Ultrasound Imaging Laboratory, as well as, Aaron Totemeier and Adam Parkison of the Texas A&M University Department of Nuclear Engineering Fuel Cycle and Materials Laboratory for the time spent assisting with portions of this research.

To my many mentors and peers at Pacific Northwest National Laboratory, the guidance and support provided has been immeasurable. Five years ago, I was looking for a career field in life that would be rewarding. I found it summer after summer under the Washington sun.

To my parents, John and Brenda, my siblings, and my friends, words cannot do justice to the thanks and appreciation that you deserve. The product that follows is a result of the good, the bad, the calm, and the crazy; none of which I would change.

This research and degree were made possible through financial support from The National GEM Consortium Master of Science in Engineering Fellowship. Additionally, this work was funded under U.S. DOE Contract DE-FG52-06NA27606 and U.S. DOE Contract DE-FC52-05NA26856.

TABLE OF CONTENTS

Page

LIST OF FIGURES

FIGURE Page

FIGURE Page

FIGURE Page

LIST OF TABLES

1. INTRODUCTION

Before Little Boy and Fat Man were dropped on Hiroshima and Nagasaki, the spread of nuclear weapons technology was a concern. Not until November 1945 when the United States (U.S.), United Kingdom (U.K.), and Canada issued the "Three Nation Agreed Declaration on Atomic Energy" was pen put to paper about the need to spread nuclear energy knowledge, but only if effective and enforceable safeguards could be established. In January 1946, the Union of Soviet Socialist Republics (U.S.S.R), the U.S., U.K., and their allies within the United Nations (UN) created the United Nations Atomic Energy Commission. Until 1948 when the commission was dissolved, the goal of member countries was not to just prevent the spread of nuclear weapons and weapons technology, but to eliminate the weapons and technology.[1]

From these initial steps to control nuclear weapons technology, the International Atomic Energy Agency (IAEA) was born. An agency initially proposed by U.S. President Dwight D. Eisenhower in his "Atoms for Peace" speech in December 1953, the IAEA was created with the ratification of the IAEA Statute in 1957. The Statute stated that the main objective of the IAEA was to spread peaceful nuclear technology, while ensuring that the assistance the IAEA provided was not used for military purposes. The IAEA achieved this objective by promoting the peaceful uses of nuclear technology, providing necessary materials and scientific information for the peaceful development of nuclear technology, and establishing and administering safeguards designed to ensure that materials and information provided by the IAEA was not used to further any military purpose. The Statute specified that should any member country use IAEA assistance to further military purposes, the UN Security Council would be responsible for determining the consequences for that member.[2]

This thesis follows the style of *Nuclear Technology*.

The Statute specified the rights and responsibilities the IAEA possessed in order to establish and administer safeguards. These rights and responsibilities included:[2]

- the verification of nuclear facility design information
- the requirement that all safeguarded facilities maintain operating records
- the call for and receipt of progress reports from UN member countries
- approval of reprocessing of spent fuel to ensure the material is not diverted
- the ability to send IAEA designated inspectors to nuclear facilities to determine if a diversion has occurred, and
- the right of the IAEA to remove any IAEA assistance or material from a State that fails to correct IAEA identified violations.

The IAEA eventually came to establish its first universal safeguards system with the January 1961 approval of Information Circular 26 (INFCIRC/26) *The Agency's Safeguards*. INFCIRC/26 defined: the official principles of IAEA safeguards; the materials, equipment, and information subject to IAEA safeguards; the initiation and termination of IAEA safeguards on these materials, equipment, and information; and specified how the safeguards measures outlined in the Statute would be applied.[3] INFCIRC/26 was extended in 1964 to cover larger reactor facilities. This safeguards system was revised again in September 1965 with INFCIRC/66 *The Agency's Safeguards System (1965)*.[4] This revision allowed the safeguards system to work more effectively and simplified the language used in the provisions to increase understanding of the safeguards system.[1] This safeguards system was later revised twice more to include application of safeguards to reprocessing plants, fuel conversion plants, and fuel fabrication plants.[4]

As the U.S. and U.S.S.R. began to rapidly expand their nuclear arsenals in the 1950s and 1960s, it became apparent to many in the international community that a treaty needed to be established that prevented the spread of nuclear weapons. Composed by countries (also known as States) within the IAEA, the *Treaty on the Non-proliferation of Nuclear Weapons (NPT)* was passed in 1968.[1] Entering into force in 1970, the NPT was comprised of 11 articles that promoted the role of the IAEA in

strengthening international security.[1] These articles focused on the non-proliferation of weapons by States, the pursuit of peaceful uses of nuclear technology, and the undertaking of "negotiations in good faith on effective measures relating to cessation of the nuclear arms race at an early date and to nuclear disarmament."[5]

Shortly following the NPT was INFCIRC/153 (Corrected) *The Structure and Content of Agreements between the Agency and States Required in Connection with the Treaty on the Non-proliferation of Nuclear Weapons*.[6] INFCIRC/153 established a Comprehensive Safeguards Agreement between the IAEA and each State party to the NPT. INFCIRC/153 defined a detailed framework for safeguards including what information on nuclear facility design was to be shared with the IAEA, operating records and reporting systems necessary for IAEA safeguards, IAEA inspection procedures, and the relationship that records, reports, and inspections would share in determining the safeguards compliancy of a state.[1] In addition, INFCIRC/153 further defined the objective of IAEA safeguards as "the timely detection of diversion of significant quantities of nuclear material from peaceful nuclear activities to the manufacture of nuclear weapons" and "deterrence of such diversion by the risk of early detection."[6]

Today, INFCIRC/153-type Comprehensive Safeguards Agreements (CSAs) are the most common agreement between the IAEA and States. The CSA framework was supplemented with the introduction of INFCIRC/540 (Corrected) the *Model Protocol Additional to the Agreements between States and the International Atomic Energy Agency for the Application of Safeguards* in September 1997. Created due to the undeclared nuclear activities of the Republic of Iraq discovered in 1991, INFCIRC/540 grants the IAEA "complementary inspection authority" to that provided in INFCIRC/153. These strengthened safeguards allow IAEA access to all civilian nuclear facilities in the nuclear fuel cycle present within a State. Previously, the IAEA could only inspect reactor facilities, fuel conversion facilities, enrichment plants, fuel fabrication facilities, and fuel reprocessing facilities. With INFCIRC/540, the IAEA now: [7]

- has access to uranium mines and nuclear waste sites;
- has access to all buildings on the site of a nuclear facility on short-notice;
- is allowed to collect environmental samples at locations besides declared facilities;
- can use internationally accepted communications systems to transmit data;
- inspectors are issued multi-entry visas to facilitate unannounced inspections;
- receives information from States about research and development occurring in-country related to the nuclear fuel cycle; and
- receive information from States about the manufacture and export of critical nuclear-related technologies.

1.1 Next Generation Nuclear Facilities

Just as the IAEA expanded its responsibilities to cover different types of nuclear facilities like fuel enrichment and fuel fabrication facilities, the IAEA must continually evaluate the effectiveness of their safeguards system for next generation designs of all types of nuclear facilities. One facility type that is constantly evolving is nuclear reactors. Dozens of designs of nuclear reactors exist in the world today, however many can be described by reactor types. Most reactor designs can be classified as the light water reactor (LWR) type. Other common reactor types include on-load fueled power reactors and research reactors. The IAEA has over-time gained much experience in safeguarding these reactors and as such, has developed robust and specific approaches to safeguarding these facilities. While the exact safeguards measures utilized at each plant can be different, the same types of measurements and activities are performed.[8]

In some cases new reactor designs cannot be classified under a current reactor type. Currently, these reactor designs are classified as “Other types of reactors”. Reactors classified in this type include fast breeder reactors and high temperature reactors with pebble fuel.[9] Due to the range of reactors present in this category, the IAEA has only developed generalized requirements that must be met by each reactor. In some cases there is only one or a handful of a particular reactor design in the world, so

the development of a standard safeguards approach for each reactor design presents a new challenge for the IAEA. The pebble-fueled high temperature gas-cooled reactor (HTGR) is such a design that has a wide range of applications including electricity generation, hydrogen production, and steam production for industrial facilities.[10]

1.2 History of Pebble-fueled High Temperature Gas-cooled Reactors (HTGRs)

The pebble-fueled HTGR design was pioneered by the Federal Republic of Germany (FRG) in the 1960s. The Arbeitsgemeinschaft Versuchsreaktor (AVR) pebble-fueled HTGR operated from 1967 to 1988 in Western Germany. The AVR was an experimental reactor was operated as a testing facility for pebble-fueled HTGRs. The AVR, although a small reactor at about 45 megawatts-thermal (MWt), was able to demonstrate that a reactor fueled by small fuel pebbles, and cooled by gas, could be safely operated. Over its lifetime, the AVR was home to tests that primarily focused on qualification of pebble fuel. Varying combinations of uranium and thorium and fuel sizes were tested under a wide range of operating conditions to determine optimum combinations for safety and economics.[11]

Using experience gained with the operation of the AVR, the FRG designed and built the Thorium High Temperature Reactor (THTR) that served as the link between the experimental AVR facility and commercial scale facilities. Although the THTR only operated from 1985 to 1988, the over 16,000 hours of operational experience laid the foundation for the pebble-fueled HTGR designs that are being pursued today by the People's Republic of China (PRC) and the Republic of South Africa (RSA).[12,13]

The PRC began their pebble-fueled HTGR program in the 1992 with the approval to build reactor at Tsinghua University's Institute of Nuclear Energy Technology site outside of Beijing. Completed in 2000, the HTR-10, a 10 MWt pebble-fueled HTGR, has been used by the PRC as a research facility. Much like the AVR, the HTR-10 has come to be a testing ground for the PRC in HTGR technology including testing of pebble fuel and verification of inherent safety features associated with pebble-fueled HTGRs.[14]

In 1995, the RSA was looking for a way to increase electrical generating capacity in anticipation of increased demand. At the time, to build a coal fossil fuel plant would have required a large capital investment and some 5 to 8 years to construct. This type of plant would be located near the coal fields in the central part of the country. Deemed not economically viable, the government was interested in pursuing a means of electricity generation that would require lower capital costs, have a construction time on the order of 18 to 24 months, and could be located in coastal regions or remote areas. Conducting a feasibility study on modular, high temperature, helium-cooled reactor design options led the RSA to pursue the pebble-fueled HTGR design.[15] Building on experience from the AVR and THTR, the RSA began to design a new facility based on proven technologies. Initially designed to generate 100 megawatts-electric (MWe), this design came to be known as the Pebble Bed Modular Reactor (PBMR).[15]

As countries like the RSA and the PRC develop their domestic nuclear industries with pebble-fueled HTGRs, it is expected that the design will be exported to additional countries.[16,17] Countries most interested in the pebble-fueled HTGR design are likely to be countries that do not have capital for a larger facility, that need to generate electricity in underdeveloped or hard to reach areas. More often than not, these will be non-nuclear weapons states. As such, it is important that a safeguards approach be developed for the pebble-fueled HTGR that can reliably meet the safeguards objectives outlined in INFCIRC/153 and INFCIRC/540.

2. BACKGROUND

2.1 South African Pebble-fueled HTGR Program[1]

The Pebble Bed Modular Reactor (PBMR) is designed as a two unit co-generation plant, meaning the facility produces electricity and steam for industrial facilities. Each unit produces 250 MWt using a helium coolant and an indirect steam cycle. The plant is designed to have a 60 year lifetime, with an expected power generation efficiency of 40%. Each reactor unit contains 360,000 fuel pebbles when operating at equilibrium.

The PBMR operates by generating heat from each pebble. This heat is removed with the helium coolant that enters the core from the bottom and is carried to a steam generator. The steam generator removes the heat from the helium, and transfers the heat to water. The water is turned into steam that drives a turbine connected to a generator to produce electricity. As the steam cools, the condensate water is fed back into the cycle to produce more steam, and the cooled helium is circulated back into the reactor core. Fig. 1 is a flow diagram for the PBMR.

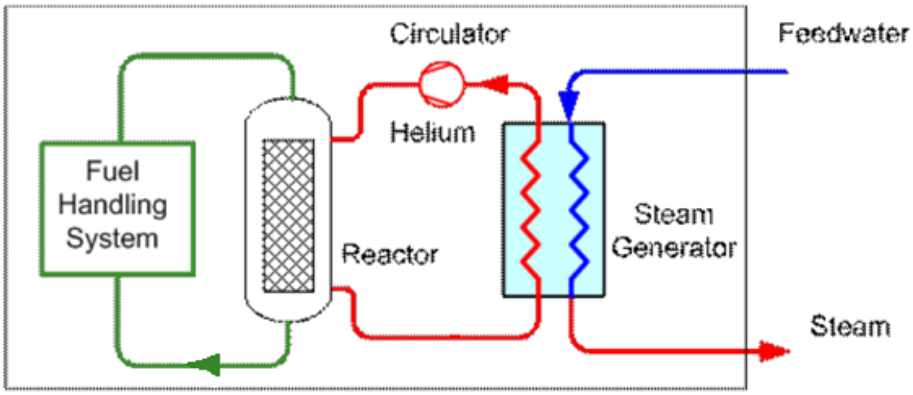

Fig. 1. Flow diagram for PBMR.[18]

[1] When this research began, the PBMR was being redesigned and marketed by Westinghouse and PBMR (Pty) Ltd. However, by late 2010 the largest investor in the design, the South African government, had withdrawn from the project and the PBMR design has since been abandoned. The information presented henceforth on the PBMR design stems from information released on the final redesign.

Unlike traditional light water reactors where the fuel remains stationary while the reactor is operating, each of the 360,000 fuel pebbles is recirculated through the reactor by a fuel handling system. As pebbles are removed from the bottom of the reactor core, the pebbles are circulated back to the top of the reactor core and reinserted. This process continues until each pebble is no longer usable as fuel and is sent to spent fuel storage. When the reactor is initially loaded, the core is filled with graphite pebbles. These pebbles are used to reduce the distance the fuel pebbles will drop when placed in the core.[18]

Each pebble spends on average 100 days in the reactor core before being recirculated. Each pebble is expected to reach an average burnup of 80,000 to 92,000 megawatt-days per ton of uranium (MWd/tU). Building on fuel experience from the AVR and THTR, each PBMR fuel pebble is comprised of Tristructural Isotropic (TRISO) fuel particles.[18] At the center of each TRISO particle is a 0.5 mm diameter uranium dioxide (UO_2) fuel kernel. Each kernel is covered in a 0.095 mm thick layer of porous carbon that acts as a buffer with additional layers and provides additional volume for fission products gases to escape. Next is a 0.04 mm thick inner layer of pyrolytic carbon (IPyC) that acts as a barrier to contain any gaseous fission products that escape the fuel kernel. A 0.035 mm thick layer of silicon carbide (SiC) is next. This layer provides structural strength to the fuel kernel, as well as, a barrier to any fission products that diffuse through the IPyC layer. Lastly, there is a 0.04 mm thick outer layer of pyrolytic carbon (OPyC) of the same thickness and composition of the IPyC that provides further structural strength to the TRISO particle.[18,19] In total, there are approximately 12,000 TRISO particles in a 50 mm diameter region in each pebble. This 50 mm diameter region is then covered in a 5 mm thick layer of graphite, making each fuel pebble 60 mm in diameter.[18] An example of this TRISO particle and fuel pebble can be seen in Fig. 2.

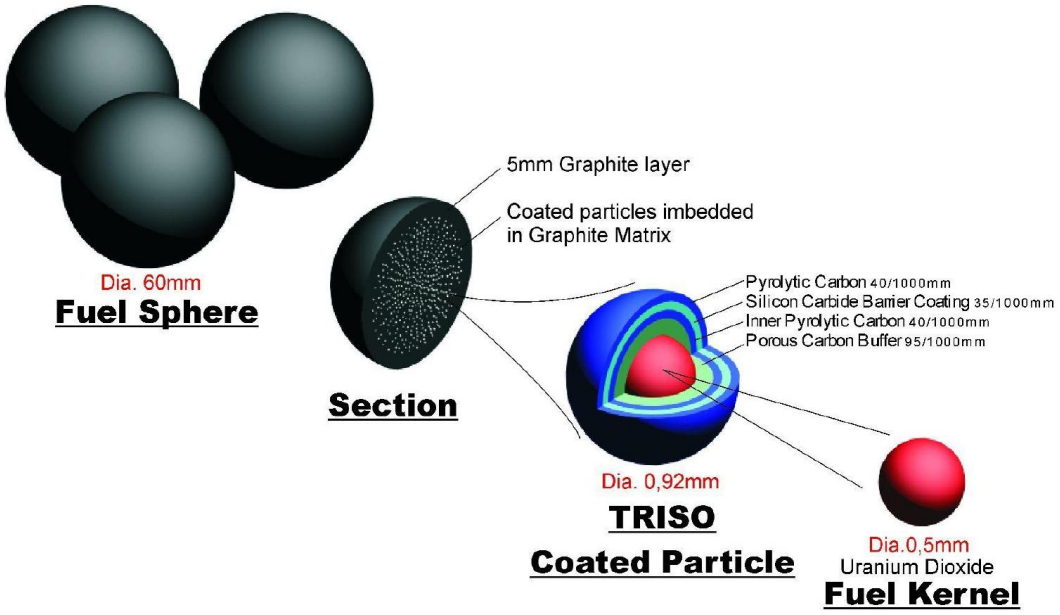

Fig. 2. TRISO particle and fuel pebble design for PBMR.[18]

Each fuel kernel contains 8 weight percent (wt%) ^{235}U; however, at the time the PBMR project was abandoned, additional research was being performed on fuel development.[18] In previous designs of the PBMR, two enrichments of pebbles, each containing 9 g of uranium, were used. The core was initially loaded with pebbles containing 5.7 wt% ^{235}U. As the reactor operated and these pebbles were discharged, the core was loaded with pebbles containing 9.6 wt% ^{235}U. The PBMR would continue to operate with this 9.6 wt% ^{235}U fuel for the remainder of the facility's operating lifetime.[20]

When operating at equilibrium, 3000 fuel pebbles are circulated throughout the system each day. Of those, approximately 350 are permanently discharged as spent fuel and are replaced with an equal number of fresh fuel pebbles. Fuel pebbles that have been permanently removed from the system are stored in large storage containers located onsite at the reactor facility.[18]

When the reactor is shutdown for long periods of time (e.g. maintenance), a Reserve Shutdown System (RSS) consisting of 18 boreholes in the inner reflector are filled with small spheres of an absorbing material. These RSS channels can also be used

to completely shutdown the reactor in an accident scenario. During normal operations, the reactor is controlled by six control rods positioned in the outer reflector.[18] In previous designs, there were 36 helium riser channels on the periphery of the outer reflector. These channels allowed the helium coolant to be pumped into the reactor vessel, up to the top of the PBMR core, where the helium was then forced down through the core and extracted at the bottom of the pressure vessel.[10]

2.2 People's Republic of China (PRC) Pebble-fueled HTGR Program

2.2.1 HTR-10

Much like the PBMR, the HTR-10 uses pebble fuel and a helium coolant to generate electricity indirectly using steam. The HTR-10 core contains 27,000 fuel pebbles, each with 8300 UO_2 fueled TRISO particles. Each pebble contains a total of 5 g of uranium enriched to 17 wt% ^{235}U. Each pebble is expected to reach an average burnup of 80,000 MWd/tU. The fuel pebble and TRISO particle composition is the same as the German developed pebble and particle also used by the RSA. The HTR-10 also contains RSS-type channels, control rods, and helium rising channels located in the same regions of the reactor as the PBMR.[14]

2.2.2 HTR-PM

Building on experience gained with the HTR-10, the PRC has made progress on designing a commercial scale prototype pebble-fueled HTGR, known as the High Temperature Reactor-Pebble bed Module (HTR-PM). Development of this new design began in 2001 and the reactor is set to start generating electricity in 2013.[21] Like the PBMR, the HTR-PM is a two unit reactor facility, where each reactor uses a helium coolant to produce steam to drive a turbine to produce electricity. Each reactor is capable of generating 250 MWt and has a design lifetime of 40 years. Each unit contains about 420,000 fuel pebbles with 7 g of uranium in each pebble enriched to 8.9 wt% ^{235}U. Each pebble is expected to reach an average burnup of 90,000 MWd/tU.[22] Unlike the PBMR, the HTR-PM does not contain a central column of solid graphite, this space is filled with

additional fuel pebbles. In the outer reflector of the HTR-PM there are eight control rods, channels for reserve shutdown, and helium coolant channels.[22]

2.3 Safeguards at Pebble-fueled HTGRs

2.3.1 Safeguards Requirements

The pebble-fueled HTGR falls into a category of safeguards requirements for "Other Types of Reactors." These requirements only apply to reactors located in countries that have concluded an INFCIRC/153-type CSA with the IAEA.[9] For the full text of requirements, refer to the *IAEA Safeguards Manual.* What follows is a summary of these requirements as they would apply to a pebble-fueled HTGR:[9]

- All records and reports at a facility are examined to ensure correctness and internal facility consistency in reporting methods. This examination is carried out during and after inspections at a facility in such a way that when the material balance period is closed, all relevant records and reports have been examined. These records and reports consist of facility records on inventory changes and material balance records.
- Each calendar year, at a reactor facility, the IAEA will carry out a physical inventory verification (PIV) of a physical inventory taking that was performed by the operator of the reactor.
    - During the PIV, fresh fuel assemblies are item counted and verified by serial number identification. If identification by serial number is not possible, gross defects in the quantity of fuel must be verified to a specified detection probability. Additional requirements apply if the fuel is a mixed oxide fuel (MOX) or highly enriched uranium (HEU) fuel.
    - For fuel that may reside in an area of the reactor system that the IAEA designates "difficult-to-access" different requirements apply. These

requirements include applying dual containment and surveillance (C/S) measures[2] to prevent any unknown removal of fuel.

- Any spent fuel that has been discharged from the reactor must be maintained under C/S measures, then counted and verified accordingly. C/S measures in place are evaluated and if necessary, the spent fuel is item counted.
- In the case of fuel assemblies that have been shipped between facilities within a country or between countries, the assemblies must be item counted and verified by serial number identification. If identification by serial number is not possible, gross defects in the quantity of fuel must be verified to a specified detection probability.
- If spent fuel is transferred out of a facility or moved between material balance areas (MBAs) within a facility, but will be "difficult-to-access", the container of spent fuel must be placed under dual C/S measures. Spent fuel discharged from a pebble-fueled HTGR would fall under this "difficult-to-access" category.
- Fuel that is moved into and out of "difficult-to-access" areas, or other strategic points in a reactor facility, is again item counted and its identification verified by the necessary means. Depending on the storage status of the fuel, a dual C/S measure may be necessary.
- The IAEA will also compare the records of transfers of fuel material between facilities.

While the IAEA does visit each reactor facility at least once a year to perform a PIV, the IAEA will also conduct inspections between PIVs. During these interim inspections:

[2] As defined in IAEA Safeguards Glossary[23]: "in a dual C/S system, each plausible diversion path is covered by two C/S measures that are functionally independent and are not subject to a common tampering or failure mode." An example of such a system would be when a container is sealed with two different types of tamper indicating devices (TIDs) or the container is sealed and placed under video surveillance.

- Facility records are examined and the amount of material present at the facility since the PIV is updated. This allows the IAEA to examine material flow through a facility between PIVs.
- Fuel present in the facility is also item counted and the identity of randomly chosen fuel material is verified. If material is under any type of C/S measure, the C/S system is evaluated to ensure its performance.[9]

At any point during PIVs or interim inspections, the IAEA must meet various timeliness goals in making the determination if a diversion of more than one significant quantity (SQ) of material has occurred. These timeliness goals vary for different types of nuclear material.[9] A significant quantity is "the approximate amount of nuclear material for which the possibility of manufacturing a nuclear explosive device cannot be excluded."[23] To determine what an SQ of material is, materials are classified as: direct or indirect use. Direct use material is "nuclear material that can be used for the manufacture of nuclear explosive devices" without having to be placed into a reactor or further enriched.[23] Indirect material is simply any nuclear material that is not direct use that requires additional processing before the material can be considered direct use.[23] When determining the timeliness goal, direct use material can be further classified as irradiated or unirradiated. Examples of direct and indirect use material and the SQ for each material can be found in Table I.

Table I. IAEA specified direct and indirect use materials and the respective SQ of material.[23]

Material	SQ
Direct use nuclear material	
Pu[a]	8 kg Pu
^{233}U	8 kg ^{233}U
HEU ($^{235}U \geq 20\%$)	25 kg ^{235}U
Indirect use nuclear material	
U ($^{235}U < 20\%$)[b]	75 kg ^{235}U
	(or 10 t natural U or 20 t depleted U)
Th	20 t Th

[a] For Pu containing less than 80% ^{238}Pu

[b] Including low enriched, natural, and depleted uranium

The timeliness goals for detection of the diversion of 1 SQ of these materials are: one month for unirradiated direct use material; three months for irradiated direct use material; and one year for indirect use material.[23] The timeliness goals set the interim inspection frequencies for the IAEA. For fresh fuel that contains low enriched uranium, the inspection frequency is yearly. In the case of fresh fuel that contains plutonium or HEU, an interim inspection is carried out monthly. In the case of low enriched uranium fuel currently in the core and spent fuel storage, the inspections are carried out once per quarter.

The IAEA also performs a design verification of each facility. Typically, the IAEA is notified when a country decides to build a nuclear facility. As the design, planning, and construction of the facility progress, the IAEA will inspect the facility to verify that the facility has been built to the specifications the agency received. The facility design information is reviewed at least once a year to: determine if any undeclared modifications have been made to the facility, apply developments that have been made in safeguards technology, or apply experience gained in verification procedures.[9]

2.3.2 Proposed Safeguards Approaches for a Pebble-fueled HTGR

The safeguards approach to satisfy the previously listed requirements for the HTR-10, as developed by the PRC and the IAEA, is not publicly available. However, work has been performed to develop a safeguards system for the PBMR design.

2.3.2.1 Dual C/S Dependent Safeguards Approach

Similar to an early approach developed for the THTR[24], today the most often referenced safeguards approach for the PBMR was developed by PBMR (Pty) Ltd.[25] Since little differs about the reactor core and fuel utilized for the pebble-fueled HTGRs described, the same safeguards approach is applicable to all pebble-fueled HTGRs.

The goal of this safeguards system - as with any safeguards system - is to provide a way to independently verify the total amount of nuclear material present at the PBMR, as well as, the amount of material present within any specified MBA of the reactor. This approach relies upon the PBMR core being designated as "difficult-to-access" by the IAEA because once a fuel pebble has been inserted into the core, direct access to a specific fuel pebble is not possible. This means the safeguards system will use dual C/S measures and item counting, not item verification, to safeguard the PBMR.

Once per year a PIV will be carried out by the IAEA, at which point:[26]

- accounting and operating records will be examined for correctness and consistency;
- all C/S measures in place at the facility will be evaluated to ensure proper performance;
- fuel pebble flow monitoring measures will be evaluated;
- all shipments and receipts of nuclear material within and outside the facility will be verified;
- environmental samples will be taken from locations throughout the facility;
- design information will be verified; and
- any nuclear material present at the reactor facility will be verified.

A fuel pebble, and maintaining continuous knowledge of its location, is in large part how the nuclear material present at the reactor is verified. This proposed system is

depicted in Fig. 3. In the figure, each step in the following description of the material flow, and the safeguards measures at each step, is designated by the letter a letter A through H.

Fresh fuel pebbles are stored in large containers that can hold 1000 pebbles. Each container is sealed and item counted. Randomly, containers of fresh fuel are selected and the presence of nuclear material is confirmed using a non-destructive assay (NDA) method that meets a specified detection probability. From fresh fuel storage, the pebble passes through a pebble counter (Fuel Flow Monitor) and the containment structure before entering the reactor core. Once a fuel pebble enters the core, the pebble cannot be counted or verified until removed later. Verification of fuel when in-core is achieved through evaluation of the dual C/S measures on all access points to the core and item counting of pebbles entering and exiting the core. Once a pebble is removed by the core unloading device, the pebble passes through the containment structure and into a fuel sorting machine. Damaged pebbles are removed and stored in a container within the core unloading device. This container of damaged pebbles is sealed with a TID, under video surveillance, and NDA measurements are taken to verify the presence of nuclear material. The material in this container is removed during maintenance and placed into a high-level waste storage area. Undamaged pebbles are identified as a fuel pebble or a graphite pebble. For fuel pebbles, their burnup is determined. If the fuel pebble can still be utilized in the reactor, the fuel pebble is counted and sent back into the core. If the fuel pebble has reached the desired burnup, the pebble is counted and sent to a spent fuel storage area for the remaining life of the reactor. Depending on the current operating status of the reactor core, graphite pebbles can be counted and sent back into the reactor core, or counted and sent to a storage area for later use. Fuel and graphite pebbles can also be removed after identification for a post-irradiation examination (PIE) in a secured location. Fuel pebbles not removed for a PIE pass into a temporary storage area where each is placed inside a large container. Once the container is full, the container is sealed with a TID and placed in long-term storage under video surveillance.

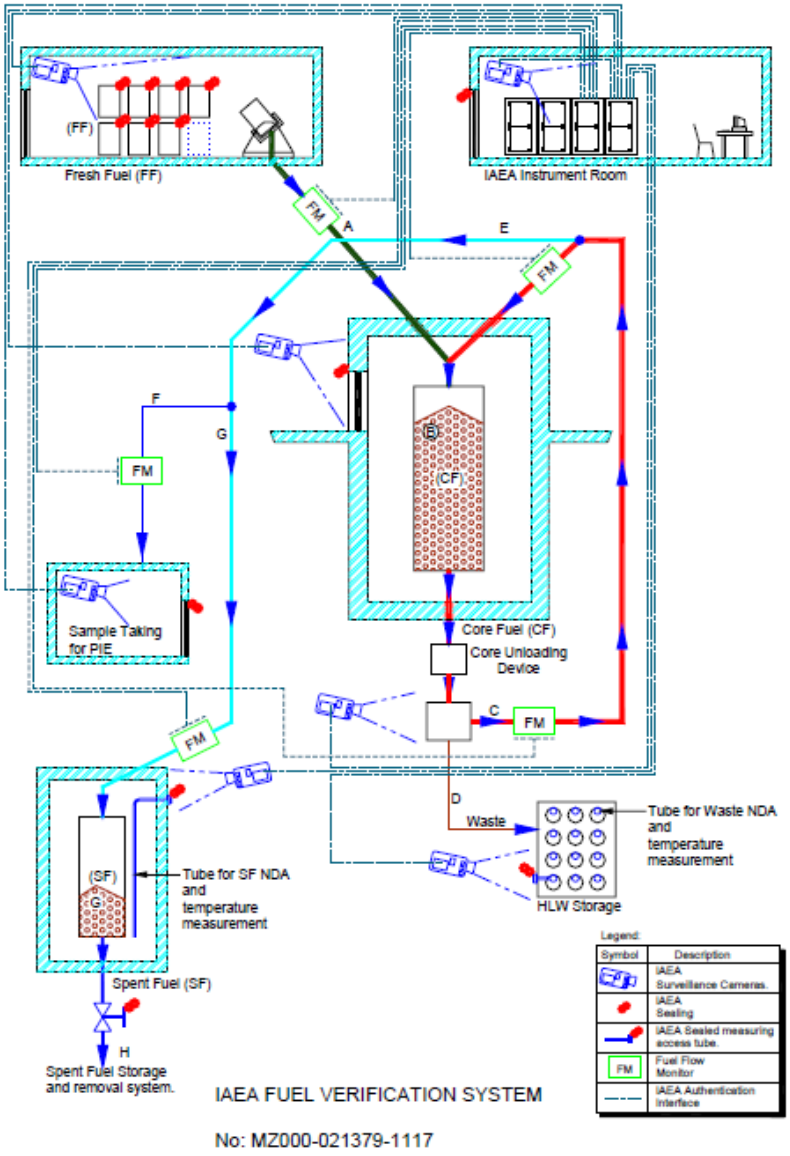

Fig. 3: Proposed dual C/S dependent safeguards system for the PBMR.[20]

As the pebbles are moved around the reactor system, access points to the various areas (e.g. core containment, PIE room, spent fuel storage areas) are sealed with tamper indicating devices (TIDs) and are under constant video surveillance. The data from these surveillance cameras and pebble counters are sent to an instrumentation room or cabinet with access limited to the IAEA. This room or cabinet is sealed with a TID and under constant video surveillance.[20,26] This approach plans to utilize unattended or remote

monitoring of the surveillance and pebble flow systems.[26] Since the TIDs and video surveillance used in this approach are "functionally independent and not subject to a common tampering or failure mode," this proposed system satisfies the dual C/S measures condition of a "difficult-to-access" core.[9,23] Should one system fail, it is expected that the other system would continue to operate, thereby preventing loss of continuity of knowledge (CoK) of pebble location. This safeguards approach also draws a safeguards conclusions through random unannounced inspections and complementary access to all facilities located on the reactor site. These unannounced inspections are carried out in the same manner as the interim inspections with examination of records, random verification and identification of nuclear material present at the site, and evaluation of any C/S measures in use.[26]

2.3.2.2 Hybrid Safeguards Approach

Since the pebble-fueled HTGR is a reactor type not commonly safeguarded by the IAEA, some researchers have determined that a new safeguards approach must be developed for this "new" reactor type.

This line of thought has resulted in a hybrid safeguards approach that uses traditional reactor safeguards methods and safeguards methods commonly applied at bulk-type material facilities. This approach argues that these methods can be combined because the fuel pebbles are indistinguishable, sufficiently small in size, and large in number that the pebble-fueled HTGR is more similar to a bulk-type material facility than item-type material facility.[27] This hybrid method is depicted in Fig. 4.

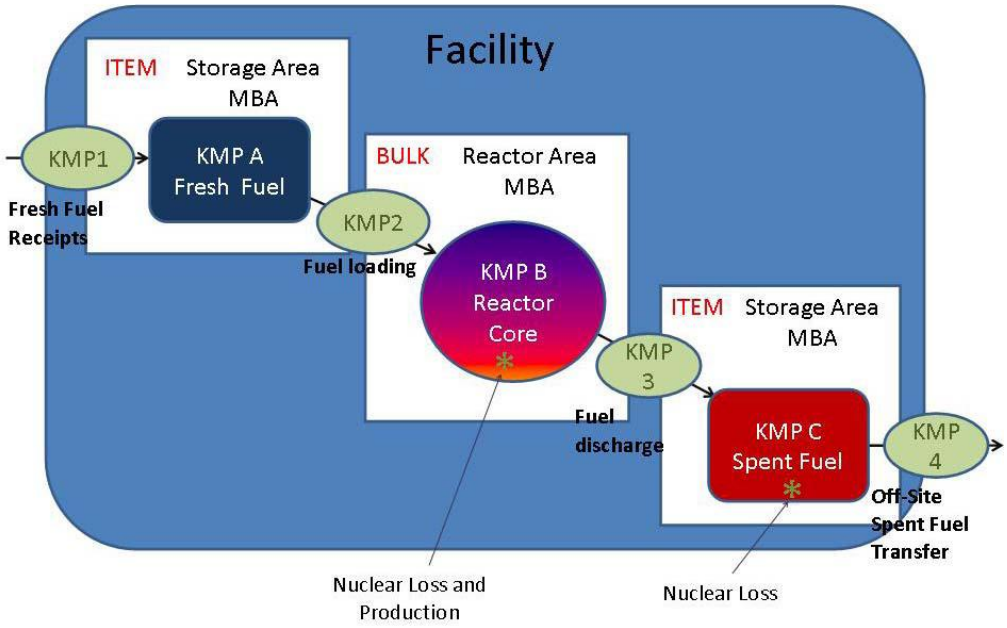

Fig. 4. Hybrid safeguards approach for a pebble-fueled HTGR.[28]

To use item- and bulk-type material accounting methods, multiple material balance areas (MBAs) must be established inside the reactor facility. This is unlike traditional LWR safeguards where the entire reactor facility is traditionally placed inside a single MBA.

The first MBA is placed around the fresh fuel storage area. Here the fuel is stored in large containers that are item counted. A serial number is placed on each container. This allows for random identity verification of containers of pebbles. Each container is also weighed to verify the approximate quantity of pebbles in the container. From this, the approximate amount of nuclear material can be estimated. The content of these containers are also verified using gross radiation attribution. This means that an NDA measurement is taken to verify the height of pebbles in each container. Comparing this approximate height to previous height estimations will reveal if large quantities of pebbles have been removed and changes in the overall radiation signature of the container can revel if pebbles in the container have been replaced. As pebbles are removed from these large containers and sent into the reactor core, each pebble is

counted. When the pebbles enter the reactor core, the pebbles enter a bulk-type material MBA.

As the reactor operates, the nuclear production and loss in the reactor core can be simulated using information provided about operating power records and pebble quantity from pebble counters.

When pebbles exit the reactor core, each pebble is counted and passed into another item-type material MBA. This MBA is a temporary spent fuel storage area where the pebbles are again placed into a large container. Once full, the container is sealed with a TID. Like the containers in fresh fuel storage, each container is marked with a serial number, is weighed, and its contents are verified using gross radiation attribution before being placed in long-term storage. By storing fuel pebbles in large containers, the amount of effort needed to determine the amount of nuclear material present is reduced. Each drum can be counted instead of attempting to count each pebble. As long as the IAEA has already verified the contents of each drum, only the TIDs and serial numbers on randomly chosen drums need to be verified during subsequent inspections. In addition to these item- and bulk-type material safeguards measures, C/S measures would also be utilized throughout the facility to supplement the safeguards system.

2.3.3 Challenges with Proposed Safeguards Approaches for Pebble-fueled HTGR

There are two vulnerabilities identified in the proposed safeguards approaches for the pebble-fueled HTGR: maintenance of continuity of knowledge (CoK) and the introduction of material unaccounted for (MUF).

In the safeguards approach proposed by PBMR (Pty) Ltd. that was described in Section 2.3.2.1, maintenance of CoK cannot be demonstrated in scenarios when C/S measures have failed, or are purposely compromised. Item counting could be used to restore some knowledge of core contents; however, experiences at the HTR-10 have proven that even these counters cannot be relied upon to accurately determine the quantity of pebbles present in the core.[27] Additionally, if an adversary were to replace the quantity of removed pebbles with borrowed pebbles, or pebbles that were produced

at an undeclared facility, item counting would not detect this diversion. In the hybrid approach, if the reactor core were emptied and C/S measures were not operable, operation of the bulk-type material measurement system, primarily the weighing system for storage containers, must remain uncompromised in order for CoK to be maintained. If at any point the bulk-type material measurement systems were inoperable, an adversary could remove pebbles, and replace the pebbles with borrowed material to carry out a diversion.

Uncertainty found with item counting and bulk-type material measurement systems, generate material unaccounted for (MUF) into the safeguards approach for a pebble-fueled HTGR. In a facility, MUF is mathematically determined from quantities obtained by measurement techniques that have some uncertainty in their measurements. As MUF is calculated, this uncertainty is propagated until a total uncertainty in MUF is determined. This uncertainty in MUF, if large due to poor measurement accuracy or measurement/counting system manipulation, can be used by an adversary to divert material.

These vulnerabilities in proposed approaches identify the hurdle that must be overcome to safeguard a pebble-fueled HTGR: the ability to verify the unique identity of each fuel pebble. Safeguards requirements, as outlined in Section 2.3.1, repeatedly reflect the necessity to verify the identity of each pebble passing through the reactor system. If each fuel pebble identity can be verified, when C/S measures are inoperable CoK can be restore and there would be a zero MUF in the facility.

Although work has been performed to demonstrate the difficulty and expense associated with reprocessing of diverted fuel pebbles[29,30] and the large quantity of fuel pebbles necessary to divert a SQ of material[3], this work does not directly address the need to uniquely identify each pebble in a pebble-fueled HTGR. As such, the focus of this safeguards system concept is to develop and evaluate a system to uniquely identify each fuel pebble. Identification of each fuel pebble would firmly place the pebble-fueled HTGR as an item-type material facility family, increasing the difficulty for an adversary

[3] 1 SQ LEU = 86,000 LEU fresh fuel pebbles; 1 SQ Pu = 52,000 LEU spent fuel pebbles (Durst et. al.[27]).

to divert material undetected. As such, safeguards approaches at different types of item-type material reactors would be applicable to this concept.

2.4 Safeguards Approaches at Different Types of Reactors

2.4.1 Light Water Reactors

There are 442 nuclear reactors currently operating in the world.[31] Of these operating reactors, the majority are light water reactors (LWRs). This reactor type is comprised of two general designs: pressurized water reactors (PWRs) and boiling water reactors (BWRs). Due to the large number of LWR facilities, LWRs are the most common reactor type safeguarded by the IAEA. LWRs, like most reactors, are considered item-type material facilities because the fuel is maintained in distinguishable fuel assemblies and fuel pins.[23] This "item" designation is what the safeguards approach for a LWR is built.

2.4.1.1 Operation of a LWR

LWRs operate on the same principle as a pebble-fueled HTGR. Unlike the pebble-fueled HTGR, a LWR uses meters long fuel assemblies that are comprised of fuel pins that contain the fuel material. In a PWR, this heat is transferred to a light water coolant, and then transferred to another water cycle to create steam. The steam drives a turbine attached to a generator to produce electricity.[33] In a BWR, the heat generated by the fuel is cooled by water that is directly converted to steam inside the reactor vessel.[32] This generation process for a PWR can be seen in Fig. 5.

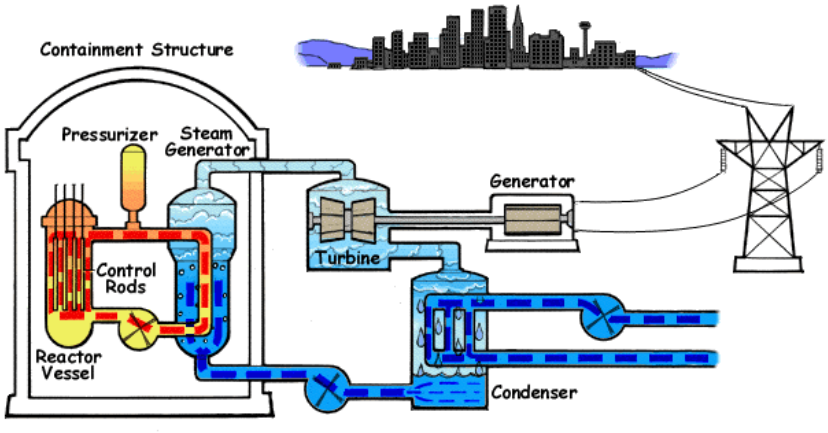

Fig. 5. Flow diagram for a PWR.[33]

To maintain the electricity generation process, the fuel in the reactor core must be replaced at regular intervals. This spent fuel typically comprises one-third of a reactor core. When spent fuel is replaced, the reactor is shutdown and the cover of the reactor vessel is removed using a large crane. Spent fuel is removed from the reactor core and transferred to an open spent fuel storage pond. Once the spent fuel has been removed, fresh fuel is inserted into the reactor core from an open storage pool. When all of the fresh fuel has been loaded, the reactor vessel cover is returned.

2.4.1.2 Safeguarding a LWR

Light water reactors are designed to store spent fuel inside or outside of reactor containment. In LWRs with spent fuel storage within containment, a single C/S measure (e.g. video surveillance) is used to monitor the area within containment. Safeguards measures implemented at this type of facility can be seen in Fig. 6.

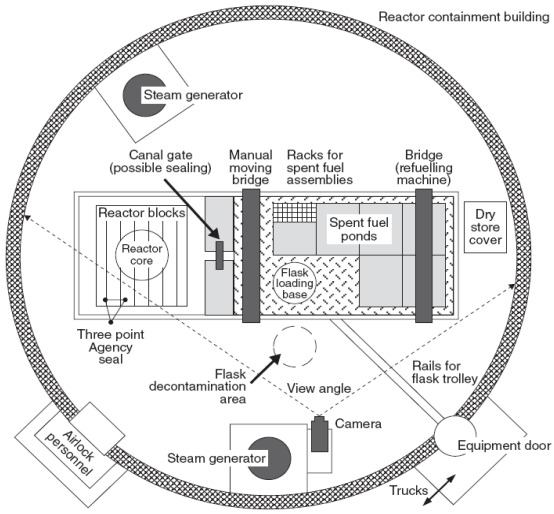

Fig. 6. Safeguards measures at a LWR with spent fuel storage inside containment.[34]

In a reactor design where the spent fuel storage pond is located outside of the containment structure, there are at least two C/S measures in place (e.g. surveillance of the spent fuel storage pool and surveillance of the reactor vessel). Implementation of safeguards measures for this type of LWR can be seen in Fig. 7.

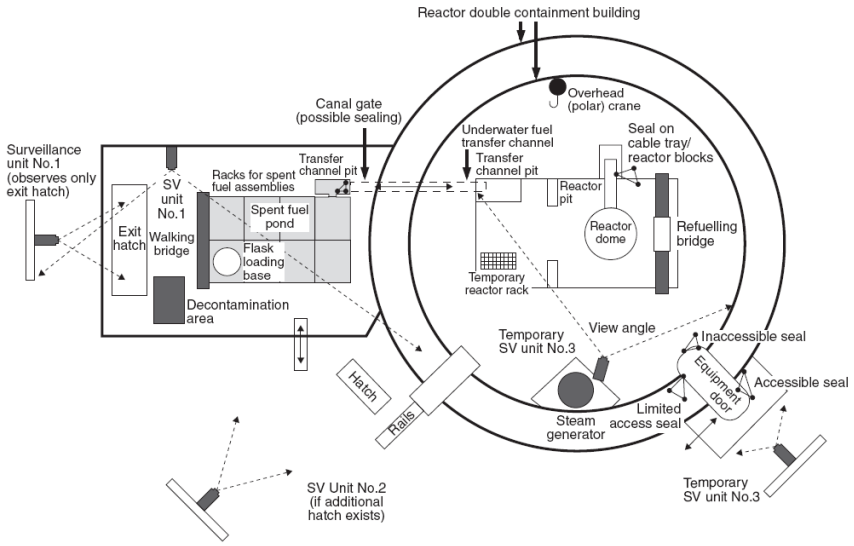

Fig. 7. Safeguards measures at a LWR with spent fuel storage outside containment.[34]

Although spent fuel location can change depending on the design, all LWRs still utilize similar measures to safeguard their nuclear material. These measures are:[8,34]

- Placement of a seal on the cover of the reactor vessel. To access core fuel, the reactor vessel cover must be removed. By placing a seal on the cover the IAEA can verify any access against facility records to determine why the cover was removed. The IAEA can then review video surveillance to determine if fuel was removed during that access.
- Each fuel assembly and fuel pin is engraved with a unique serial number during manufacturing. When fuel assemblies are transferred between facilities and within the reactor facility, the assemblies are counted and the identity of randomly chosen fuel assemblies is verified by the serial number.
- Seals are applied to shipping containers for fresh fuel and any storage containers for spent fuel. The seal must be removed in order to open the containers. The IAEA can then verify this access against facility records and review video surveillance.
- The reactor crane used to move fuel assemblies and the reactor vessel cover is also utilized in safeguarding a LWR. A seal can be placed on a key component of the crane such that operation could not occur without removal of the seal.
- The reactor core, storage areas, and reactor crane are monitored by video surveillance.
- The canal that connects the fuel storage pool to the core is lined with detector systems. When radiation is detected, video surveillance will activate allowing the IAEA to determine the number of fuel assemblies moved and where the assemblies were transferred. The IAEA can also verify the identity of the fuel assembly if the system is setup to capture images of each assembly serial number.
- In the spent fuel storage pool, visibility through water allows the IAEA to use a Cerenkov Viewing Device to verify that spent fuel assemblies have not been replaced with fake assemblies or fresh fuel assemblies.

- The IAEA less frequently uses facility operating records and fuel manufacturing records to simulate the burn of core fuel. When the fuel is removed, the IAEA can use various types of detectors to verify the fission product content of the spent fuel against the simulation to ensure that there was no undeclared operations at the facility.

The IAEA verifies these safeguards measures at LWRs quarterly, or once every three months. These measures are also verified yearly during the PIV.

2.4.2 On-load Fueled Reactors

On-load fueled reactors refer to reactor types that are refueled while the reactor is operating. The most common reactor designs of this type are CANada Deuterium Uranium (CANDU) reactors and Magnox reactors. There are currently no plans for additional Magnox reactors to be built, however there are plans for additional CANDU reactors and a similar style reactor built by The Republic of India. The CANDU reactor is the most commonly safeguarded on-load refueled reactor, as such the CANDU will serve as the reference facility.

2.4.2.1 Operation of On-load Fueled Reactors

The operating principles of a CANDU reactor are similar to LWRs. A flow diagram of a CANDU facility can be seen in Fig. 8. Heat is generated by fission of low enriched uranium in fuel bundles. This heat is transferred to water that generates steam in a secondary cycle. The steam drives a turbine that is attached to a generator. However, there are several differences between a CANDU and LWR:[35]

- the reactor vessel of a CANDU is oriented horizontally instead of vertically;
- the fuel bundles are placed in fuel channels that penetrate the reactor vessel from end to end;
- a CANDU uses heavy water (D_2O) to moderate neutrons and cool the fuel bundles (in the most recent design, the Advanced CANDU, D_2O is placed inside the reactor vessel to moderate neutrons, while light water (H_2O) is placed in the fuel channels to cool the fuel assemblies);

- the fuel assemblies are considerably smaller (approximately 0.5 m in length) than a typical LWR fuel assembly; and
- natural uranium is used instead of low enriched uranium (in the Advanced CANDU, varying low enrichments of uranium are used in a single fuel bundle).

The CANDU operates by placing several fuel bundles in each of the hundreds of fuel channels. Once a fuel bundle has reached the desired burnup, the bundle is pushed out one end of the reactor vessel and a fresh fuel bundle is added to the fuel channel. This action is performed by a fuel handling machine that simultaneously inserts the fresh fuel bundle, while removing the spent fuel bundle. The fresh fuel is taken from a fresh fuel storage area and loaded into the fuel handling machine. Spent fuel bundles that have been removed are placed in a spent fuel storage bay.[35]

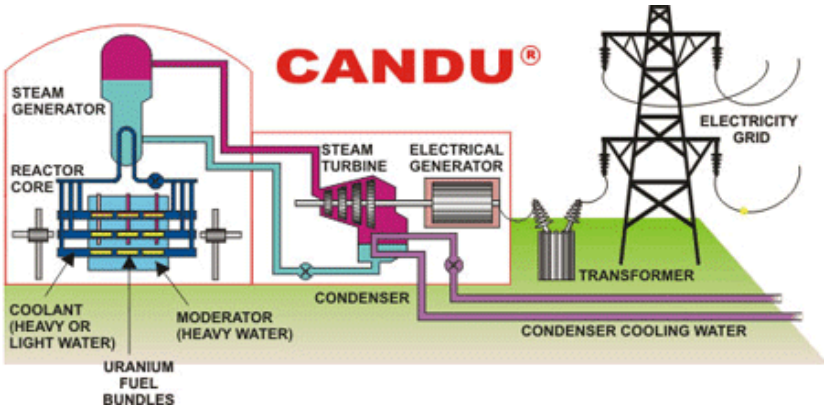

Fig. 8. Flow diagram for an Advanced CANDU reactor.[36]

2.4.2.2 Safeguards for CANDU Reactor

Depending on the equipment available at the time and the safeguards agreement between the IAEA and the State, the safeguards measures used to maintain CoK at a CANDU-type facility may be different. One method to maintain CoK relies upon video surveillance of the fuel bundle flow paths. The implementation of the safeguards measures can be seen in Fig. 9. An additional method to maintain CoK on the pebble flow paths is to mount a neutron and gamma radiation detector above each end of the

reactor core. Implementation of safeguards measures using this core discharge monitor can be seen in Fig. 10.

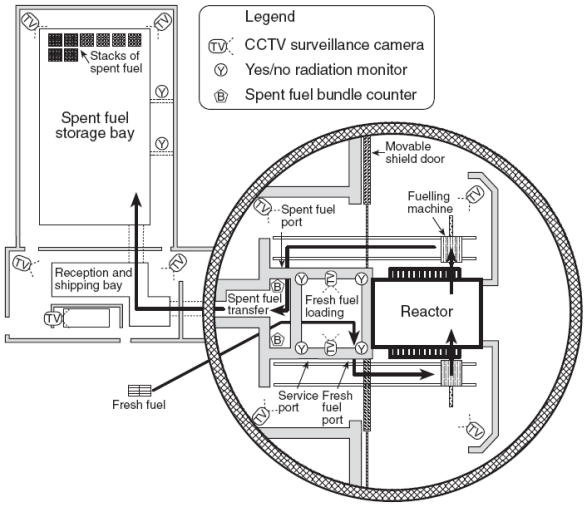

Fig. 9. Implementation of safeguards measures at a CANDU facility using video surveillance and radiation monitors.[34]

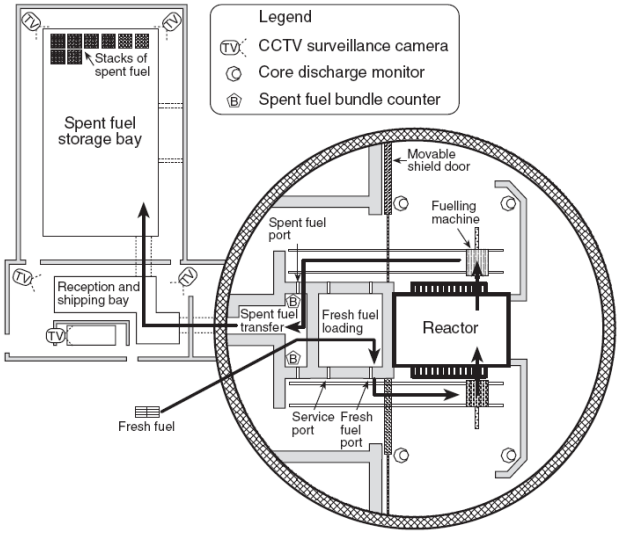

Fig. 10. Implementation of safeguards measures at a CANDU facility using core discharge monitor.[34]

The CANDU presents an interesting challenge to safeguards for a reactor because the reactor has characteristics like a LWR and a pebble-fueled HTGR. Like a

LWR, use of easily distinguishable fuel bundles makes item counting and identity verification possible. However, the reactor vessel is penetrated by hundreds of fuel channels. Each channel has fuel being inserted and withdrawn, meaning there is not a single reactor vessel cover that would have to be sealed, but hundreds. Similar to a pebble-fueled HTGR, once a fuel bundle has been placed inside a fuel channel, the bundle cannot be physically seen until the bundle has been removed on the other end of the fuel channel. Furthermore, CANDU fuel is discharged as spent fuel at a much lower burnup than LWR or pebble-fueled HTGR fuel. This results in a spent fuel bundle with a plutonium content more desirable to an adversary. As such, the safeguards measures focus on the spent fuel bundles. CANDUs still rely upon similar safeguards measures as a LWR, but applied differently. Safeguards measures utilized at a CANDU:[8,37]

- Fuel bundles are manufactured with serial numbers and shipped in sealed containers.
- When fresh fuel is brought into the reactor facility, the bundles are placed in storage before being loaded into the fuel handling system. Bundles are loaded under constant video surveillance.
- The fuel handling machines are controlled remotely and semi-automated. Each machine is under constant video surveillance.
- Spent fuel bundles are remotely transferred to the storage bay. The transfer path is under video surveillance.
- As the bundles pass through the containment structure, detectors use the radiation emitted to count the number of bundles that pass.
- Once the bundles enter the storage area, radiation detectors are again used to monitor movement within the storage area, as well as video surveillance.

As depicted in Fig. 10, video surveillance of transfer paths can be replaced with a core discharge monitor. This monitor is capable of detecting the characteristic variations in gamma and neutron radiation emitted when the fuel channels are opened and closed for loading and unloading of fuel. This distinct variation in the amount of radiation emitted is used to count the number of bundles inserted or removed. The IAEA also uses

this radiation to verify the flow of the fuel bundles through the fuel handling machines, unlike when C/S measures monitor flow by monitoring access to the handling machines.

The increased focus on spent fuel is important because the more desirable spent fuel bundles accumulate quickly. Instead of counting and verifying the identity of each, the bundles are loaded into large storage racks. Once a rack is full, a seal is applied. Now, instead of counting and verifying hundreds of fuel bundles, the IAEA can count the full racks and verify the integrity of the seals. Additionally, like LWRs, the coolant visibility allows use of a Cerenkov Viewing Device to determine if fuel present in the storage racks has been irradiated or replaced with dummy bundles. Additionally, a radiation detector can be lowered into the spent fuel area during IAEA inspections to verify the authenticity of the spent fuel.

Although there is an increased focus on the spent fuel present at a CANDU facility, the interim inspection frequency is three months, in addition to a yearly PIV.

2.4.3 Fast Reactors

Fast reactors use a liquid metal as the coolant. This liquid metal is typically sodium or lead, or some alloy of sodium or lead. While almost fifty experimental, demonstration, and commercial fast reactor facilities have been built across the world, very few have been under full scope IAEA safeguards. As such, of all reactor types, the IAEA has the least amount of safeguards experience with commercial fast reactors.

2.4.3.1 Operation of Fast Reactors

Fast reactors operate on the same principle as the other reactors considered. The nuclear fuel generates heat that is transferred to the liquid metal coolant. This coolant then transfers the heat to additional cycles that eventually drive a turbine. Different between fast reactors and LWRs is the type of fuel assembly used. LWRs typically use low-enriched uranium in slightly varying enrichments. In fast reactors some assemblies contain large quantities of plutonium, while some primarily contain depleted uranium. The fresh fuel assemblies contain the most plutonium; as such, fresh fuel is the focus of the safeguards approach. The most safeguarded fast reactor is the sodium cooled fast reactor; this design will serve as the reference facility.

2.4.3.2 Safeguarding Fast Reactors

Fast reactors are treated as item-type material facilities. The largest difficulty in safeguarding a fast reactor is the opaque nature of the coolant and the large amount of plutonium in some assemblies. Thus, the approach primarily relies upon item counting and extensive C/S measures to maintain CoK.

The facility layout and implemented safeguards measures at the MONJU sodium-cooled fast reactor located in Japan can be seen in Fig. 11. The safeguards measures utilized are:[8,38]

- Fresh fuel assemblies arrive at the reactor facility in sealed cans. The cans are unloaded into a fresh fuel storage pit. Fresh fuel assemblies that contain the large quantities of plutonium are unloaded to the storage pit in the presence of an IAEA inspector. This storage pit is under dual C/S measures.
- Fuel to be loaded into the reactor is unloaded in the fresh fuel handling room. As the assembly leaves the fuel handling room to enter the reactor, the assembly passes an Entrance Gate Monitor (ENGM). The monitor uses an NDA system to count each assembly and to determine the type of assembly that is being transferred.
- Each fuel assembly is loaded into the reactor core by a series of remotely controlled machines. After passing the ENGM, the assembly is placed into the Ex-Vessel Transfer Machine (EVTM). Here, radiation monitors are again used to count and verify the fuel assembly type.
- The EXTM then transfers the assembly to the Ex-Vessel Storage Tank (EVST). In the EVST, each assembly is immersed in the sodium coolant. Radiation monitors (EVST Monitors) line the tank to count each assembly, verify assembly type, and determine direction of movement in or out of the reactor vessel.
- Once in the reactor core, an internal transfer machine is used to place each assembly. The Radiation Power Monitor (RPM) is similar in function and purpose to the EVST Monitors but tracks fuel movement inside the reactor vessel.

- Once the fuel has been placed inside the reactor core, the assemblies are inaccessible. Thus, seals and video surveillance are used to ensure there is no undeclared removal of fuel from the reactor core.
- When fuel assemblies are removed from the reactor core, the assemblies travel through the EVST. The EVST then transfers the assemblies into a spent fuel cleaning and canning station.
- Once cleaned and dried, the fuel assembly is placed into a can. When fuel assemblies have been removed from the core and cleaned, verification of the serial number is possible, but not heavily relied upon because the serial number could not be verified when the assembly was in the core.
- The spent fuel storage can is then sealed, the transferred through an Exit Gate Monitor (EXGM). This monitor is similar in function and purpose to the ENGM, but instead monitors the flow of assemblies into the spent fuel storage pit.
- Once placed in the spent fuel storage pit, the can is placed under video surveillance.
- Fuel assemblies that originally contained only depleted uranium, now contain some amount of plutonium usable in more reactor fuel. These assemblies are placed into sealed shipping containers and sent to a reprocessing plant.

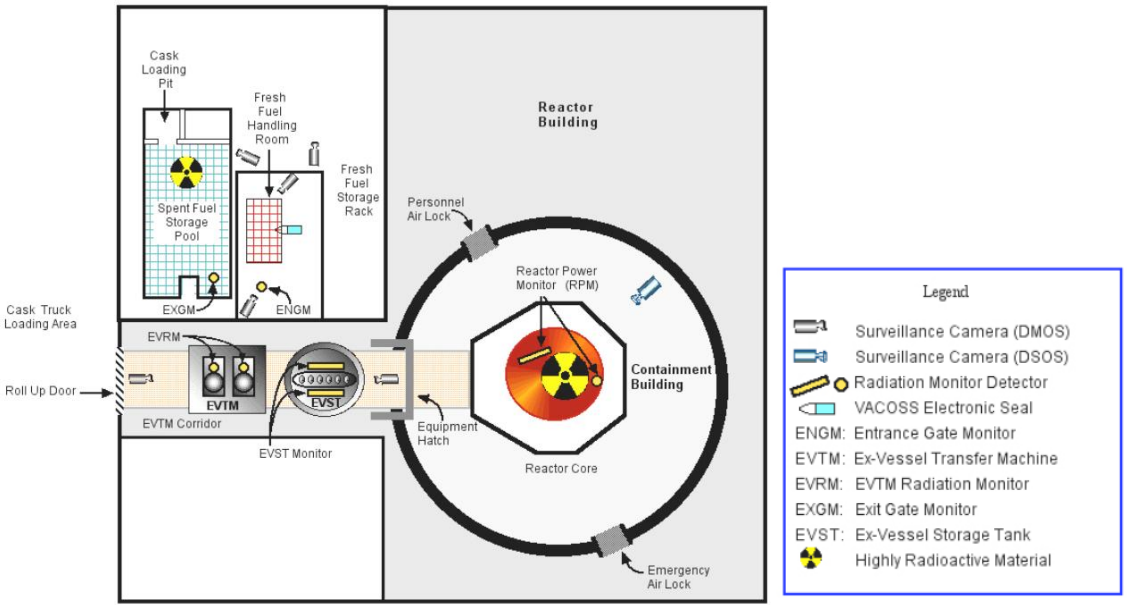

Fig. 11. Primary safeguards measures at MONJU Fast Reactor in Japan.[38]

Since there are large quantities of plutonium in fresh fuel assemblies, the fresh fuel is considered unirradiated direct use material. Thus, fast reactors are inspected monthly in addition to the yearly PIV.

2.4.4 Review of Item-based Approach for Pebble-fueled HTGR Safeguards System Concept

This review of safeguards approaches at different types of reactors demonstrated a wide definition of the item-based approach. The easiest reactor to safeguard was the LWR because the fuel assemblies are easily distinguishable, remain visible throughout the reactor facility, and can be marked with a serial number. The limitation of visibility of assemblies while in the core is overcome by placing a seal on the core cover to indicate any access.

On-load fueled reactors are similar to pebble-fueled HTGRs since fuel is added to the reactor while operating. However, on-load reactors utilize fuel bundles that are still fairly physically distinguishable for item counting and can be marked with serial numbers. Like pebble-fueled HTGRs, once the fuel is inserted into fuel channels, the

bundles are inaccessible. This was overcome by increasing the number of C/S measures applied in the safeguards approach.

The safeguards approach for fast reactors is very similar to the approach for on-load fueled reactors. Item counting and extensive C/S measures are used to ensure no diversion of fuel assemblies. However, fast reactor safeguards had to overcome the additional challenge that the opaque coolant prevents direct verification of serial numbers when fuel assemblies are submerged. Additionally, spent fuel assemblies are stored in cans that prevent their visual verification. Nonetheless, should the fuel assemblies ever be removed from the coolant or storage can, the serial number on each assembly can still be used to restore continuity of knowledge.

The review of these approaches furthers the notion that any approach for a pebble-fueled HTGR should be item-based. While item verification may not be heavily relied upon, like with on-load fueled reactors and fast reactors, the availability of identity verification supplemented by item counting and C/S measures increases the difficulty for an adversary to unknowingly divert nuclear material from the reactor facility.

3. DEVELOPMENT OF A NEW SAFEGUARDS SYSTEM CONCEPT

3.1 Potential Methods to Uniquely Identify Individual Pebbles

To develop methods to identify the fuel pebbles, we first considered the placement of the identifier wither within the pebble (internal) or on the outside of the pebble (external).

3.1.1 External Identifier

The external identifier addressed is a serial number that is commonly applied as an identifier to item materials like the fuel present in a LWR, on-load fueled reactor, or fast reactor. This serial number would be engraved in the graphite that comprises the non-fueled region of the pebble, after the fuel pebble has been fully manufactured.

Any concern of the neutronics affects of removing some amount of the graphite reflector due to engraving would be minimal because the quantity of graphite removed would be low compared to the total graphite present in a fuel pebble. An additional concern is how the engraving of serial number would affect the structural integrity of the pebble. As the pebble moves down the reactor core in-contact with other fuel pebbles and core components, the edges created by the engraving make the location a likely spot for damage to occur. This could result in loss of the serial number or a complete failure of the pebble fuel.

By far, the greatest concern with any type of external identifier would be the ease with which the identifier could be reproduced. While the idea of a serial number is simple and easily verifiable, that is also a vulnerability to the system. In LWRs this vulnerability is overcome with the use of C/S measures since the fuel assemblies in an LWR are quite large, thus one can be distinguished from the removal of another. As long as video surveillance of the reactor vessel and surrounding areas was not compromised, it would be quickly revealed if fuel assemblies were being diverted.

3.1.2 Internal Identifier

Concerns of pebble structural integrity and identifier reproducibility can be overcome with use of an internal identifier. The internal identifier conceived uses

microspheres, of similar size as TRISO particles, whose random placement within the fueled region of the pebble would act as a fingerprint for each pebble.

During pebble manufacturing, these microspheres could be added to the graphite matrix mixture that contains the TRISO particles. Once the mixture is transferred to the pebble mold for pressing, the microspheres would be randomly distributed inside the pebble. A detailed flow chart for the production of the TRISO particles and fuel pebbles can be found in Appendix A.

The microsphere material must be able to withstand the expected thermal and radiation environment, as well as not chemically react with the graphite matrix. The microspheres should have a minimal impact on the reactivity in the pebble, meaning the material chosen should have a small neutron absorption cross section so as not to disrupt the neutron flux thereby impacting reactor operation. Additionally, an imaging system must be found that can reliably locate microspheres inside each fuel pebble. This imaging system must be capable of imaging fresh fuel, core fuel, and spent fuel pebbles, otherwise this safeguards systems would not be able to maintain CoK. Reproducibility of the random location of microspheres would be very difficult for an adversary to repeat, further increasing the difficulty of an undetected diversion of material.

3.2 Development of Internal Identifier

To determine the material for the microspheres, consideration was given to two types of microspheres. First, a microsphere comprised of a material that once irradiated, would emit a specific gamma energy that would be detected using a radiation based imaging system. The second type of material considered, was an inert material that could be imaged using a non-radiation based imaging system. The radiation based systems considered for detecting the microspheres were computed tomography (CT) and single photon emission tomography (SPECT). The non-radiation based imaging system considered was ultrasound imaging. Other imaging systems could be used in the concept but these systems were considered the most likely to be successful.

3.2.1 Computed Tomography (CT) Imaging

Computed tomography (CT) is traditionally used in the medical field on biological material. CT operates by using a collimated x-ray source located directly across from a series of detectors that rotate around the patient as the source is rotated. The source is exposed to a one "slice" of the patient at a time, producing a series of one-dimensional projections (images) at different angles around the patient. This process continues until enough projections have been taken to produce a good spatial resolution close to 1 mm. Using computer software, these one-dimensional projections are combined to create a two-dimensional image of the patient's body. This operating principle can be seen in Fig. 12. CT scanners used in most hospitals today are third generation scanners that operate in the 70-80 keV energy range.[39]

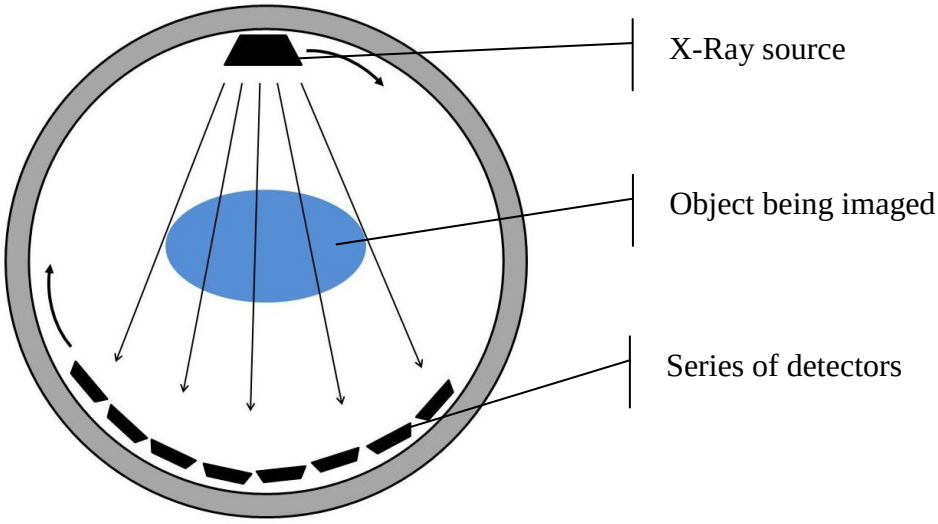

Fig. 12. Operating principle of CT scanner.

CT has been previously investigated for use in the nuclear industry:[40]

- individual fuel pellets have been imaged to determine density gradients;
- fuel samples from Unit 2 at Three Mile Island were examined after the accident to determine the degree of damage to the fuel;

- CANDU fuel bundles used in a simulated loss of coolant accident were examined to determine temperature and radiation damage; and
- PWR assemblies have been examined to form a detailed analysis of materials and flaws in subassemblies.

If CT was used to image each pebble, the microspheres could be gamma emitting or inert because there is an exterior source that produces the x-rays necessary for imaging. However, there are two limitations to the use of CT for this approach. First, nuclear material is dense, much denser than the typical biological materials traditionally imaged using CT.[40] This means the x-rays from the source are attenuated more. As such, the source must generate x-rays of high energy that can fully penetrate the object and be detected on the opposite side. An additional limitation is that the radiation emitted from irradiated pebbles can saturate the detectors in the scanner.[40] Once a fuel pebble has been irradiated, the radiation emitted from the TRISO particles or any gamma emitting microspheres would likely saturate the detectors 70-80 keV operating range. Also, the detectors used in CT scanners cannot differentiate between the radiation emitted from the pebble from the x-rays emitted by the source. This would result in an inaccurate fingerprint for the pebble that could not be matched to the correct image. With a fuel pebble, these limitations of CT prevent the system from being a viable imaging system for this safeguards systems concept.

3.2.2 Single Photon Emission Computed Tomography (SPECT) Imaging

Radiation emitted from irradiated fuel pebbles presented difficulties in the CT imaging process. To overcome the limitations of an imaging system that emits the radiation, a system that detects emitted radiation was considered. Locating radioactive source material within an object is the operating principle behind single photon emission computed tomography (SPECT).

SPECT does not produce an image of tissue within a patient, but instead produces an image of the distribution of radiopharmaceuticals in that tissue. The radiopharmaceuticals, known as radiotracers, are typically gamma emitting isotopes that are produced by irradiating a stable element causing the element to transmute into the

gamma emitting isotope desired. Elements with isotopes used as radiotracers include technetium, gallium, thallium, xenon, indium, and iodine. Each has isotopes with half-lives on the order of hours to days with gamma energies ranging from 70 to 400 keV. Much like CT, SPECT uses a series of gamma cameras to detect the gamma radiation emitted by the radiotracers to create two-dimensional images of the patient's body. Unlike CT, the spatial resolution of SPECT cannot be improved by generating additional images, so a resolution of 1 cm is typical.[39]

SPECT has been previously investigated for use in the nuclear industry to detect the removal of fuel rods in fresh and spent LWR fuel assemblies. A system was designed such that a fuel assembly that has been shortly cooled (3-4 weeks) is placed inside of a housing while still in the spent fuel pool. Inside this housing, several collimated detectors record the radiation emitted by the fuel assembly. The detectors are moved vertically along the fuel assembly, recording measurements at set intervals. The investigation concluded that SPECT could successfully be used to detect the removal or replacement of fuel pins from fuel assemblies without having to disassemble the fuel assembly.[41]

In application with this developed safeguards system concept, if the microspheres in the fuel pebble were emitting gamma radiation, the microspheres could act as the radiotracer for use with SPECT. However, there would be a few issues.

Imaging of fresh fuel pebbles is not possible because the gamma emitting "radiotracer" microspheres have not been irradiated, so no gamma radiation could be detected by the SPECT system. Once the fuel pebble has been irradiated the same limitations seen with CT arise. Much like CT, SPECT:

- is incapable of differentiating between radiation emitted by the microspheres and radiation emitted by the irradiated fuel material;
- is vulnerable to detector saturation from radiation emitted from irradiated fuel pebbles in its 70-400 keV operating range;

- has a poorer resolution than CT, meaning the microspheres would have to be physically larger than the TRISO particles due to the 1 cm resolution of a SPECT system; and
- Lastly, the energy of the radiation released by the microspheres would have to be large enough that any attenuation caused by the dense fuel material could be overcome.

Taken together, these limitations prevent SPECT from being a viable imaging system this concept. While SPECT could determine the location of microspheres larger than 1 cm in diameter, this size microsphere is likely to disrupt the TRISO particle quantities, thus changing the fuel characteristics, an undesired outcome.

3.2.3 Ultrasound Imaging

By considering an imaging system that does not rely upon detection of emitted radiation, the problems associated with detector saturation and source differentiation can be overcome. The non-radiation based system considered for application in this developed safeguards system is ultrasound imaging.

Ultrasound imaging operates by sending a short pulse of energy into the body using an ultrasound transducer. The transducer produces a narrow ultrasound beam that moves through the body as a pressure wave. When the wave encounters tissue surfaces, boundaries between tissues, or objects within the body, part of the wave energy is lost due to absorption or scattering.[39] The direction and magnitude of scattered waves is dependent upon the physical and acoustic properties of the scattering object.[39]

Some of the waves backscatter, or scatter back towards the transducer. The transducer then acts as a receiver, converting the returning pressure waves into voltages that are amplified, filtered, and then converted into a digital signal. This concept is depicted in Fig. 13. An image can be constructed from this digital signal because the time delay between transmission of the pressure wave and its return is known, as well as the speed at which the wave travels. From these two values, the system can determine the depth of the boundary or object within the body. The transmission and receipt of the wave takes 100-300 microseconds. After the transducer has received all of the

backscattered waves from this initial wave, the narrow ultrasound beam is electronically directed adjacent to the initial wave. Depending on the ultrasound system, this is repeated some 64 to 256 times, each acquiring a line of the image. These lines are then compiled by the system to create an image of the body in tens of milliseconds.[39]

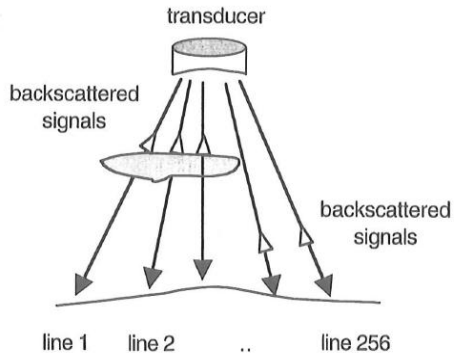

Fig. 13. Basic operating principle for an ultrasound system.[39]

Generally operating in the frequency range of 1-10 MHz, ultrasound imaging has been used in the medical field for many years. When possible, ultrasound is the preferred imaging method because ultrasound imaging is fast, with real time imaging capabilities and possesses a high intrinsic spatial resolution at high frequencies. Ultrasound imaging does have some limitations in that ultrasound wave transmission is greatly reduced in gases and differentiation between biological material boundaries is poor.[39]

Within the nuclear industry, ultrasound systems are extensively used to measure the flow of liquids through pipes in nuclear reactors. In the area of nuclear safeguards, ultrasound imaging has been investigated for use in safeguarding in-core fuel at sodium fast reactors.[42] As previously discussed in Section 2.4.3, once a fuel assembly has been placed in the opaque liquid metal coolant, no serial number can be visually read. However, by using an ultrasound system, the response of sound waves can be used to reconstruct an image of the serial number engraved on a fuel assembly.

In this safeguards system concept, ultrasound imaging presents no immediately discernable limitations. Since ultrasound operates using mechanical properties of materials, and not nuclear properties of materials, an ultrasound system should be able to

image fresh, core, and spent fuel pebbles. This assumes that the ultrasound equipment itself has been radiation hardened or not affected by the radiation emitted from irradiated fuel pebbles. With an ultrasound system it is not necessary for the microspheres to emit radiation. This opens the options for materials that could be used for the microspheres.

The major unknown about ultrasound imaging for this concept that could not be determined was the transmission behavior of ultrasound waves in graphite. However, it was established through experimentation. Other than the unknown transmission characteristics, since no conclusive disadvantages of ultrasound imaging could be demonstrated from literature, ultrasound imaging was chosen as the system to be used in this concept.

3.2.4 Microsphere Material

With the imaging system chosen, it was possible to determine the material for the microspheres. The field was quickly narrowed to ceramic materials due to their high temperature resistance. This is a desired characteristic because the pebble-fueled HTGR is a high temperature reactor, operating with a helium outlet temperature near 900^{o}C.[18] A ceramic microsphere is more likely to remain stable at these temperatures over the lifetime of the fuel pebble, as well as remain stable past 1600^{o}, the temperature at which metallic fission products begin to diffuse through the SiC layer of the TRISO particle.[43] The two ceramics considered for the microsphere material were zirconium carbide (ZrC) and zirconium oxide (ZrO_2).

Both ZrC and ZrO_2 have been investigated for use in nuclear reactors. Each are being considered as candidate materials for use in inert matrix fuels for LWRs and high temperature reactors to burn excess plutonium from fuel reprocessing and nuclear weapons.[44,45] Additionally, ZrC is being considered for application in pebble fuel as a replacement for the SiC layer of the TRISO particle for improved fission product retention. ZrC has also been investigated as an additional layer around the fuel kernel to react with free oxygen to prevent failure of the TRISO particle due to fuel kernel migration.[46]

With regards to the microspheres proposed, ZrC and ZrO_2 have melting temperatures of approximately 3500^{o}C and 2700^{o}C, respectively.[47] These temperatures are well above the 1600^{o}C fission product diffusion limit of SiC near the 2800^{o}C melting temperature of UO_2.[48] This means at very high temperatures, failure of the microspheres will not be of primary concern because prevention of a fuel failure would be more consequential.

Either ZrC or ZrO_2 can be used as the ceramic material for the microspheres imagined in this safeguards system concept. For this work, ZrO_2 was chosen as the material for the microspheres. ZrO_2 is not commonly used in a pure form, more often ZrO_2 is doped with an additive that stabilizes the ZrO_2 for use in a wider range of applications.[47] For the microspheres considered in this concept the additive chosen was yttrium oxide (Y_2O_3).

An additional ideal characteristic of ZrO_2 is its low neutron absorption cross section. Fig. 14 shows a plot of the neutron absorption cross section of ^{235}U, natural zirconium, natural yttrium (^{89}Y), and carbon (^{12}C) from *Evaluated Nuclear Data File (ENDF) B Version VI.8*. In Fig. 14, a line marks 0.025 eV, the average thermal neutron energy. At this energy, the absorption cross section for natural zirconium, ^{89}Y, and ^{12}C are very low compared to ^{235}U. This means the probability that the microsphere will parasitically absorb a neutron is low compared to the probability that the fissionable ^{235}U in each TRISO particle will absorb a neutron.

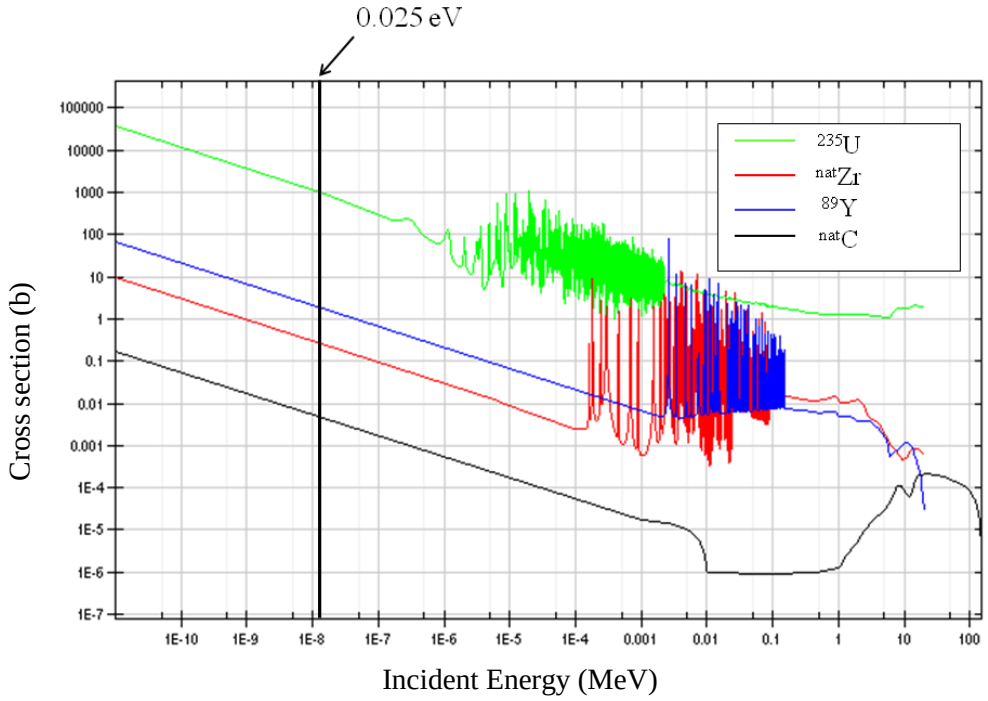

Fig. 14. Absorption cross section plot of ^{235}U, natural zirconium, ^{89}Y, and ^{12}C.

3.3 Implementation of the Developed System Concept

The fully developed system consists of 1 mm ZrO_2 microspheres that have been randomly dispersed inside of each fuel pebble. The random configuration of these microspheres will be imaged using an ultrasound imaging system. For this safeguards system concept, the microspheres will be placed in the fueled region of each fuel pebble, meaning the microspheres will be dispersed among the TRISO particles. Consideration was given to placement of the microspheres in the non-fueled region of the pebble, but was decided against due to the unknown amount of the graphite shell that would be removed as each pebble circulated through the reactor core.

This safeguards system concept would be implemented at the reactor facility in such a way that the microsphere fingerprint would be verified at key measurement points throughout the reactor system. These key measurement points are highlighted in red boxes in Fig. 15. Use of this safeguards system concept does not replace the need of C/S measures. While the extensive C/S measures used the dual C/S dependent approach will probably not be necessary, some level of C/S protection will be required. The supplementation of C/S measures is necessary because of the lack of access to fuel pebbles for random verification when the pebbles are in the reactor core and fuel storage containers.

Most likely, this system can replace the functionality of the pebble counters utilized in previous approaches. The imaging of each pebble acts as a pebble counter, much like in CANDU safeguards when detection of radiation emitted from fuel bundles is used to count the number of bundles.

To prevent tampering, the ultrasound system will need to be sealed with a TID and possibly maintained under video surveillance. This judgment must be made by the agency utilizing the system to safeguard the reactor. An additional part of the determination will need to be the cost associated with implementation of this design. While ultrasound systems can be less expensive than other imaging systems considered in this research, the higher the resolution of the system needed, the larger the cost associated. For this research, these costs were not considered.

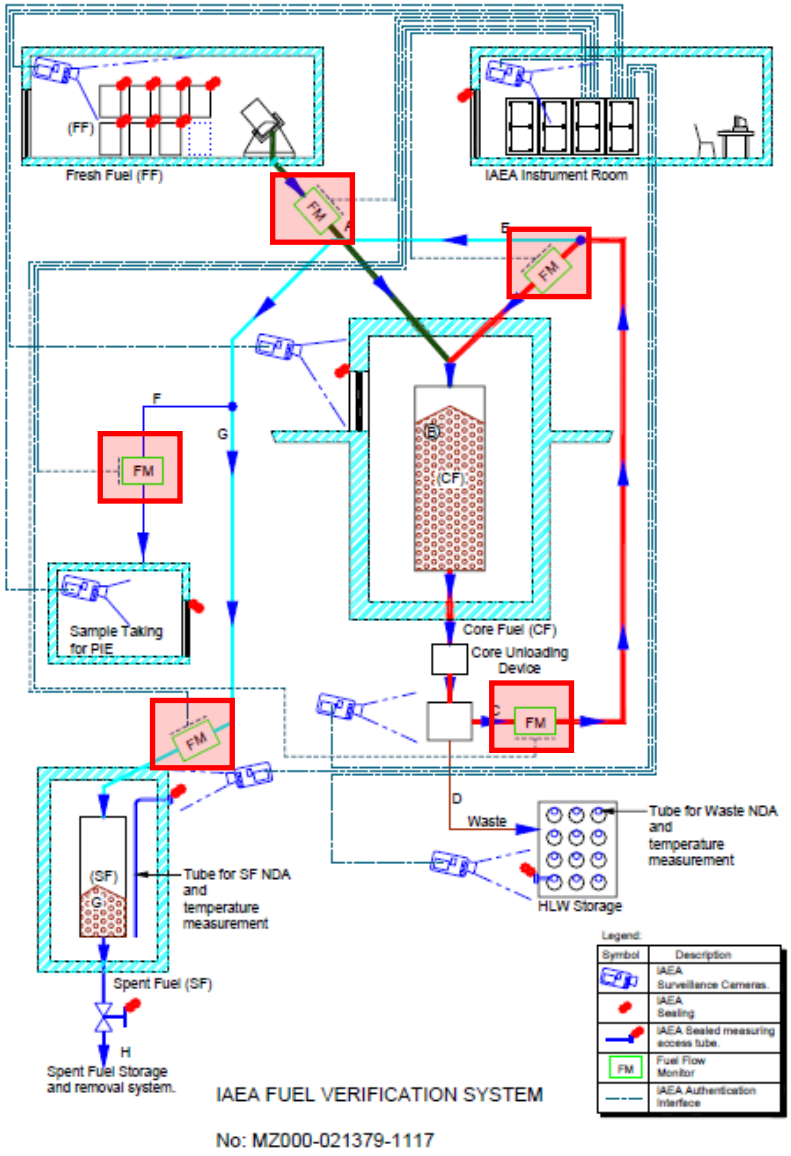

Fig. 15. Key measurement points where the developed safeguards system concept would be implemented at a pebble-fueled HTGR facility.

3.4 Conclusions on the Development of the System Concept

The main challenge to safeguarding a pebble-fueled HTGR was identified as the current inability to restore continuity of knowledge (CoK) in situations where large quantities of pebbles are removed from the core and containment and surveillance (C/S) measures in place have failed or been purposely compromised. This challenge could be

overcome if a method were developed to uniquely identify each fuel pebble supplemented by C/S measures, much like the safeguards systems used at light water reactors, on-load fueled reactors, and fast reactors. Based on the pebble-fueled HTGR core environment and material challenges with the fuel pebbles, the best placement of an identifier for the system was determined to be inside the pebble. The identifying method chosen was the use of small microspheres that could be randomly distributed inside each fuel pebble to create a unique fingerprint for each pebble. To verify this internal identifier it was determined that an imaging system must be found that could operate in the presence of unirradiated and irradiated fuel pebbles. The imaging system most likely capable of imaging these types of pebbles was determined to be ultrasound imaging. Zirconium based ceramic materials were identified as the preferred material for the microspheres based on high temperature resistance and small thermal neutron absorption cross section. The final chosen material for this safeguards system concept was zirconium oxide with the additive yttrium oxide. Implementation of this concept was also considered. It was determined that the system would be placed at key measurement points in the reactor facility, replacing the functionality of pebble counters utilized in currently proposed approaches.

4. STATISTICAL ANALYSIS OF SAFEGUARDS SYSTEM CONCEPT

For this statistical analysis, there are two questions that need to be answered:

1. What is the minimum number of microspheres necessary to be able to uniquely identify some number of pebbles?
2. What is the probability that one pebble will have a configuration that randomly matches another pebble?

4.1 Total Number of Pebbles Passing Through the Reactor Core

The total number of pebbles that will pass through the reactor in its lifetime was determined. This number sets the lower limit for the total number of configurations of microspheres necessary. The total number of fuel pebbles in the reactor system was set to 520,000. This number corresponds to the number of pebbles found in the HTR-PM core when the reactor is operating at equilibrium. Several assumptions were made: [49]

1. the number of pebbles initially loaded into the reactor core will be the same as the number of pebbles in the equilibrium core;
2. the initial load of pebbles remains in the core for three years before pebbles are permanently discharged;
3. once equilibrium status has been reached, the average number of pebbles being discharged daily is 8036;
4. on average, approximately 10% (803 pebbles) are permanently discharged daily as spent fuel and replaced with an equal number of fresh fuel pebbles, the remaining being recirculated back into the core; and
5. the reactor is operating 365 days per year for its design lifetime of 40 years.

Using these assumptions, it is possible to determine the total number of pebbles the reactor will "see" in its lifetime:

$$520{,}000 + \left(803\,\frac{pebbles}{day}\right)\left(365\,\frac{days}{year}\right)(37\ years) = 11{,}364{,}515\ pebbles$$

In real world conditions this number would fluctuate due to the true number of pebbles in the initial core and the operating statistics of each reactor, such as capacity factor and availability factor. Additionally, this value corresponds to the number of pebbles that pass through a single reactor in its lifetime. When implemented, this total number of pebbles must at least be multiplied by at least the number of reactors in each country.

To make simplify subsequent calculations, the number of pebbles seen in the reactor lifetime was rounded to 10,000,000 pebbles. This means that there must be at least 10,000,000 unique configurations of microspheres that can be used to identify a pebble.

4.2 Minimum Number of Microspheres

Consider a simple square divided into four smaller squares in Fig. 16. These squares are labeled 1, 2, 3 and 4. Assume a circle is placed in two of the four squares.

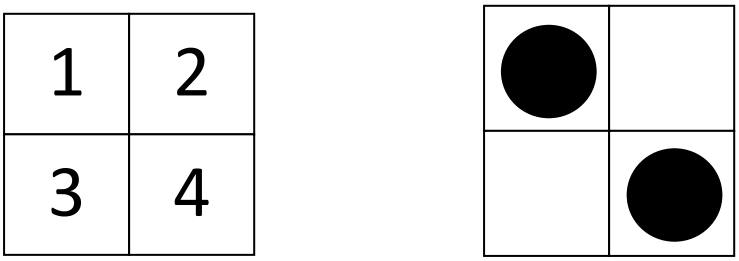

Fig. 16. Graphical representation of one of the possible ways to fill a 2 by 2 set of squares with two circles.

There are six, or configurations, that two squares can each be filled with one circle (1,2; 1,3; 1,4; 2,3; 2,4 and 3,4). This total number of configurations can be analytically determined using the binomial coefficient,[50] noted as $\binom{n}{k}$:

$$\binom{n}{k} = \frac{n!}{k!(n-k)!} \qquad \text{Eq. (1)}$$

where, *n* is the number of objects and *k* is the number of chosen objects. In the case of the above example with the four squares and two circles, Eq. (1) would be:

$$\binom{4}{2} = \frac{4!}{2!\,(4-2)!} = \frac{4 \cdot 3 \cdot 2 \cdot 1}{(2 \cdot 1) \cdot (2 \cdot 1)} = 6$$

Using this same process, it is possible to determine the minimum number of microspheres necessary to create enough unique configurations of microspheres to identify at least 10,000,000 pebbles.

We consider the number of possible positions in which microspheres can be placed must be determined. The microspheres will be placed in the fueled region of the pebble. the volume of this region is:

$$V_{FR} = \frac{4}{3}\pi r^3 = \frac{4}{3}\pi\,(25mm)^3 = 65{,}449.85\,mm^3$$

Also present in this fueled region of the pebble are TRISO particles. The volume that these TRISO particles occupy must be removed because a microsphere cannot occupy the same volume as a TRISO particle.

If the volume of all the TRISO particles was simply subtracted from the volume of the fueled region, this volume would not represent the volume available for a microsphere. Even if the entire fueled region of the pebble were occupied by TRISO particles, in reality there would be some volume that would not be occupied due to the lattice structure created by the TRISO particles. In 2D this principle can be seen in Fig. 17, where the black region represents the area occupied by a TRISO particle and the crosshatch region represents the vacant area due to the nature of the lattice structure.

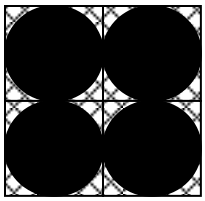

Fig. 17. Voxel created by each TRISO particle and microsphere.

This crosshatch region must be accounted for in the volume calculation for a TRISO fuel particle. In reality, the TRISO particles could form a lattice structure that has a higher packing fraction. However, by using the structure in Fig. 17 the a larger volume will be attributed to each TRISO particle, meaning the volume available for the microspheres will be a conservative estimate.

To account for this volume correction, the diameter of the TRISO particle is used as the side length of a cube around the TRISO particle. Thus, the volume of this TRISO voxel is:

$$V_{TRISO\ voxel} = (0.92\ mm)^3 = 0.7787\ mm^3$$

The total volume of the fueled region of the pebble occupied by all 15,000 TRISO particle voxels is:

$$V_{15{,}000\ TRISO} = 15\ ,00 \cdot (0.92\ mm)^3 = 11{,}680.32\ mm^3$$

Subtracting this total TRISO particle volume from the volume of the fueled region, the remaining volume of the fueled region that can be occupied by the microspheres is:

$$V_{FR\ remaining} = 65{,}449.85\ mm^3 - 11{,}680.32\ mm^3 = 53{,}769.53\ mm^3$$

Applying the same lattice principle to the microspheres, the volume of a voxel created by a single microsphere is:

$$V_{Zr\ cube} = (1.0\ mm)^3 = 1\ mm^3$$

Dividing the remaining volume in the fueled region by the volume of the microsphere cube, the total number of positions a microsphere could occupy would be:

$$\begin{matrix} Total\ number\ of\ voxels \\ for\ Zr\ microsphere \end{matrix} = \frac{53{,}769.53\ mm^3}{1.0\ mm^3} = 53{,}769 \qquad \text{Eq. (2)}$$

These 53,769 voxels are the number of positions in the fueled region of the pebble available for a microsphere. Since a fraction of a microsphere cannot be placed inside one of these positions, the total number of voxels for microspheres was rounded down to the nearest integer. This total number of voxels should be considered an average value. In manufacturing processes, random differences in pebbles could increase or decrease the total number of positions possible in the fueled or non-fueled region.

Now that the number of voxels that can be occupied by a microsphere has been determined, the binomial coefficient can be used to determine the number of unique configurations of microspheres as follows:

$$\binom{53{,}769}{k} = \frac{53{,}769!}{k!(53{,}769-k)!} \qquad \text{Eq. (3)}$$

where there are *n* (or 53,769) voxels to choose from and *k* voxels chosen to be filled with a microsphere. The simplest way to determine the lowest *k* is to begin at 1 and increase *k* by 1. When the number of unique configurations exceeds the lower limit of 10,000,000, the minimum number of microspheres necessary to uniquely identify each pebble has been found. This is as follows:

For *k*=1

$$\binom{53{,}769}{1} = \frac{53{,}769!}{1!\,53{,}768!} = \frac{53{,}769}{1} = 53{,}769\ unique\ configurations$$

For *k*=2

$$\binom{53{,}769}{2} = \frac{53{,}769!}{2!\,53{,}767!} = \frac{53{,}769 \cdot 53{,}768}{2 \cdot 1} = 1{,}445{,}525{,}796\ unique\ configurations$$

The lower limit is exceeded by randomly filling only two, of the 53,769 available positions with microspheres. This means that the minimum number of microspheres necessary to create enough unique configurations of microspheres to uniquely identify at least 10,000,000 pebbles is two. However, in application, to determine which voxel the microsphere has been placed in, or really the *x*-, *y*-, and *z*-coordinate of each microsphere, there must be a reference point with a known location. Taking this into consideration, there must really be at least three microspheres in each pebble whose positions can be precisely measured, no matter where each microsphere resides inside the pebble.

4.3 Identifying Each Pebble

To identify each pebble, a set of "characteristic lengths" is determined. These lengths are shown in Fig. 18.

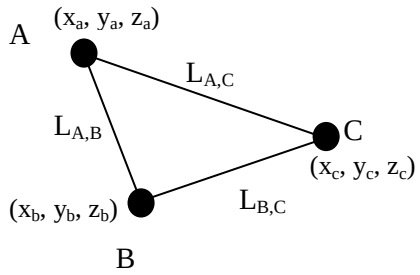

Fig. 18. Naming scheme for characteristic lengths identified in template image.

These lengths are determined by subtracting the *x*-, *y*-, and *z*-coordinates of the center of each microsphere from the opposite microsphere used to create the line. Those coordinates can be placed in a matrix from which the matrix of the connecting microsphere coordinates can be subtracted. This creates a 3 x 3 matrix of the difference in the *x*-,*y*-, and *z*-coordinates. This matrix operation can be seen below:

$$\begin{bmatrix} x_A & y_A & z_A \\ x_B & y_B & z_B \\ x_C & y_C & z_C \end{bmatrix} - \begin{bmatrix} x_B & y_B & z_B \\ x_C & y_C & z_C \\ x_A & y_A & z_A \end{bmatrix} = \begin{bmatrix} x_A - x_B & y_A - y_B & z_A - z_B \\ x_B - x_C & y_B - y_C & z_B - z_C \\ x_C - x_A & y_C - y_A & z_C - z_A \end{bmatrix} = \begin{bmatrix} x_{A,B} & y_{A,B} & z_{A,B} \\ x_{B,C} & y_{B,C} & z_{B,C} \\ x_{C,A} & y_{C,A} & z_{C,A} \end{bmatrix}$$

If this matrix of differences is then transposed and multiplied by the original differences matrix, the diagonal of the resulting matrix is the square of the line lengths of interest referenced in Fig. 18. This can be seen below:

$$\begin{bmatrix} x_{A,B} & y_{A,B} & z_{A,B} \\ x_{B,C} & y_{B,C} & z_{B,C} \\ x_{C,A} & y_{C,A} & z_{C,A} \end{bmatrix} \begin{bmatrix} x_{A,B} & x_{B,C} & x_{C,A} \\ y_{A,B} & y_{B,C} & y_{C,A} \\ z_{A,B} & z_{B,C} & z_{C,A} \end{bmatrix}$$

$$= \begin{bmatrix} x_{A,B}^2 + y_{A,B}^2 + z_{A,B}^2 & \cdots & \cdots \\ \cdots & x_{B,C}^2 + y_{B,C}^2 + z_{B,C}^2 & \cdots \\ \cdots & \cdots & x_{C,A}^2 + y_{C,A}^2 + z_{C,A}^2 \end{bmatrix}$$

By taking the square root of each of these diagonal values, the line lengths referenced in Fig. 18 are determined as seen below:

$$\begin{bmatrix} x_{A,B}^2 + y_{A,B}^2 + z_{A,B}^2 & x_{B,C}^2 + y_{B,C}^2 + z_{B,C}^2 & x_{C,A}^2 + y_{C,A}^2 + z_{C,A}^2 \end{bmatrix} = \begin{bmatrix} L_{A,B}^2 & L_{B,C}^2 & L_{C,A}^2 \end{bmatrix}$$

$$\begin{bmatrix} L_{A,B}^2 & L_{B,C}^2 & L_{C,A}^2 \end{bmatrix}^{\frac{1}{2}} = \begin{bmatrix} L_{A,B} & L_{B,C} & L_{C,A} \end{bmatrix}$$

This set of characteristic lengths identifies each configuration of microspheres, and thereby each pebble. In application, this method will have some uncertainty. This uncertainty is introduced by the ultrasound imaging machine. The machine has a

resolution at which the position of each microsphere can be determined and subsequently, the length of the line between two microspheres. The functionality of the ultrasound system and the computer software used determines where this resolution uncertainty is applied. Most likely, this uncertainty will be applied to the characteristic lengths.

4.4 Matching Pebbles

When a pebble is imaged before being placed in the reactor core, an initial image is recorded and an initial set of characteristic lengths can be found. This set of lengths is considered the template. As subsequent images of the pebble are recorded and the characteristic lengths found in those images, this subsequent set of lengths is compared to the template set in Fig. 19. If the two sets of characteristic lengths match within the statistical error of the imaging system, then it can be concluded that the subsequent pebble was indeed the initial pebble placed into the reactor.

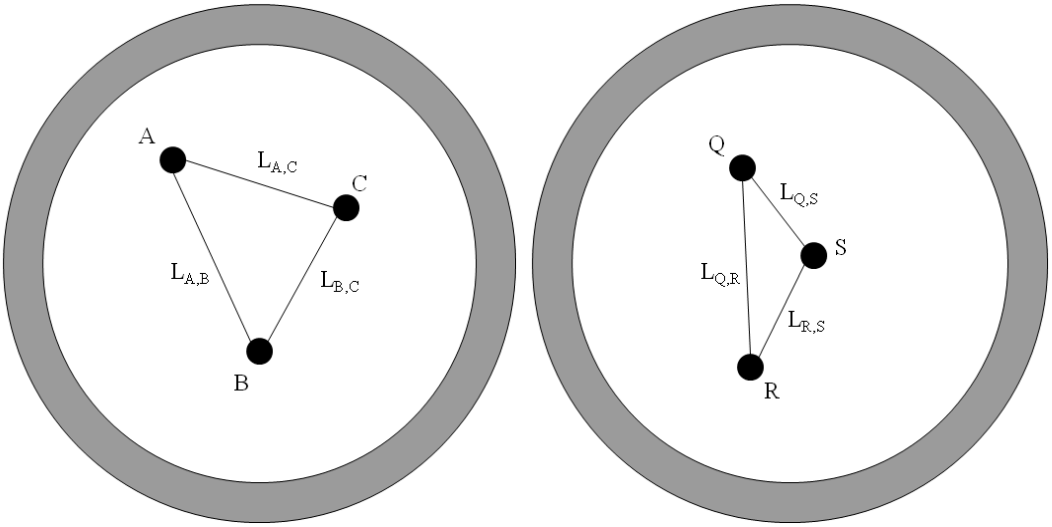

Fig. 19. Initial image (left) of some pebble placed in reactor core and a (right) a subsequent image of some pebble removed from the reactor core.

The microspheres in the subsequent image in Fig. 19 are labeled *Q*, *R*, and *S* because when the pebble is imaged by the ultrasound system it will not be oriented in the

same manner as when the template image was originally taken. Thus, it cannot be stated that microsphere *Q* in the subsequent image is in fact microsphere *A, B, or C* in the template image. To overcome this limitation, to determine if the two images match, each of the characteristic lengths found in the subsequent image must be subtracted from the lengths from the template image. Much like when determining the characteristic lengths, this creates a matrix of characteristic length differences. The calculation of this matrix can be seen below:

$$\begin{bmatrix} L_{A,B} & L_{B,C} & L_{C,A} \\ L_{A,B} & L_{B,C} & L_{C,A} \\ L_{A,B} & L_{B,C} & L_{C,A} \end{bmatrix} - \begin{bmatrix} L_{Q,R} & L_{R,S} & L_{Q,S} \\ L_{R,S} & L_{Q,S} & L_{Q,R} \\ L_{Q,S} & L_{Q,R} & L_{R,S} \end{bmatrix} = \begin{bmatrix} \left|\Delta_{(A,B),(Q,R)}\right| & \left|\Delta_{(B,C),(R,S)}\right| & \left|\Delta_{(C,A),(Q,S)}\right| \\ \left|\Delta_{(A,B),(R,S)}\right| & \left|\Delta_{(B,C),(Q,S)}\right| & \left|\Delta_{(C,A),(Q,R)}\right| \\ \left|\Delta_{(A,B),(Q,S)}\right| & \left|\Delta_{(B,C),(Q,R)}\right| & \left|\Delta_{(C,A),(R,S)}\right| \end{bmatrix}$$

To determine which length from the subsequent image is in fact $L_{A,B}$, $L_{B,C}$, or $L_{A,C}$ from the initial image, first the absolute value of the minimum difference between $L_{A,B}$ and $L_{Q,R}$, $L_{R,S}$, or $L_{Q,S}$ is found. Assuming the minimum difference is between $L_{A,B}$ and $L_{Q,R}$. This means that $L_{B,C}$ cannot also be $L_{Q,R}$. $L_{B,C}$ must either be $L_{R,S}$ or $L_{Q,S}$. Again, the absolute value of the minimum difference is identified; assume it is $L_{Q,S}$. This then means that $L_{A,C}$ and $L_{R,S}$ have the best chance of matching because $L_{Q,S}$ cannot also be $L_{A,C}$.

With the characteristic lengths in the subsequent image now tied to a length from the template, we can determine if the two pebbles do indeed match. If the absolute values of the minimum differences calculated and identified previously are each less than the resolution of the system, the two pebbles are considered to match and the subsequent pebble is identified.

An additional limitation of this method that must be highlighted is that since the lines created are between microspheres and not some known reference, the possibility exists for there to be a repetition in the lengths of line. Two microspheres with a characteristic length of 1.05 cm can actually be oriented in many different ways within

the pebble and still be 1.05 cm apart. It is the combination of the three characteristic lengths that make the identification more unique, and thus less likely to repeat.

4.5 Results

A Microsoft Excel macro was written that performed the procedure described in Sections 4.3 and 4.4.

In the numerical simulation, a set of three characteristic lengths was randomly generated. These lengths were considered the characteristic lengths for the initial image of a pebble, like $L_{A,B}$, $L_{B,C}$, or $L_{A,C}$ in Fig. 19.

Next, a set of three characteristic lengths between 0.1 cm and 4.9 cm were randomly generated. This set of lengths was considered the characteristic lengths determined from a subsequent image of a pebble, like $L_{Q,R}$, $L_{R,S}$, or $L_{Q,S}$ in Fig. 19. The lower limit of the range was 0.1 cm because the minimum length between the centers of any two microspheres can be 0.1 cm, or twice the radius of a single microsphere. The upper limit of the range was 4.9 cm because the closet a center of a microsphere can lie to the interface between the fueled and non-fueled region of the pebble is 0.05 cm. These limits are depicted in Fig. 20.

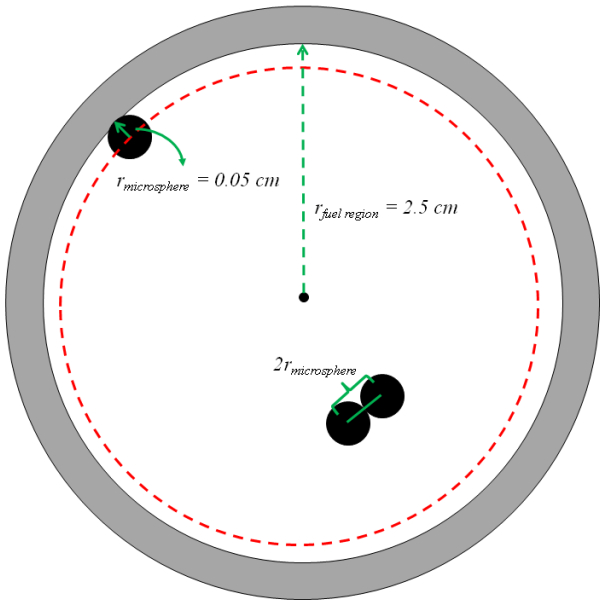

Fig. 20. Depiction of limits on characteristic lengths for computer simulation.

After the set of characteristic lengths for the subsequent image was created, the matrix of differences from Section 4.4 was calculated. Each column of characteristic lengths in the matrix of differences represents one of the characteristic lengths in the initial image of the pebble. The simulation then finds the minimum difference in each column as described in Section 4.4. Finally, if each of the three minimum differences found is less than the resolution of the imaging system, the simulated subsequent image of a pebble was considered a match to the set of characteristic lengths generated for the initial image of a pebble. This process was repeated 10,000,000 times, simulating the 10,000,000 pebbles expected to pass through the reactor during its operating lifetime. After 10,000,000 pebbles were simulated, the resolution was increased by 0.01 cm and the process was repeated. The macro written to execute this simulation can be found in Appendix B.

The results of the numerical evaluation can be seen plotted on a log scale in Fig. 21. In the simulation, the resolution of the imaging system was increased in 0.1 cm increments from 0.0 cm.

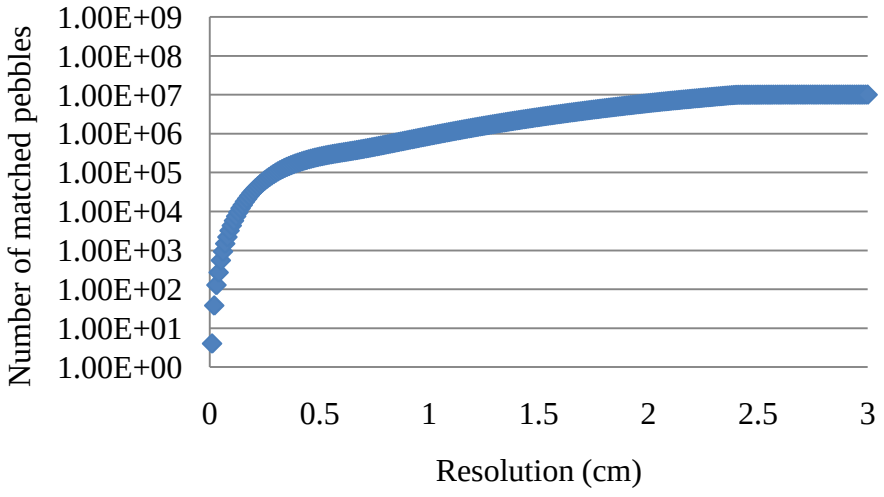

Fig. 21. Plot of the number of repeated pebbles calculated from the numerical simulation.

The calculate values for the simulation 0.3 cm (3000 micrometers) can be found in Appendix C. In this developed safeguards system concept, the ultrasound imaging system is expected to have a resolution less than 0.05 cm (500 micrometers). The simulation predicts there will be 551 pebbles that will be deemed matches to an initial image of a pebble in the lifetime of the reactor. Over the operating lifetime of the reactor, this would amount to 0.00551% of pebbles that may be misidentified. Albeit this value is very small, it will ultimately be decided by the respective safeguards agency implementing this concept that will decide if this is an acceptable risk. At the very least it is recommended that the number of microspheres be increased to 4 or 5, further increasing the uniqueness of each set of characteristic lengths. This number of repeated pebbles due to repeated line lengths could also be further reduced if an exterior reference point was introduced and each pebble was oriented in the same manner each time it was imaged.

In the results from the computer simulation, it can be seen that number of pebbles matched to the template pebble begins to increase immediately as the resolution of the system is increased. This is expected since the characteristic lengths, generated to represent the subsequent pebble images, were randomly generated in Microsoft Excel. As expected, the larger the resolution became, the larger the number of pebbles with characteristic lengths deemed matches to the initial set of characteristic lengths.

Upon review of the macro written for the simulation, the random numbers generated by Microsoft Excel used to generate a set of characteristic lengths are actually pseudorandom. These pseudorandom numbers are used to restrict the generated values of characteristic lengths to within the range of 0.1 to 4.9 cm. This limitation causes an inflation in the number of "randomly" generated sets of characteristic lengths that would be considered a match to the initial value of characteristic lengths.

4.6 Statistical Analysis Conclusions

The minimum number of microspheres necessary to identify at least 10,000,000 pebbles was determined to be two. However, to determine the location of these two

microspheres in an *x*, *y*, *z* coordinate system, a third reference point of known location is necessary. This limitation can be overcome by including a third microsphere and measuring the lengths between the three microspheres. This set of lengths was identified as the characteristic lengths used to uniquely identify each pebble. Comparing sets of characteristic lengths, it was shown that the determination can be made if two pebbles will randomly match.

To determine the number of pebbles that could be expected to have a repeated microsphere fingerprint, a simulation was run. In the simulation, sets of characteristic lengths were generated and compared to a "true" set of values. It was found that over the lifetime of the reactor, at a realistic resolution of 500 μm for an ultrasound imaging system, the total number of repeated pebbles will be less than 0.01% of pebbles. Well below a significant quantity for either LEU or Pu, this value can be further reduced by including more microspheres in each pebble or by orienting the pebbles the same way when imaged.

5. ASSESSMENT OF REACTOR SYSTEM RESPONSE TO MICROSPHERE INCLUSION

To determine how the use of the microspheres would affect the performance of a pebble-fueled HTGR, the South African-designed Pebble Bed Modular Reactor (PBMR) 400 was modeled using the Monte Carlo N-Particle Transport Code System Version 5.1 (MCNP).

Two types of models were developed: a model where the fuel pebble contained no zirconium microspheres and a model where the zirconium microspheres were placed in the fuel region of the pebble. An additional model was later created to determine effects of placement of zirconium microspheres in the non-fueled region of the pebble. Each model contained the same overall reactor design, only the fuel pebble was modified.

5.1 Overview of MCNP

A detailed description of MCNP and how the code is utilized can be found in *MCNP – A General Monte Carlo N-Particle Transport Code, Version 5 Volumes I and II*. MCNP is a general purpose transport code that uses the Monte Carlo method to simulate individual particle behavior within a modeled system. For each particle simulated, MCNP determines an average behavior. Using a set of average behaviors, MCNP infers the average behavior of all particles in the modeled system.[51]

The multiplication factor of a system can be defined as the measure of the increase or decrease in the neutron flux of a system. A system can be modeled as an infinite geometry, but at times a more accurate determination of the multiplication factor is needed for a realistic system that has a finite geometry. In these cases, k_{eff} is determined. For the models developed for this research, the effective multiplication factor (k_{eff}) was determined using MCNP. The effective multiplication factor (k_{eff}) accounts for neutrons that leak out of a finite system, providing a more complete

description of the neutron life cycle in the system. Mathematically expressed as a ratio of fission neutron in two subsequent genereations, k_{eff} is determined by:[52]

$$k_{eff} = \frac{(neutron\ production\ from\ fission\ in\ one\ generation)}{\left(\begin{matrix}neutron\ absorption\ in\\ preceeding\ generation\end{matrix}\right) + \left(\begin{matrix}neutron\ leakage\\ in\ preceeding\ generation\end{matrix}\right)} \qquad \text{Eq. (4)}$$

Using Eq. (4), the state of a reactor system can be determined. If k_{eff} is greater than 1, the reactor is considered supercritical. If k_{eff} is less than 1, the reactor is considered to be subcritical. If k_{eff} is equal to 1, the reactor system is considered to be critical.[52]

The MCNP models were also used to determine the impact of the microspheres on the temperature coefficient of reactivity (α_T). The temperature coefficient of reactivity is a measure of the change in the reactivity of the reactor system per degree change in the temperature of the reactor system. While there are many different temperature coefficients of reactivity, the moderator temperature coefficient of reactivity and the fuel temperature coefficient of reactivity have the most dominant effects on the reactor system. The temperature coefficient of reactivity can be negative or positive; however, a negative coefficient is preferred. A negative temperature coefficient means as the temperature of the reactor increases, the reactivity of the reactor system will decrease, reducing power. This self shutdown mechanism helps to prevent a "runaway" reactor that could lead to an accident.[52]

The temperature coefficient of reactivity can be calculated with Eq. (5) by determining k_{eff} for the same reactor system at two different temperatures and using:

$$\propto_T = \left(\frac{1}{\Delta T}\right)\left(\frac{\Delta k}{k_1 k_2}\right) \qquad \text{Eq. (5)}$$

5.2 Description of MCNP Model

5.2.1 Core Structure

The main structure of the reactor core is composed of three concentric circles. This structure can be seen in Figs. 22 and 23. The central cylinder of the reactor is composed of graphite. This cylinder is 2.0 m in diameter. Around the periphery of this central graphite column, there are nine equally spaced reserve shutdown system (RSS) channels, each 15.4 cm in diameter. These RSS channels extend the entire length of the reactor core and through the top and bottom reflectors. In the PBMR design, when the reactor is shutdown for long periods of time, and the core temperature is expected to fall below 100^{o}C, these channels are filled with 1 cm diameter borated graphite spheres.[53] In the MCNP models, these nine channels are filled with helium. The annular region created by the first two concentric circles is where the fuel pebbles reside. This region is 3.7 m in diameter. Outside of this annular core region, there is a graphite reflector that is 5.6 m in diameter. On the edge closest to the annular region, there are 24 equally spaced control rod channels, each 15.4 cm in diameter. Each control rod was withdrawn 1.85 m, the critical rod height for the model. These control rods are modeled as B_4C. On the outer edge of this graphite reflector region, there are 36 equally spaced helium gas rising channels, each 17.0 cm in diameter. The helium rising channels also extend the entire length of the reactor core and through the top and bottom reflectors. Also modeled was a 0.95 m thick slab of graphite reflector on the top and bottom of the reactor core. In total, the height of the reactor core in the model is 12.9 m.[53]

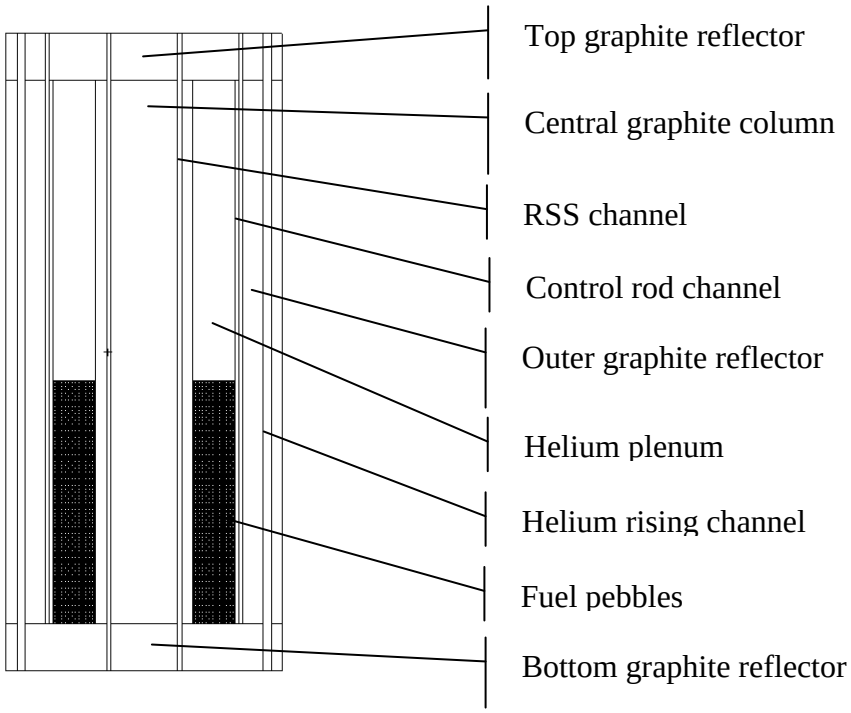

Fig. 22. Axial view of the modeled reactor core.

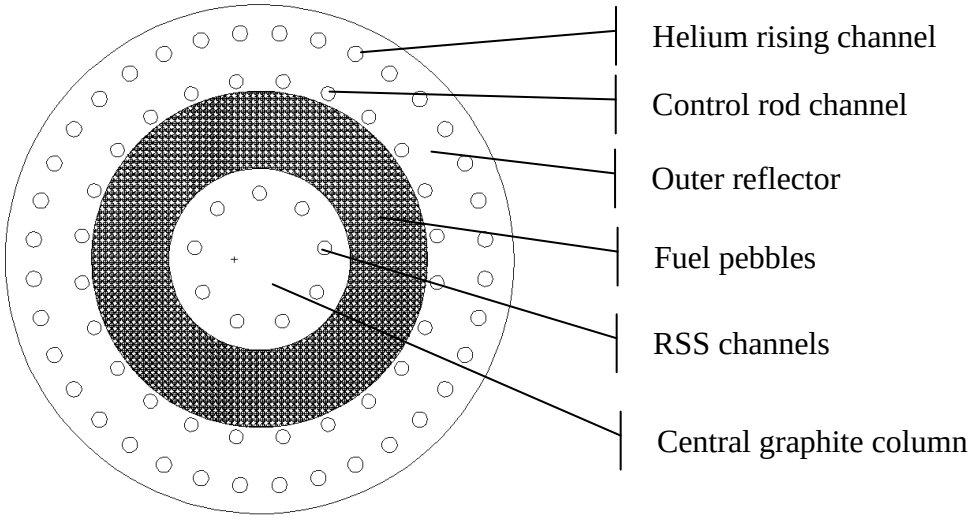

Fig. 23. Cross section of the modeled reactor core.

In Figs. 22 and 23 the central graphite column, outer graphite reflector, and top and bottom graphite reflectors have a density of 1.76 g/cm^3 and 2 ppm boron impurities. The helium coolant has a density of 0.01163 g/cm^3 at a pressure of 70 bar.[54] The control

material, B_4C, has a density of 2.50 g/cm^3.[47] The region filled with black lines represents the annular core that is occupied by approximately 450,000 fuel pebbles. This annular region is 11 m tall[10], with the fuel pebbles occupying 9.83 m. Above the fuel occupied region of the core is the helium plenum.

5.2.2 TRISO Particle

The TRISO particle modeled can be seen in Fig. 24. In each model, the TRISO particle is enriched to 5.7 wt % ^{235}U. This corresponds to the expected enrichment of the PBMR core when loaded with its initial load of fresh fuel.[20] Each TRISO particle is comprised of a fuel kernel with 0.5 mm diameter and density of 10.85 g/cm^3. The kernel is then covered in a 0.095 mm thick inner layer of porous carbon with a density of 0.98 g/cm^3. Next, there is a layer of pyrolytic carbon (IPyC) that is 0.04 mm thick with a density of 1.865 g/cm^3. Then there is a layer of silicon carbide that is 0.035 mm thick with a density of 3.20 g/cm^3. The silicon carbide is comprised of natural silicon with 92.23% ^{28}Si, 4.67% ^{29}Si, and 3.1% ^{30}Si. The outermost layer of the TRISO particle is pyrolytic carbon (OPyC) that is the same thickness and density as the IPyC layer. In total, the TRISO particle is 0.92 mm in diameter.[18, 55, 56]

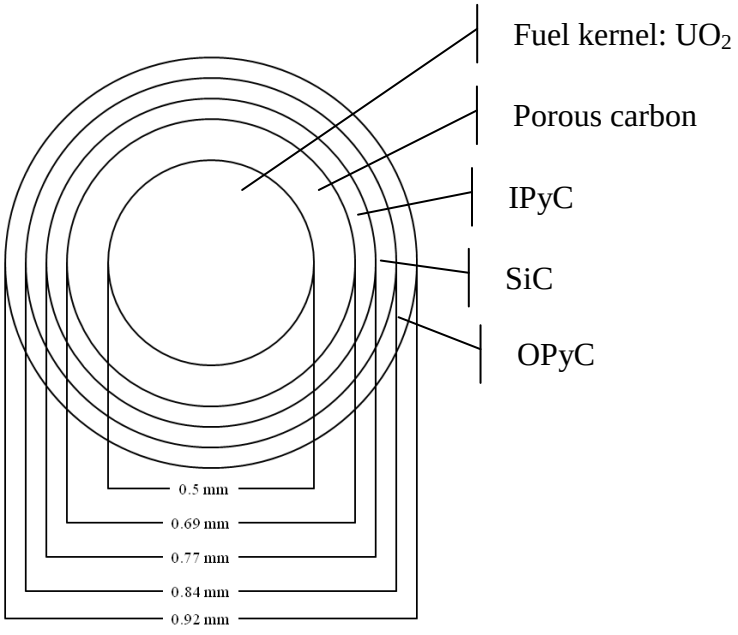

Fig. 24. Cross section view of the model TRISO particle.

5.2.3 Fuel Pebble with No Microspheres

The fuel pebble is made up of two regions, the inner fueled region which contains the TRISO particles, and the outer non-fueled region. The fueled region of the pebble is 5.0 cm in diameter and the non-fueled region is 0.5 cm thick. The fuel pebble model can be seen in Fig. 25. The graphite matrix that contains the TRISO particles and entirely comprises the non-fueled region of the pebble has a density of 1.76 g/cm^3 and a boron impurity of 2 ppm. The TRISO particles were modeled centered within an evenly spaced cubic lattice structure that represents approximately 15,000 TRISO particles.[57] In total, the TRISO particles occupy approximately 9.34% of the total volume of the fueled region. There is approximately 9.0 g of uranium in each fuel pebble. The input for this model can be found in Appendix D.

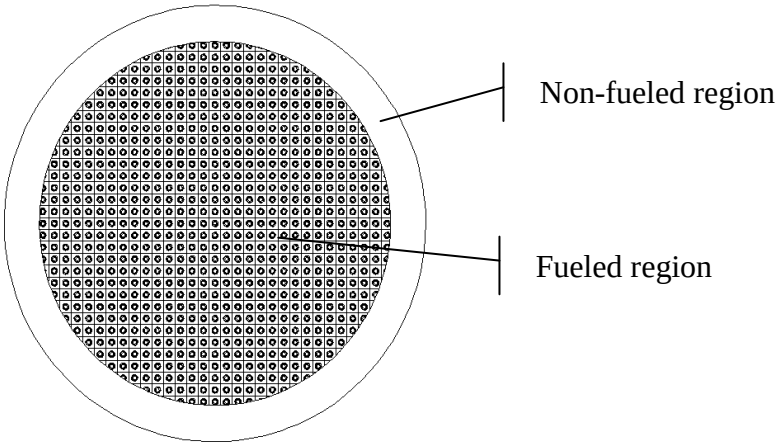

Fig. 25. Cross section view of the modeled fuel pebble.

5.2.4 Fuel Pebble with Microspheres

In the model with the microspheres in the fueled region, the microspheres were explicitly placed at random intersections of the TRISO lattice structure. An example of a pebble with microspheres in the fueled region can be seen in Fig. 26. Due to the nature of the pebble lattice structure, the microspheres were placed in the same position in each pebble in the core. This input file can be found in Appendix E.

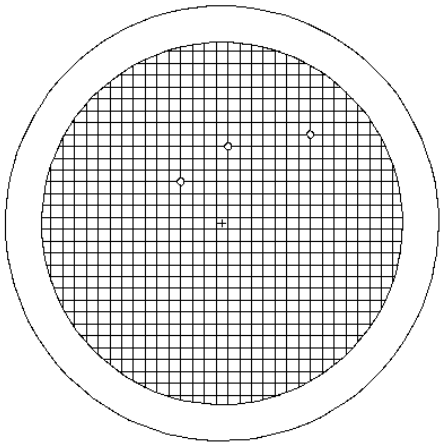

Fig. 26. Example of a pebble with microspheres in the fueled region (TRISO particles have been removed to better show placement of microspheres).

The microspheres used in the models are composed of zirconium oxide with 3% yttrium oxide (97% ZrO_2-3% Y_2O_3). The zirconium is natural zirconium containing 51.45% ^{90}Zr, 11.22% ^{91}Zr, 17.15% ^{92}Zr, 17.38% ^{94}Zr, and 2.8% ^{96}Zr. The 3% yttrium oxide is comprised of natural yttrium, ^{89}Y.[56]

5.2.5 Pebble Lattice Structure

In the actual reactor design, as pebbles are inserted into the PBMR core, each pebble is explicitly placed to achieve the best burnup. As the pebbles move toward the bottom of the reactor core, their movement is random. Within MCNP, this random packing cannot be explicitly modeled, however by placing the fuel pebbles in a body centered cubic (BCC) lattice structure, a 68% packing fraction can be achieved. This is close to the PBMR 61% average packing fraction.[57] This means a fuel pebble is located in the center of a cube such that in each of the eight corners of the cube, one eighth of the volume of a fuel pebble is also placed. This BCC lattice structure can be seen in Fig. 27. In all of the MCNP models, the core contained approximately 450,000 fuel pebbles.

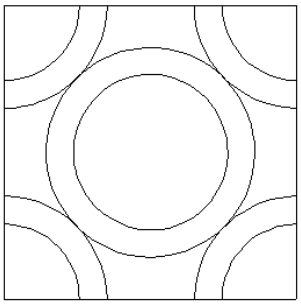

Fig. 27. BCC lattice structure created in modeled core (TRISO particles have been removed from fueled region).

5.2.6 Source Definition

For each model, the source point was placed inside a fuel kernel in an individual TRISO particle. Each model was run with 700 active cycles of 1000 particles each.

5.3 Results

Of interest in this neutronics analysis is the determination of the reactivity effects the 1 mm diameter microspheres will have on the reactor core and what impact this subsequent reactivity effect may have on the safety of the core, mainly the temperature coefficient of reactivity.

5.3.1 Impact of Microsphere Inclusion on Reactivity of Reactor System

To determine the reactivity effects of the microspheres, the effective multiplication factor (k_{eff}) was calculated by MCNP. Each model was at 300 K with the control rods withdrawn 1.85 m and RSS channels filled with helium. Models were created modeling 0 to 50 microspheres in the fueled region, in increments of five microspheres. The resulting k_{eff} was graphed with the standard deviation for each value, and the average k_{eff} for all models. The MCNP calculated k_{eff} values can be seen in Table II and graphed in Fig. 28.

Table II. MCNP calculated k_{eff} values for microspheres in the fueled region of pebble at 300 K.

	Microspheres in fueled region of pebble	
Number of Microspheres	k_{eff}	Standard deviation
0	1.00321	0.00095
5	1.00203	0.00098
10	1.00310	0.00098
15	1.00341	0.00100
20	1.00548	0.00097
25	1.00343	0.00100
30	1.00129	0.00098
35	1.00286	0.00099
40	1.00520	0.00103
45	1.00371	0.00097
50	1.00081	0.00098

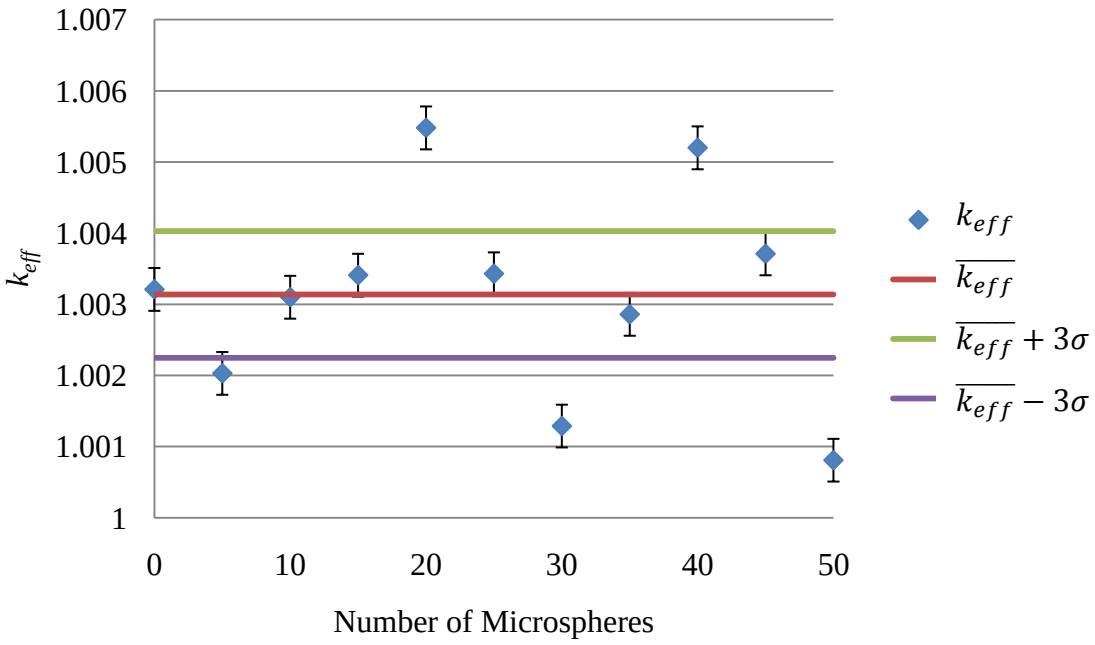

Fig. 28. Plot of k_{eff} with microspheres in the fueled region at 300 K.

With the microspheres in the fueled region of the pebble, the average k_{eff} at 300 K was 1.00313 ± 0.000297.

In order to determine the temperature coefficient of reactivity, the same models with 0 to 50 microspheres were used, but with the temperature of the entire reactor at 600 K. The density of the helium coolant was changed from 0.01163 g/cm^3 to 0.00553 g/cm^3 at 70 bar. It should be noted that the densities of other materials in the reactor were not changed and subsequently, thermal expansion of the materials has not been accounted for in the models. The MCNP calculated k_{eff} values can be seen in Table III and graphed in Fig. 29.

Table III. MCNP calculated k_{eff} with microspheres in the fueled region of the pebble at 600 K.

	Microspheres in fueled region of pebble	
Number of Microspheres	k_{eff}	Standard deviation
0	0.97045	0.00097
5	0.97223	0.00103
10	0.97330	0.00097
15	0.97013	0.00100
20	0.97110	0.00093
25	0.97237	0.00100
30	0.97109	0.00095
35	0.97080	0.00095
40	0.97246	0.00099
45	0.97057	0.00096
50	0.97298	0.00096

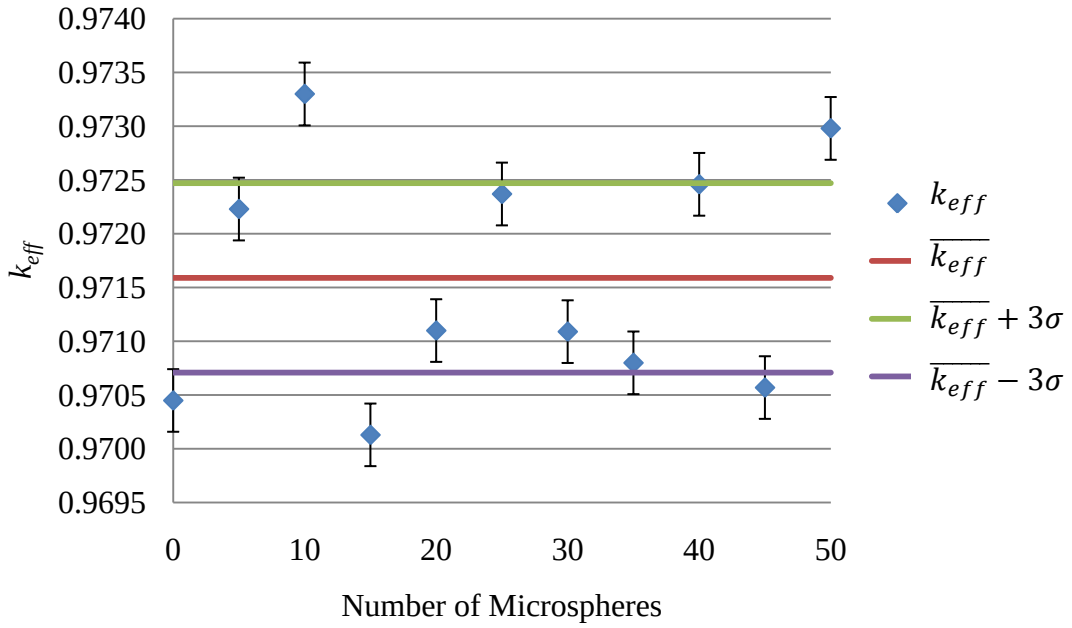

Fig. 29. Plot of k_{eff} with microspheres in the fueled region at 600 K.

With the microspheres in the fueled region of the pebble, the average k_{eff} at 600 K was 0.97159 ± 0.000294.

From the results obtained, it is clear that there is no discernable trend in k_{eff} with an increasing quantity of microspheres. At 300 K, with no microspheres in the pebble, k_{eff} was determined to be 1.00321 ± 0.00095 and with 50 microspheres in the pebble k_{eff} was determined to be 1.00081 ± 0.00098. With no microspheres in the pebble at 600 K, k_{eff} was determined to be 0.97045 ± 0.00097 and with 50 microspheres in the pebble k_{eff} was determined to be 0.97298 ± 0.00096. When compared to the overall average k_{eff} of all models, each k_{eff} is within, or very close to within, three standard deviations of the average. Since no quantity of microspheres resulted in a k_{eff} that fell well outside of the average, from these results it can be concluded that the inclusion of 1 mm diameter ZrO_2 microspheres is not statistically significant, thus having no impact on the reactivity of the reactor system.

5.3.2 Impact of Microsphere Inclusion on Temperature Coefficient of Reactivity

Now that k_{eff} at each interval of microspheres has been determined at two temperatures, Eq. (5) can be used to calculate the temperature coefficient of reactivity (α_T) at each interval. The results of this calculation for microspheres in the fueled region of the pebble can be seen in Table IV and graphed in Fig. 30.

Table IV. Calculated α_T with microspheres in the fueled and non-fueled regions of pebble.

	Microspheres in fueled region of pebble	
Number of Microspheres	α_T ($\Delta k/k/^oC$)	Uncertainty
0	-0.000112	0.000005
5	-0.000102	0.000005
10	-0.000102	0.000005
15	-0.000114	0.000005
20	-0.000117	0.000005
25	-0.000106	0.000005
30	-0.000104	0.000005
35	-0.000110	0.000005
40	-0.000112	0.000005
45	-0.000113	0.000005
50	-0.000095	0.000005

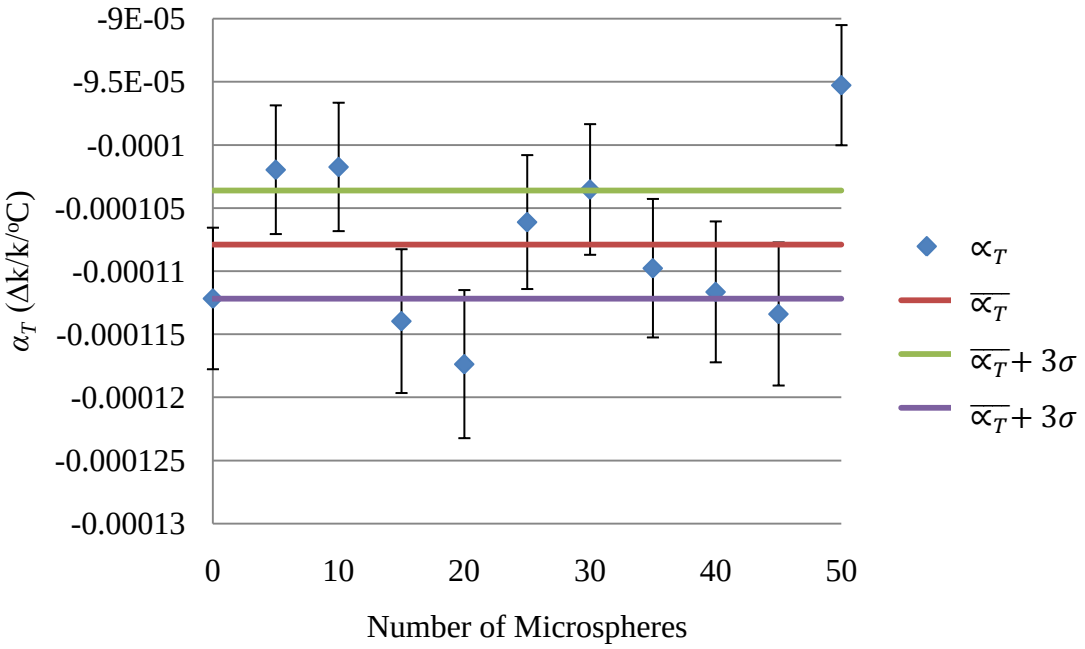

Fig. 30. Plot of α_T with microspheres in the fueled region.

For microspheres in the fueled region, the average temperature coefficient of reactivity was calculated to be -0.000108 ± 0.000001 Δk/k/^{o}C.

With no microspheres present, α_T was calculated to be 0.000112 ± 0.000005 and with 50 microspheres present α_T was calculated to be -0.000095 ± 0.000005. These results confirm that the pebble-fueled HTGR model has the desired negative temperature coefficient of reactivity. Like the impact of the microspheres on k_{eff}, for each interval of microspheres, when compared to the average, the calculated temperature coefficient of reactivity fell within statistical variance essentially showing no change with the inclusion of the microspheres. With no discernable trend in this data, it can be concluded that the inclusion of 1 mm diameter ZrO_2 microspheres would not impact the temperature coefficient of reactivity.

5.3.3 Placement of Microspheres in the Non-Fueled Region

The impact of microspheres placed in the non-fueled region of the pebble was also considered. An example of a pebble with microspheres in the non-fueled region can be seen in Fig. 31. This input can be found in Appendix F.

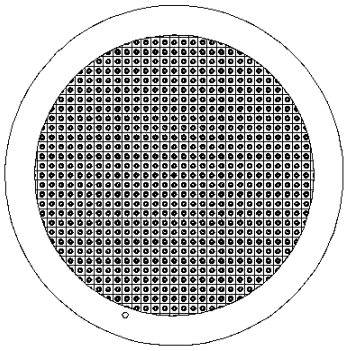

Fig. 31. Example of a pebble with microspheres in the non-fueled region.

These models were simulated under the same conditions as the models with the microspheres in the fueled region. Models were at 300 K and 600 K with the control rods withdrawn 1.85 m and RSS channels filled with helium. In 600 K models, helium density was adjusted to 0.00553 g/cm^3 at 70 bar. Thus, thermal expansion of other materials was not accounted for in these results. The MCNP calculated k_{eff} values can be seen in Table V and graphed in Figs. 32 and 33.

Table V. MCNP calculated k_{eff} values for microspheres in non-fueled regions of pebble at 300 K and 600 K.

	Microspheres in nonfueled region of pebble at 300 K		Microspheres in nonfueled region of pebble at 600 K	
Number of Microspheres	k_{eff}	Standard deviation	k_{eff}	Standard deviation
0	1.00321	0.00095	0.97045	0.00097
5	1.00345	0.00098	0.97182	0.00094
10	1.00366	0.00098	0.97153	0.00100
15	1.00390	0.00096	0.97152	0.00095
20	1.00252	0.00099	0.97030	0.00098
25	1.00227	0.00102	0.97301	0.00095
30	1.00392	0.00104	0.97125	0.00096
35	1.00265	0.00098	0.97140	0.00099
40	1.00422	0.00098	0.97415	0.00099
45	1.00196	0.00097	0.97127	0.00100
50	1.00273	0.00101	0.97249	0.00095

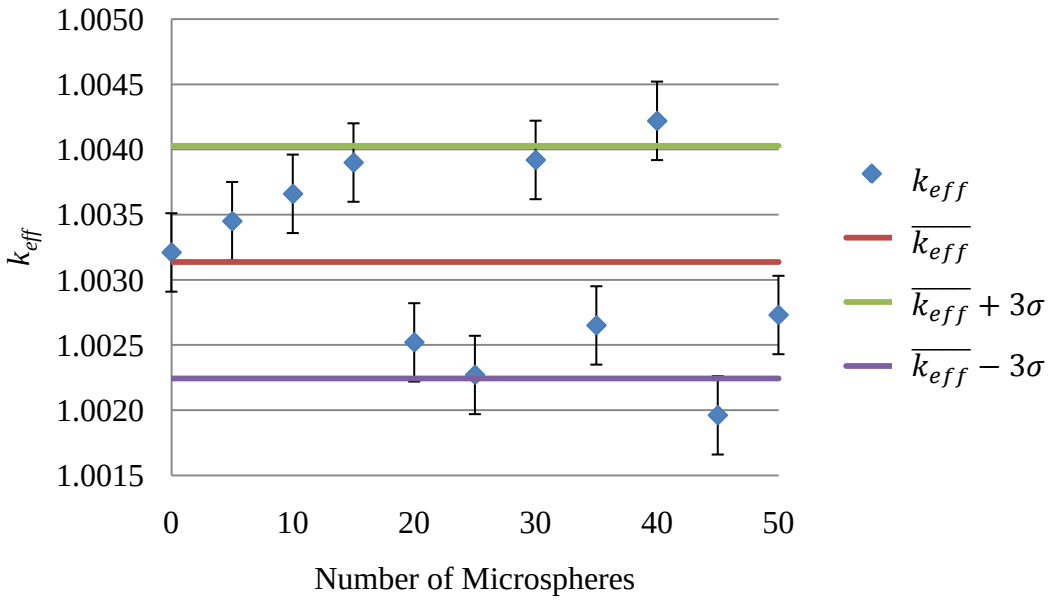

Fig. 32. Plot of k_{eff} with microspheres in the non-fueled region at 300 K.

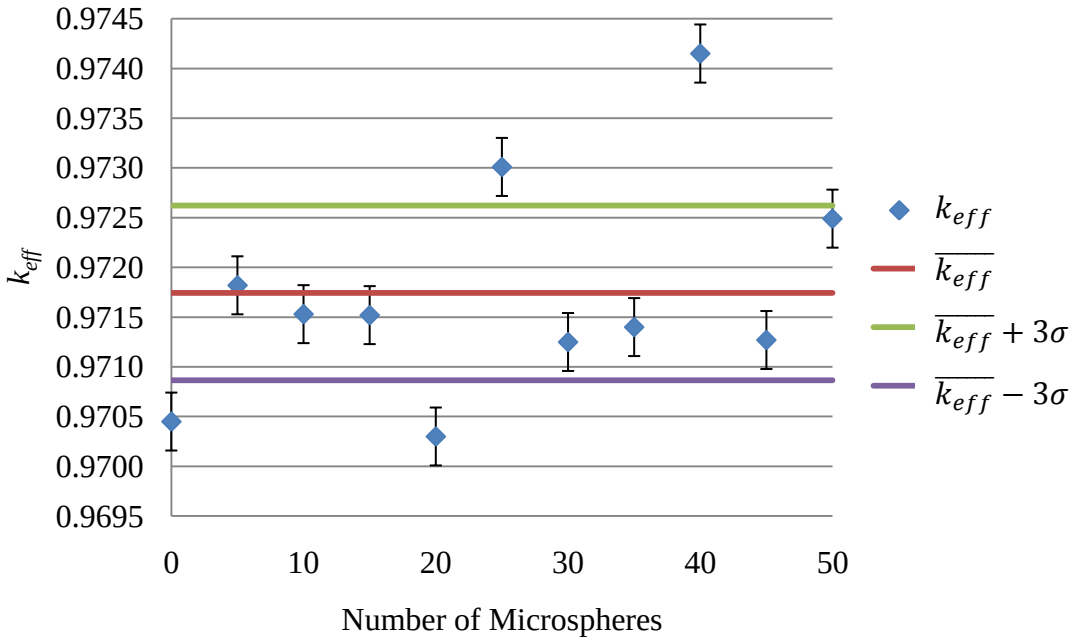

Fig. 33. Plot of k_{eff} with microspheres in the non-fueled region at 600 K.

When the microspheres were present in the non-fueled region of the pebble at 300 K, the average k_{eff} was 1.00314 ± 0.000298. At 600 K, the average k_{eff} was 0.97175 ± 0.000293.

The temperature coefficient of reactivity was again calculated using Eq. (5). The calculated results can be seen in Table VI and graphed in Fig. 34.

Table VI. Calculated α_T with microspheres in the fueled and non-fueled regions of pebble.

	Microspheres in nonfueled region of pebble	
Number of Microspheres	α_T ($\Delta k/k/^oC$)	Uncertainty
0	-0.000112	0.000005
5	-0.000108	0.000005
10	-0.000110	0.000005
15	-0.000111	0.000005
20	-0.000110	0.000005
25	-0.000100	0.000005
30	-0.000112	0.000005
35	-0.000107	0.000005
40	-0.000102	0.000005
45	-0.000105	0.000005
50	-0.000103	0.000005

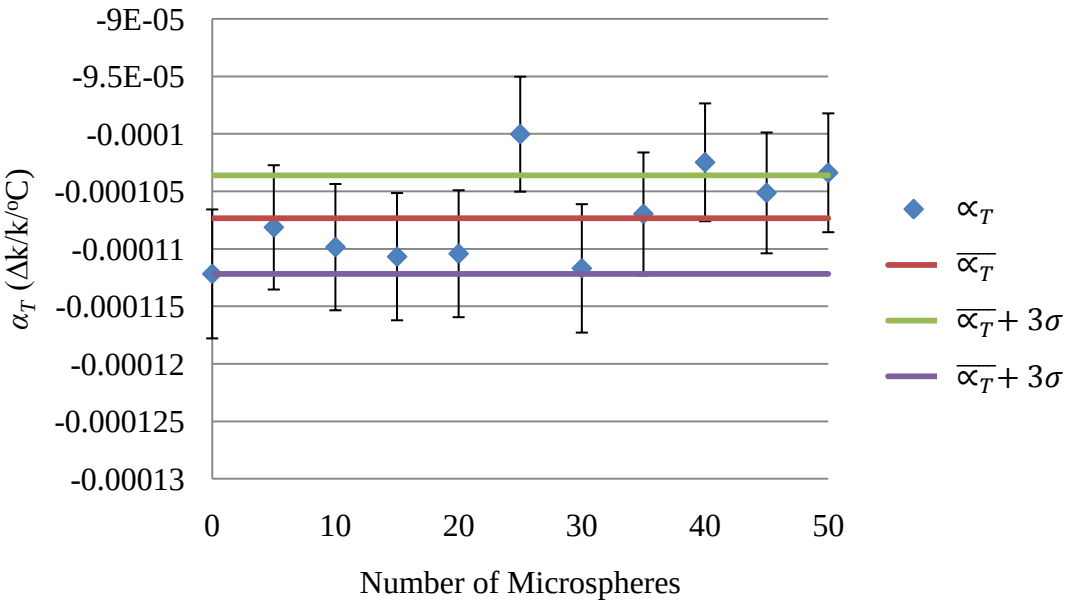

Fig. 34. Plot of α_T with microspheres in the non-fueled region.

The average temperature coefficient of reactivity for microspheres in the non-fueled region was -0.000107 ± 0.000001 $\Delta k/k/^{o}C$.

Like microsphere placement in the fueled region, inclusion of 1 mm ZrO_2 microspheres in the non-fueled region of the pebble had no discernable impact on the reactivity or the temperature coefficient of reactivity of the modeled reactor.

5.3.4 Identifying a Trend

Since no trend was seen in the results with a 1 mm microsphere, additional models were created with larger microspheres to determine if the microspheres would have any effect on k_{eff}. Models were created that contained 2 mm, 3 mm, and 4 mm microspheres in the non-fueled region of the pebble. These microspheres could only be placed in the non-fueled region because placement in the fueled region would have required removal of fuel material in the model. Maintaining the same amount of fuel in the pebble is key to ensuring that this safeguards concept does not negatively impact the reactor design. Again, models were created that contained 0 to 50 microspheres in increments of 5 microspheres at 300 K. The calculated k_{eff} results for 1 mm, 2 mm, 3 mm, and 4 mm microspheres in the non-fueled region of the pebble can be seen in Table VII and plotted in Fig. 35.

Table VII. MCNP calculated k_{eff} with various diameters of microspheres in the non-fueled region of pebble at 300 K.

	1 mm microsphere		2 mm microsphere	
Number of Microspheres	k_{eff}	Standard deviation	k_{eff}	Standard deviation
0	1.00321	0.00095	1.00321	0.00095
5	1.00345	0.00098	1.00168	0.00100
10	1.00366	0.00098	1.00393	0.00094
15	1.00390	0.00096	1.00207	0.00095
20	1.00252	0.00099	0.99966	0.00093
25	1.00227	0.00102	1.00190	0.00100
30	1.00392	0.00104	1.00238	0.00096
35	1.00265	0.00098	1.00143	0.00098
40	1.00422	0.00098	1.00332	0.00099
45	1.00196	0.00097	1.00111	0.00099
50	1.00273	0.00101	1.00207	0.00100
	3 mm microsphere		4 mm microsphere	
Number of Microspheres	k_{eff}	Standard deviation	k_{eff}	Standard deviation
0	1.00321	0.00095	1.00321	0.00095
5	1.00142	0.00099	0.99959	0.00102
10	1.00165	0.00095	0.99821	0.00099
15	1.00100	0.00098	0.99631	0.00101
20	0.99846	0.00100	0.99829	0.00098
25	1.00024	0.00100	0.99758	0.00099
30	1.00046	0.00102	0.99618	0.00097
35	1.00006	0.00100	0.99161	0.00097
40	0.99832	0.00099	0.99135	0.00099
45	0.99620	0.00100	0.98974	0.00099
50	0.99787	0.00097	0.98832	0.00094

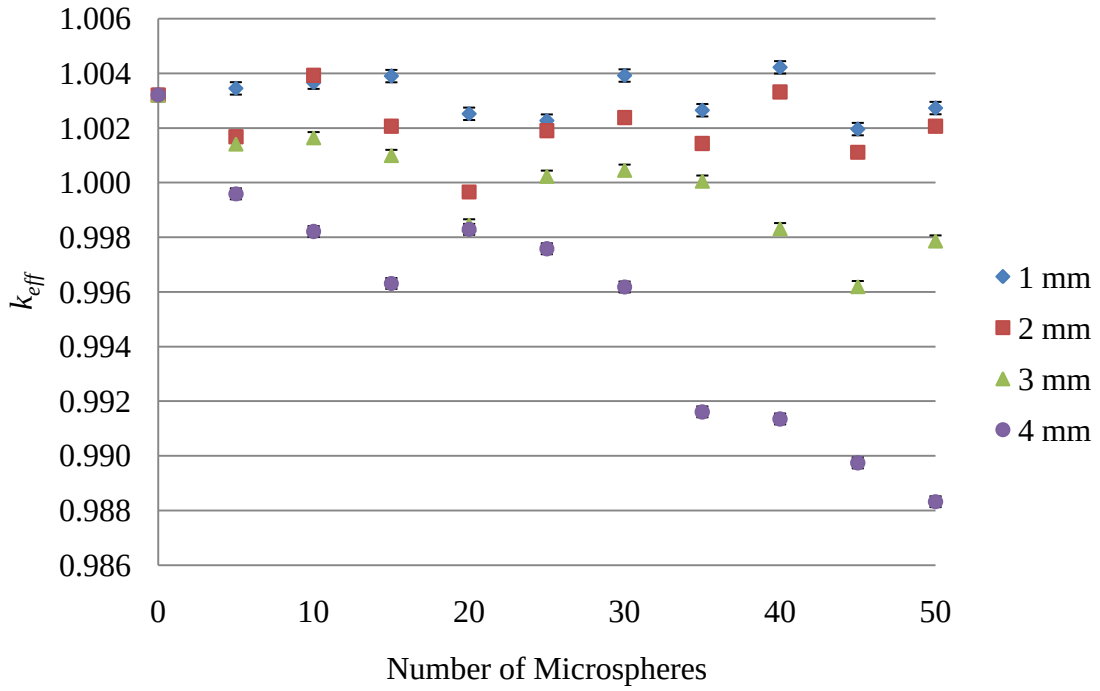

Fig. 35. Plot of k_{eff} with various diameters of microspheres in the non-fueled region at 300 K.

From these results it is possible to see that as an increasing quantity of larger diameter microspheres are placed in the non-fueled region of the pebble, k_{eff} is reduced. This can be attributed to the increasing amount of graphite that is removed as larger microspheres are added to the non-fueled region. This graphite that encases each TRISO particle and each pebble acts as a local reflector and moderator for neutrons created in the fuel kernel and those that escape the pebble. As the graphite material is removed, more neutrons are allowed to escape the system and interact with materials that are not fissionable. The resulting impact on the temperature coefficient of reactivity was not calculated because it can be reasonably expected that at 600 K there will be a decrease in k_{eff} as microsphere diameter increases. This would subsequently result in a negative trend in the temperature coefficient of reactivity.

5.4 Reactor Response Conclusions

By developing a reactor model in MCNP, it was possible to determine what impact inclusion of ZrO_2 microspheres would have on the reactivity of the reactor (k_{eff}), as well as their impact on the temperature coefficient of reactivity of the reactor (α_T). When the k_{eff} for each model is compared to the average k_{eff} all of the models, inclusion of the 1 mm ZrO_2 microspheres was found to be statistically insignificant. From the obtained k_{eff} values, α_T was calculated. Again, the inclusion of 1 mm ZrO_2 was found to be insignificant. When the microspheres were moved to the non-fueled region of the pebble, their impact on k_{eff} and α_T was again found to be insignificant. A trend in k_{eff} in the models that contained microspheres was found when the size of the microspheres was increased. It was found that as the size of the microspheres increased, the increasing amount of graphite reflector and moderator removed would eventually have a negative impact on k_{eff}, reducing system reactivity. While this model was not benchmarked to standard PBMR models, by addressing the relative change in k_{eff} and α_T due to microsphere inclusion it can be concluded that inclusion of less than fifty 1 mm ZrO_2 microspheres will have no impact on the reactivity or the temperature coefficient of reactivity of the pebble-fueled HTGR.

6. EVALUATION OF ULTRASOUND IMAGING SYSTEM

The transmission characteristics of ultrasound waves through graphite are unknown. A proof-of-concept experiment was developed to determine the effectiveness of ultrasound in imaging the microspheres.

Two samples were created that contained a known number of 1 mm ZrO_2-Y_2O_3 microspheres. Using an ultrasound imaging system, an image of the configuration of the microspheres was taken. To determine the effectiveness of ultrasound wave transmission through graphite, two graphite plates of 1 mm and 5 mm thickness were placed on top of the samples. The 5 mm thick graphite plate corresponds to the thickness of the non-fueled region of the pebble. Images of the microsphere fingerprint were again acquired using the ultrasound imaging system. The resulting image was then compared to either a visual photograph of the configuration or previous ultrasound image to determine if all the microspheres could be accounted for.

6.1 Equipment

The ultrasound imaging system used was an Ultrasonix Sonix RP System. The energy range of operation for the system is 4.8 to 14 MHz. This system has a 3.8 cm long transducer with a 1 mm wide ultrasound beam. The beam can be moved into 128 elements to produce 128 lines.

6.2 Experimental Procedure

For the first sample, or phantom, a base layer of gelatin was created. This layer was created from 156 g of water containing 5.1 g (approximately 3%) of Porcine skin gelatin type A. The gelatin was allowed to semi-firm. Next, twenty 97% ZrO_2-3% Y_2O_3 microspheres were randomly dispersed on top of this layer of gelatin. Then, an additional layer of gelatin was poured over the microspheres and previous layer of gelatin. This layer was comprised of approximately the same composition of water and gelatin as the base layer. The entire sample was then allowed to completely firm.

A second phantom was created using the same procedure as above, but this phantom was created with approximately 5% gelatin and approximately 3% of the additive agar. Agar is a common thickener and impurity added when imaging phantoms of biological material. It mimics the noise expected in biological material. In this application, the agar was added to increase the noise in the image. If the microspheres were not visible among this low level "biological" noise that was still closer to a liquid than a solid material, it could be concluded that imaging would not be possible in a solid inorganic sphere.

Each phantom was removed from its plastic mold, placed on top of a 1 cm thick rubber mat, and the frequency used for imaging was 10 MHz. To image the phantoms, the transducer was placed perpendicular to the plane containing the microspheres. The transducer was then moved across the plane until all of the microspheres had been passed. This placement is depicted in Fig. 36.

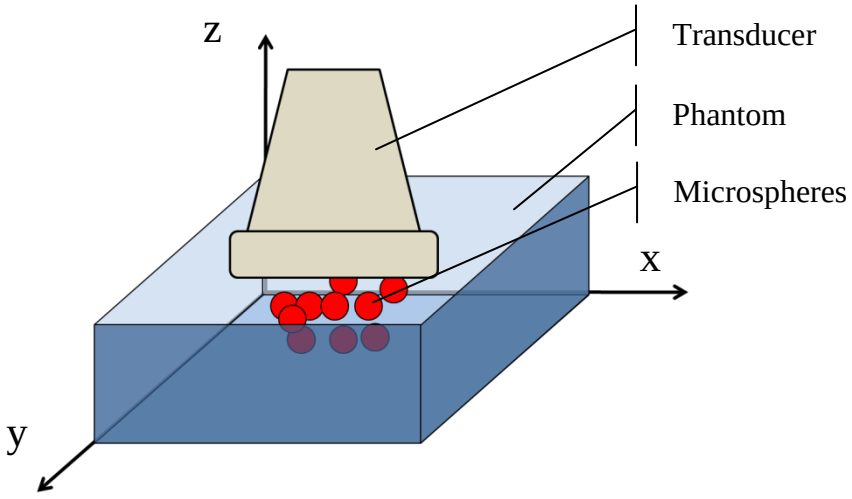

Fig. 36. Placement of ultrasound transducer on phantom containing microspheres.

By moving the transducer in this manner, an image of each the *xz*-, *yz*-, and *xy*-planes is a produced. The system software is then capable of generating a three-dimensional (3D) image of the microspheres.

6.3 Results[4]

6.3.1 Non-Agar Sample

Photographs of the non-agar sample can be seen in Figs. 37 and 38. Following the axis orientation in Fig. 36, the resulting *xz*-, *yz*-, and *xy*-plane images can be seen in Fig. 39.

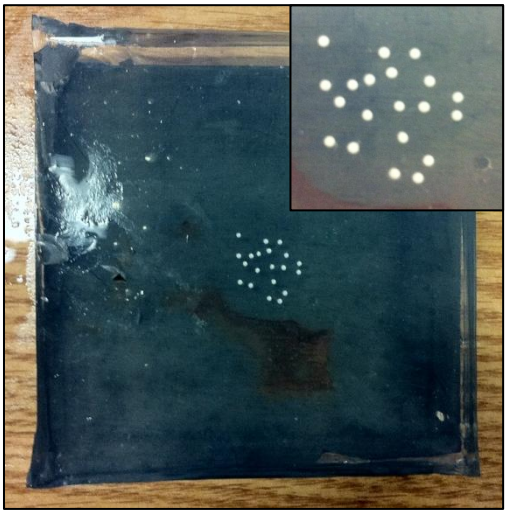

Fig. 37. Axial image of the non-agar phantom, showing placement of microspheres. Insert is a close up of microspheres.

Fig. 38. Cross section image of the non-agar phantom, showing placement of microspheres.

[4] It is important to note that all images presented as part of these results were filtered using the Ultrasonix Sonix RP System. After the images were taken off the system, no manipulation other than cropping and orientation was performed on the images.

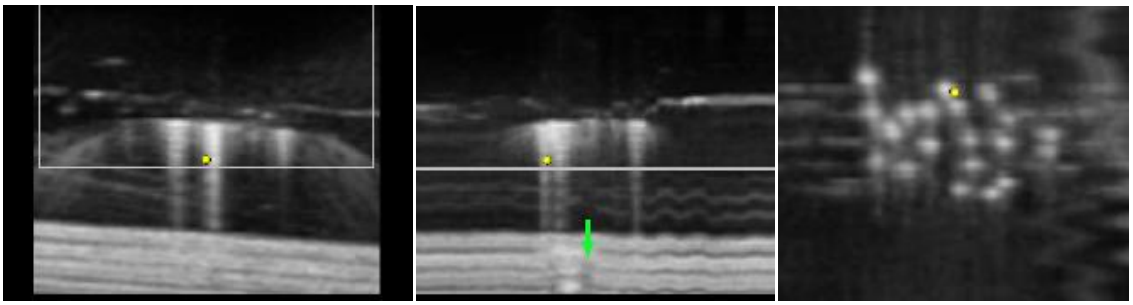

(a) (b) (c)

Fig. 39. Ultrasound images of (a) *xz*-plane (b) *yz*-plane (c) *xy*-plane produced in 3D imaging mode. The yellow dot and green arrow are produced by the imaging software and do not represent characteristics of the microsphere fingerprint.

In Figs. 39 (a) and (b) the microspheres lie parallel to the imaging plane. The *xy*-plane image seen in Fig. 39 (c) clearly shows the twenty microspheres suspended in the gelatin. A side-by-side comparison of the *xy*-plane image in Fig. 39 with the configuration shown in Fig. 37 can be seen in Fig. 40.

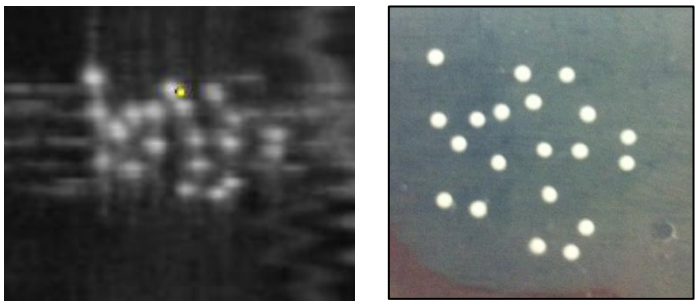

Fig. 40. Side-by-side comparison of ultrasound produced microsphere placement in *xz*-plane (left) and microsphere placement seen in initial image (right).

The distortion in the ultrasound image can be attributed to the speed at which the transducer is moved by the operator across the area containing microspheres. The system captures 128 frames, 1 mm wide, as the transducer is moved across the area with the microspheres. The faster the transducer is moved, the 1 mm slices are taken further apart, capturing less of each microsphere. The slower the image moved, the slices are closer, together or maybe even overlapping, stretching the appearance of the

microspheres. Depicted in Fig. 41 is the principle is when the transducer is moved too quickly.

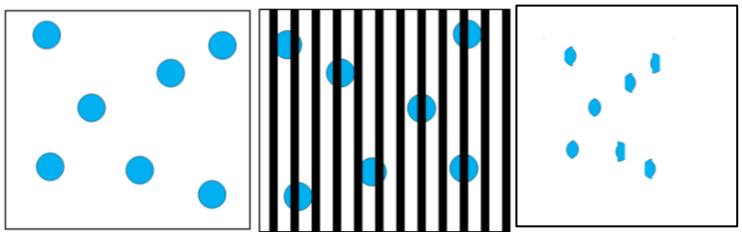

(a) (b) (c)

Fig. 41. When the transducer is moved too quickly in 3D imaging mode, (a) the original configuration can be distorted. This occurs when ultrasound beam is transmitted, missing some areas blacked-out in (b). Once reconstructed, (c) the resulting image has a distorted configuration.

As can be seen in side-by-side comparison of the system rendered 3D image in Fig. 42, all twenty microspheres that were suspended in the non-agar phantom are visible. This image was manually filtered using the ultrasound system to obtain the best image possible.

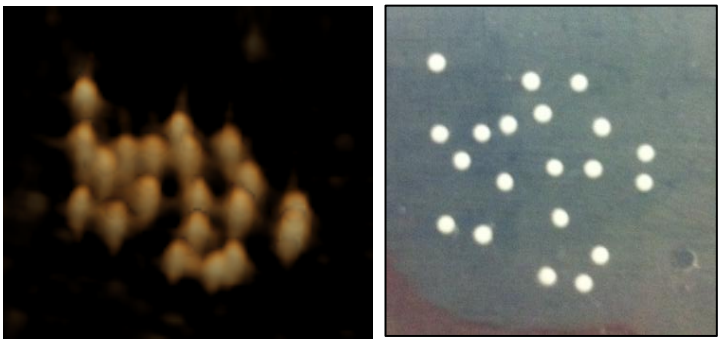

Fig. 42. Side-by-side comparison of ultrasound produced microsphere placement in 3D rendered image (left) of non-agar phantom , with no graphite plates, and microsphere placement seen in initial image (right).

Following these results, next a 1 mm thick graphite plate was placed on top of the phantom. This layout can be graphically depicted in Fig. 43. A thin layer of water was placed between the graphite and phantom and the graphite and transducer to act as a

buffer medium. The manually filtered 3D rendered image of this setup can be seen in Fig. 44. All twenty microspheres were identified in Fig. 44 (a).

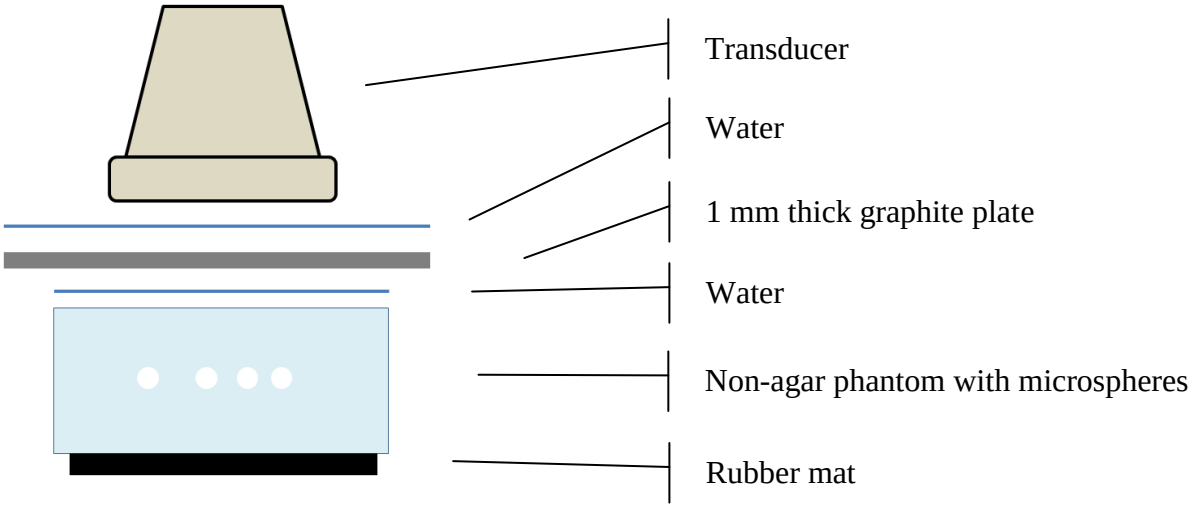

Fig. 43. Arrangement of transducer, graphite, phantom, and rubber mat for imaging.

An issue with the use of the water buffer was the non-uniform thickness of the water layer. As the transducer was moved across the phantom, in some areas air bubbles were may have crossed the imaging plane. As mentioned in Section 3.2.3, ultrasound wave transmission in gases is greatly reduced. This transmission reduction will result in distortions in the resulting image. Air bubbles could have been introduced at several steps during the experiment like preparation of the phantom. However, since these distortions were not apparent in the 3D rendered image the phantom without graphite, it is likely that the air was introduced in one of the layers of the water buffer. For example, if the graphite was shifted or lifted, air could be trapped in the water buffer between the graphite and phantom. Suspected air bubble distortions in Fig. 44 (a) have been marked in Fig. 45.

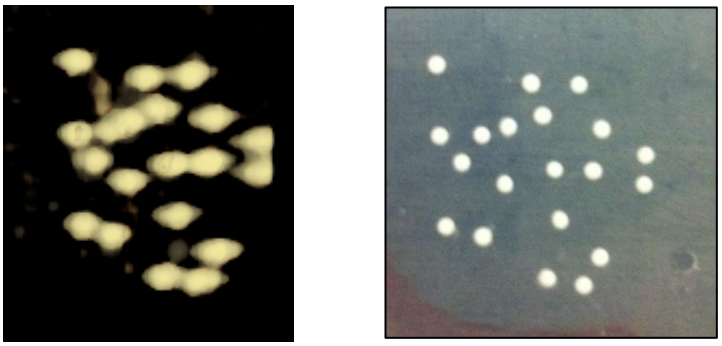

(a) (b)

Fig. 44. Side-by-side comparison of ultrasound produced microsphere placement in 3D rendered image (left) of non-agar sample, with 1 mm thick graphite plate, and microsphere placement seen in initial image (right).

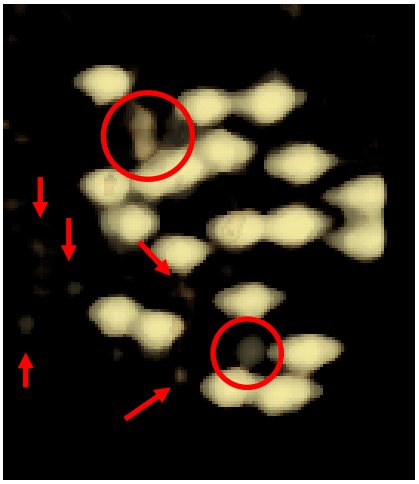

Fig. 45. Distortions produced in 3D image (marked by red arrows and circles) suspected to be caused by air bubbles in path of transducer.

In an attempt to produce a clearer image, the water buffer between the transducer and graphite was replaced with ultrasound gel. The manually filtered 3D rendered image using this setup can be seen in Fig. 46.

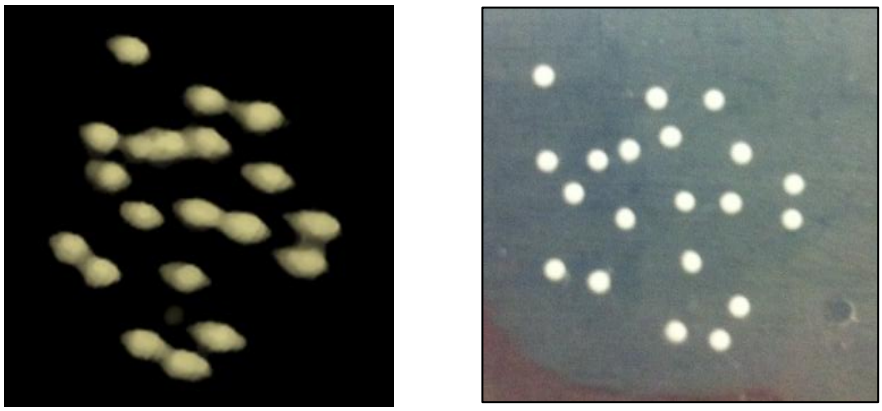

Fig. 46. Side-by-side comparison of ultrasound produced microsphere placement in 3D rendered image (left) of non-agar sample, through 1 mm thick graphite plate with ultrasound gel buffer between transducer and graphite plate. Image on right is microsphere placement seen in initial image.

In the left image of Fig. 46, all twenty microspheres were identified and there are no viewable distortions that can be attributed to air bubbles. As such, for the remainder of the experiment, ultrasound gel was used as the buffer between the transducer and graphite.

Next, the 1 mm thick graphite plate was removed and replaced with a 5 mm thick plate. The resulting 3D rendered image can be seen in Fig. 47.

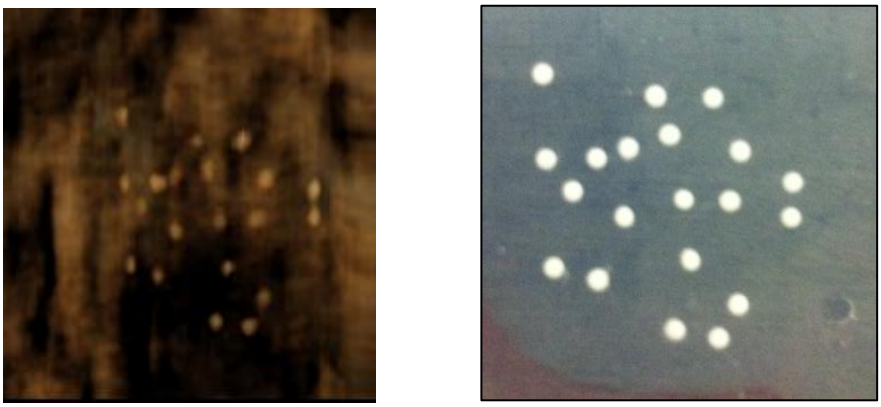

Fig. 47. Side-by-side comparison of ultrasound produced microsphere placement in 3D rendered image (left) of non-agar sample, through 5 mm thick graphite plate with ultrasound gel buffer between transducer and graphite plate. Image on right is microsphere placement seen in initial image.

In Fig. 47, all twenty microspheres can be identified in the 3D rendered image. However, as can been seen, there is a large distortion across the entirety of the image. This distortion is due to large air bubbles in the ultrasound gel.

6.3.2 Agar Sample

A close-up picture of the agar phantom with the microspheres can be seen in Fig. 48. The cloudy appearance of the phantom prevented visual confirmation of the microsphere configuration before images were taken. To overcome this, the agar phantom was imaged without a graphite plate. A side-by-side comparison of this image and the 3D rendered image taken through the 5 mm graphite plate can be seen in Fig. 49.

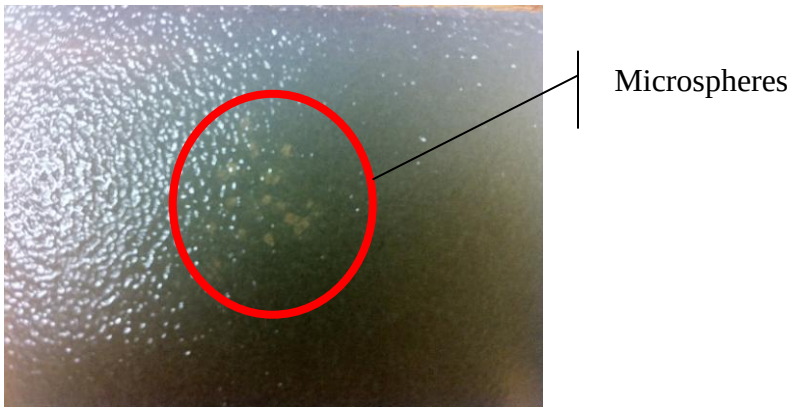

Fig. 48. Close-up photo of agar containing sample with microsphere placement highlighted by red circle.

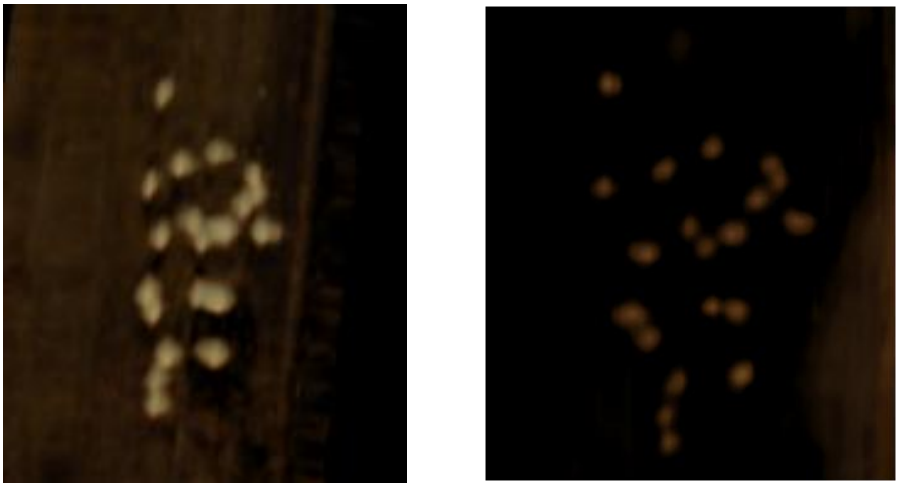

Fig. 49. Side-by-side comparison of ultrasound produced microsphere placement in 3D rendered image (left) of agar sample, through 5 mm thick graphite plate with ultrasound gel buffer between transducer and graphite plate. Image on right is microsphere placement in 3D rendered image of sample phantom without 5 mm thick graphite plate.

Comparing the two resulting images, it is possible to discern twenty microspheres. The layout with the 5 mm thick graphite plate provides better clarity than the sample without the graphite plate. However, the microspheres in Fig. 49 (b) appear smaller than those in Fig. 49 (a). Due to the lack of clarity in the image with no graphite plate, and the lack of a pre-imaging visual confirmation of the configuration, it cannot be stated that these images show the *true* configuration of microspheres placed in the agar sample.

6.3.3 Determination of Ultrasound System Resolution

Using the images in Fig. 40 it is possible to determine an approximate resolution of the ultrasound system. In the initial photograph of the non-agar sample, it is known that the microspheres each have a nominal 1 mm diameter. By measuring the distance between the microspheres positioned closely together in the initial image and comparing that to the respective distance in the ultrasound image, it is possible to gauge the ability of the ultrasound system to discern between two microspheres. Circled in Fig. 50 are the microspheres used to determine this resolution.

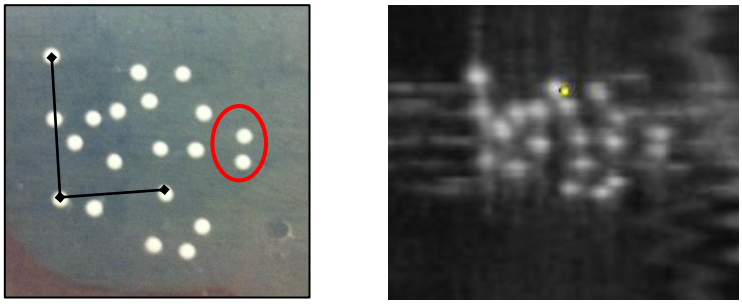

Fig. 50. Comparison of initial image and ultrasound image and microspheres used to approximate a resolution for the imaging system.

For the two microspheres in the initial image, the distance between the centers of the microspheres was determined to be approximately 1.4 mm. To determine the distance between these two microspheres in the ultrasound image, the distortion associated with the translation speed of the transducer had to be accounted for. This was done by calculating the percent difference between the line lengths connecting the centers of microspheres approximately in direct line of each other. The microspheres used for this purpose are connected by lines in Fig. 50. From this it was determined that the microsphere fingerprint in the ultrasound image appears 25% larger horizontally and 22% smaller vertically than the initial image. Accounting for this distortion, the distance between the two microspheres was measured to be approximately 1 mm. This means, that the imaging system is capable of determining microsphere position to within 0.4 mm (400 microns).

6.4 Ultrasound Imaging Conclusions

The experiment developed tested the effectiveness of ultrasound imaging of the ZrO_2 microspheres through graphite plates of two thicknesses, 1 mm and 5 mm. It was found that a configuration of microspheres is visible through graphite when the microspheres are suspended in a gelatin phantom and a gelatin phantom that contained the noise additive agar.

Some limitation to the use of ultrasound was found in this experimental setup. Near-liquid state gelatin and ultrasound gel have a tendency to form air bubbles during

the fabrication and imaging processes. As such, the transmission of the ultrasound waves through these air bubbles is hindered, reducing image quality and producing distortions that can be misinterpreted as microspheres.

This experiment showed that ultrasound imaging of a microsphere configuration through thin graphite plates is possible. The resolution of the system was determined to be approximately 0.04 cm. However, it cannot be conclusively stated that an ultrasound system can or cannot image a microsphere configuration in a spherical pebble. Focus must be placed on the limited scope of the experiment. These results are of ultrasound imaging of microspheres *through* graphite, not ultrasound imaging of microspheres *embedded* in graphite. Also, this experiment imaged samples that only contained microspheres. In reality, the microspheres will be dispersed among TRISO particles. Thus, additional work must be performed to certify the use of an ultrasound system to image placement of microspheres in a fuel pebble.

7. CONCLUSIONS

To deter and detect the diversion of nuclear material, nuclear facilities must be safeguarded. As new types of nuclear facilities are designed and built, the IAEA must address the challenges associated with safeguarding the design against diversion. The pebble-fueled HTGR is not a new reactor design. However, the recent developments in the design by the Republic of South Africa and the export potential of a People's Republic of China-designed pebble-fueled HTGR have placed an increased importance on developing a safeguards approach that can adequately account for the nuclear material present at such a facility.

Two safeguards approaches have been previously proposed for the pebble-fueled HTGR. The first approach relies upon extensive application of dual C/S measures and the second approach combines safeguards techniques commonly applied in bulk-type material facilities with measures traditionally utilized at a reactor facility. By reviewing safeguards approaches at other types of reactor facilities, it was determined that neither proposed safeguards approach can fully restore the CoK in cases when C/S measures have failed or been compromised, or when bulk-type material measurement techniques have been failed or been manipulated. Additionally, each proposed approach introduces an amount of material unaccounted for that could be exploited by an adversary to divert material from the reactor facility.

A new safeguards system concept for the pebble-fueled HTGR that would be capable of restoring CoK in most, if not all, failure scenarios, was developed and evaluated. It was determined that to restore CoK, each fuel pebble must be uniquely identifiable. Identification methods addressed determined that internal placement of microspheres in a random configuration to create a unique fingerprint was best. To determine the location of each microsphere an imaging system had to be chosen that could be used on fresh, core, and spent fuel present at the reactor facility. Ultrasound-based imaging was found to be unhindered by the radiation emitted by core and spent fuel and as such, was the chosen imaging system evaluated as part of this concept. The

chosen material for the microspheres was ZrO_2, doped with the additive Y_2O_3. ZrO_2 was chosen for it stability at high temperature, low neutron absorption cross section, and chemical stability in the graphite environment of a fuel pebble.

The system was evaluated to determine the minimum number of microsphere necessary to uniquely identify each fuel pebble, the probability that a configuration inside a pebble will randomly match another, the impact that these microspheres would have on the neutronics and safety of the reactor system, and the effectiveness of ultrasound in imaging microspheres through graphite.

It was found that the minimum number of microspheres necessary to be able to uniquely identify each pebble is three. Using these three microspheres it was possible to determine that only 0.00551% of pebbles that pass through the reactor in its lifetime may be misidentified. It was found that less than fifty 1 mm diameter zirconium oxide microspheres will have no negative or positive impact on the reactivity of the reactor or the temperature coefficient of reactivity. Lastly, an ultrasound imaging system was used to evaluate the effectiveness of ultrasound imaging through graphite plates. These results of the experiments showed that ultrasound wave transmission through thin graphite plates is possible and that a small grouping of twenty microspheres can be imaged to within 0.04 cm.

Overall the evaluation of the proposed safeguards system concept showed that using a unique microsphere fingerprint to identify each fuel pebble is possible. However, additional work must be completed to certify the use of an ultrasound system to determine the location of the microspheres. There are several recommendations for future research in developing and implementing this safeguards concept:

- The method use to determine the minimum number of microspheres necessary to uniquely identify each pebble was built by using unique microsphere locations. The later developed method to identify each pebble was based upon characteristic lengths. The minimum should be re-evaluated to determine if the minimum number of microspheres would change if the possible number of unique lengths was considered.

- A better model that determines the random probability of matching microsphere fingerprints based on characteristic lengths, and not volumes, should be found and compared to the developed computer simulation results.
- Further imaging experiments with ultrasound imaging should utilize a computerized, mechanically controlled system to move the transducer.
- Future samples should embed the microspheres in graphite.
- Radiation damage, and its effect, to the ultrasound system from irradiated pebbles should be quantified.
- The impact of the microspheres on the manufacturing of the fuel pebbles and what affects their inclusion may have.
- The costs associated with implementation of the concept should be evaluated to determine if the system would be cost prohibitive.

REFERENCES

1. D. FISCHER, *History of the International Atomic Energy Agency: The First Forty Years*, International Atomic Energy Agency, Vienna (1997).

2. "Statute of the International Atomic Energy Agency," United Nations Conference on the Statute of the International Atomic Energy Agency (Oct.1956).

3. "The Agency's Safeguards," INFCIRC/26, International Atomic Energy Agency (March 1961).

4. "The Agency's Safeguards System ," INFCIRC/66/Rev. 2, International Atomic Energy Agency (Sept. 1968).

5. "Treaty on the Non-proliferation of Nuclear Weapons," International Atomic Energy Agency (June 1968).

6. "The Structure and Content of Agreements Between the Agency and States Required in Connection with the Treaty on the Non-proliferation of Nuclear Weapons (NPT)," INFCIRC/153 (corrected), International Atomic Energy Agency (June 1972).

7. "Model Protocol Additional to the Agreement(s) between State(s) and the International Atomic Energy Agency for the Application of Safeguards," INFCIRC/540 (corrected), International Atomic Energy Agency (Sept. 1997).

8. "IAEA Safeguards: Implementation at Nuclear Fuel Cycle Facilities," IAEA/SG/INF/6, International Atomic Energy Agency (1985).

9. "Safeguards Manual: Safeguards Criteria - Section 3 Other Types of Reactors," International Atomic Energy Agency (2003).

10. D. MATZNER, "Chapter 14: The Pebble Bed Modular Reactor," *Future Energy*, Elsevier, Oxford, 239-257 (2008).

11. E. ZIERMANN, "Review of 21 years of power operation at the AVR experimental nuclear power station in Jülich," *Nucl. Eng. Des.*,**121**, 135-142 (1990).

12. R. BÄUMER, I. KALINOWSKI, E. RÖHLER, J. SCHÖNING, and W. WACHHOLZ, "Construction and operating experience with 300-MW THTR nuclear power plant," *Nucl. Eng. Des.*,**121**, 155-166 (1990).

13. D. SCHWARZ, R. BÄUMER, "THTR operating experience," *Nucl. Eng. Des.*, **109**, 199-205 (1988).

14. "Evaluation of high temperature gas cooled reactor performance: Benchmark analysis related to initial testing of the HTTR and HTR-10," IAEA-TECDOC-1382, International Atomic Energy Agency (2003).

15. M. FOX and E. MULDER, "Pebble Bed Modular Reactor – South Africa. Design and Development of Gas Cooled Reactors with Closed Cycle Gas Turbines," IAEA-TECDOC-899, International Atomic Energy Agency, 251-256 (1996).

16. E. STERNFELD, "Development of civil nuclear power industry in China," Nuclear Monitor, **665**, 5-8 (May 2007).

17. "Annual Report 2010," Pebble Bed Modular Reactor (Pty) Limited (2010); available online at http://www.pbmr.co.za/contenthtml/Annual2010/PBMR_AR_0910.pdf (current as of June 17, 2011).

18. "Status Report for Advanced Nuclear Reactor Designs: Pebble Bed Modular Rector (PBMR)," Report 70, International Atomic Energy Agency (Sept. 2010).

19. G.D. DEL CUL, B.B. SPENCER, C.W. FORSBERG, E.D. COLLINS, and W.S. RICKMAN, "TRISO-Coated Fuel Processing to Support High-Temperature Gas-Cooled Reactors," ORNL/TM-2002/156, Oak Ridge National Laboratory, Oak Ridge, TN (Sept. 2002).

20. J. SLABBER, "PBMR Nuclear Material Safeguards," *Proc. 2nd International Topical Meeting on High Temperature Reactor Technology*, Beijing, China, September 22-24, 2004.

21. "Nuclear Power in China," World Nuclear Association (2011); available online at http://www.world-nuclear.org/info/inf63.html (current as of March 15, 2011).

22. Z. ZHANG, Z. WU, D. WANG, Y. XU, Y. SUN, F. LI, and Y. DONG, "Current status and technical description of Chinese 2 x 250 MWth HTR-PM demonstration plant," Nucl. Eng. Des., **239**, 1212-1219 (2009).

23. "IAEA Safeguards Glossary 2001 Edition," International Nuclear Verification Series No. 3, International Atomic Energy Agency (June 2002).

24. H. BÜKER, "A Safeguards-System for Pebble Bed Reactors," *Proc. of the Institute of Nuclear Materials Management 17th Annual Meeting*, Seattle, WA, June 22, 1976.

25. D.L. TILLWICK and J.L. SHAYI, "Cooperation on international safeguards between the IAEA and South Africa," *J. Nucl. Mater. Manag.*, **35**, 4, 55-60 (2001).

26. C. CHARLIER, R. FAGERHOLM, J. SLABBER, and J.L. SHAYI, "Safeguarding the Pebble Bed Modular Reactor: A new challenge for the IAEA," *Proc. of the Institute of Nuclear Materials Management 48th Annual Meeting*, Tucson, AZ, July 8-12, 2007.

27. P.C. DURST, D. BEDDINGFIELD, B. BOYER, R. BEAN, N. COLLINS, M. EHINGER, D. HANKS, D.L. MOSES, and L. REFALO, "Nuclear Safeguards Considerations for the Pebble Bed Modular Reactor (PBMR)," INL/EXT-09-16782, Idaho National Laboratory, Idaho Falls, ID (Oct. 2009).

28. D.H. BEDDINGFIELD and M. HORI, "Nuclear Material Safeguards at Reactors Types That Defy Traditional Item Counting," presented at JAEA-IAEA Workship on Advanced Safeguards Technology for the Future Nuclear Fuel Cycle, November 13-16, 2007; see also LA-UR-07-6878, Los Alamos National Laboratory, Los Alamos, NM (2007).

29. A.M. OUGOUAG, H.D. GOUGAR, and T.D. TODD, "Evaluation of the Strategic Value of Fully Burnt PBMR Spent Fuel," INL/EXT-06-11272, Idaho National Laboratory, Idaho Falls, ID (May 2006).

30. C.W. FORSBERG and D.L. MOSES, "Safegaurds Challenges for Pebble-Bed Reactors Designed by People's Republic of China," ORNL/TM-2008/229, Oak Ridge National Laboratory, Oak Ridge, TN (Nov. 2009).

31. Power Reactor Information System (PRIS), International Atomic Energy Agency (2011); available at http://www.iaea.org/programmes/a2/ (current as of March 1, 2011).

32. "Boiling Water Reactors Information Page", Nuclear Regulatory Commission (2007); available at http://www.nrc.gov/reactors/bwrs.html (current as of March 1, 2011).

33. "Pressurized Water Reactors", Nuclear Regulatory Commission (2008); available online at http://www.nrc.gov/reactors/pwrs.html (current as of March 1, 2011).

34. "Design Measures to Facilitate Implementation of Safeguards at Future Water Cooled Nuclear Power Plants," International Atomic Energy Agency Technical Reports Series No. 392 **(**1998).

35. J.J. WHITLOCK and A.G. LEE, "CANDU: Setting the standard for proliferation resistance of Generation II and III+ reactors," *Proc. International Conference on Opportunities and Challenges for Water Cooled Reactors in the 21st Century,* Vienna, Austria, October 27-30, 2009.

36. CANDU technology, Canadian Nuclear Association (2010); available online at http://www.cna.ca/english/how_works/CANDU_technology.html, (current as of March 1, 2011).

37. P. BUTTON, "Radiation monitoring techniques for monitoring the movement of discharged fuel," Technical sheet for European Safeguards Research and Development Association (ESARDA) (2011); available online at http://esarda2.jrc.it/references/ Technical_sheets/ts-RM-Discharged-Fuel-070830.pdf (current as of March 1, 2011).

38. P.C. DURST, I. THERIOS, R. BEAN, A. DOUGAN, B. BOYER, R.L. WALLACE, M.H. EHINGER, D.N. KOVACIC, and K. TOLK, "Advanced Safeguards Approaches for New Fast Reactors," PNNL-17168, Pacific Northwest National Laboratory, Richland, WA (Dec. 2007).

39. A. WEBB, *Introduction to Biomedical Imaging* (IEEE Press Series in Biomedical Engineering), John Wiley & Sons, Inc., Hoboken, NJ (2003).

40. B.D. SAWICKA, R.V. MURPHY, G. TOSELLO, P.W. REYNOLDS, and T. ROMANISZYN, "Computed tomography of radioactive objects and materials," *Nucl. Instrum. Methods Phys. A*, **299**, 468-479 (1990).

41. S.J. SVÄRD, "A tomographic measurement technique for irradiated nuclear fuel assemblies," Doctoral Dissertation, Actas Universitatis Upsaliensis, Uppsala, Sweden (2004).

42. R.N. ORD and R.W. SMITH, "Development of an Under-Sodium Ultrasonic Scanner for In-Reactor Surveillance," HEDL-TME 72-91, Hanford Engineering Development Laboratory, Richland, WA (1972).

43. H. NICKEL, K. HOFMANN, W. WACHHOLZ, and I. WEISBRODT, "The helium-cooled high-temperature reactor in the Federal Republic of Germany: safety features, integrity concept, outlook for design codes and licensing procedure," *Nucl. Eng. Des*., **127**, 181-190 (1991).

44. G. VASUDEVAMURTHY, T.W. KNIGHT, E. ROBERTS, and T.M. ADAMS, "Laboratory production of zirconium carbide compacts for use in inert matrix fuels," *J. Nucl. Mat.*, **374**, 241-247 (2008).

45. C. DEGUELDRE and J.M. PARATTE, "Concepts for an inert matrix fuel: an overview, "*J. Nucl. Mat.*, **274**, 1-6 (1999).

46. D. WONGSAWAENG, "Performance modeling of deep burn TRISO fuel using ZrC as a load-bearing layer and an oxygen getter," *J. Nucl. Mat.*, **396**, 149-158 (2010).

47. ASM International Handbook Committee, ASM Handbooks Online, ASM International (2011); available online by subscription at http://products. asminternational.org/hbk/index.jsp (current as of March 1, 2011).

48. H. HAUSNER, "Determination of the melting point of uranium dioxide," *J. Nucl. Mat.*, **15**, 179-183 (1965).

49. Z. ZHANG, Z. WU, Y. XU, Y. SUN, and F. LI, "Design of Chinese Modular High-Temperature Gas-cooled Reactor HTR-PM," *Proc. Conference on High Temperature Reactor Technology (HTR-2004)*, Vienna, Austria, September 22-24, 2004.

50. D.C. MONTGOMERY and G.C. RUNGER, *Applied Statistics and Probability for Engineers (4th ed.)*, John Wiley & Sons, Hoboken, NJ (2007).

51. X-5 MONTE CARLO TEAM, "MCNP – A General Monte Carlo N-Particle Transport Code, Version 5. Los Alamos National Laboratory," LA-UR-03-1987, Los Alamos National Laboratory, Los Alamos, NM (Apr. 2003).

52. "DOE Fundamentals Handbook: Nuclear Physics and Reactor Theory," DOE-HDBK-1019/1-93, United States Department of Energy (Jan. 1993).

53. A. KOSTER, H.D. MATZNER, and D.R. NICHOLSI, "PBMR design for the future," *Nucl. Eng. Des.*, **222**, 231-245 (2003).

54. H. PETERSEN, "The Properties of Helium: Density, Specific Heats, Viscosity, and Thermal Conductivity at Pressures from 1 to 100 bar and from Room Temperature to about 1800 K," Report No. 224, Research Establishment Risö, Danish Atomic Energy Commission (Sept. 1970).

55. C. TANG, T. TANG, Y. ZHU, J. LI, and X. NI, "Design and manufacture of the fuel element for the 10 MW high temperature gas-cooled reactor," *Nucl. Eng. Des.*, **218**, 91-102 (2002).

56. Table of Nuclides, Korea Atomic Energy Research Institute (2000); available online at http://atom.kaeri.re.kr/ (current as of March 1, 2009).

57. “Status of innovative small and medium sized reactor designs 2005,” IAEA-TECDOC-1485, International Atomic Energy Agency (Mar. 2006).

APPENDIX A

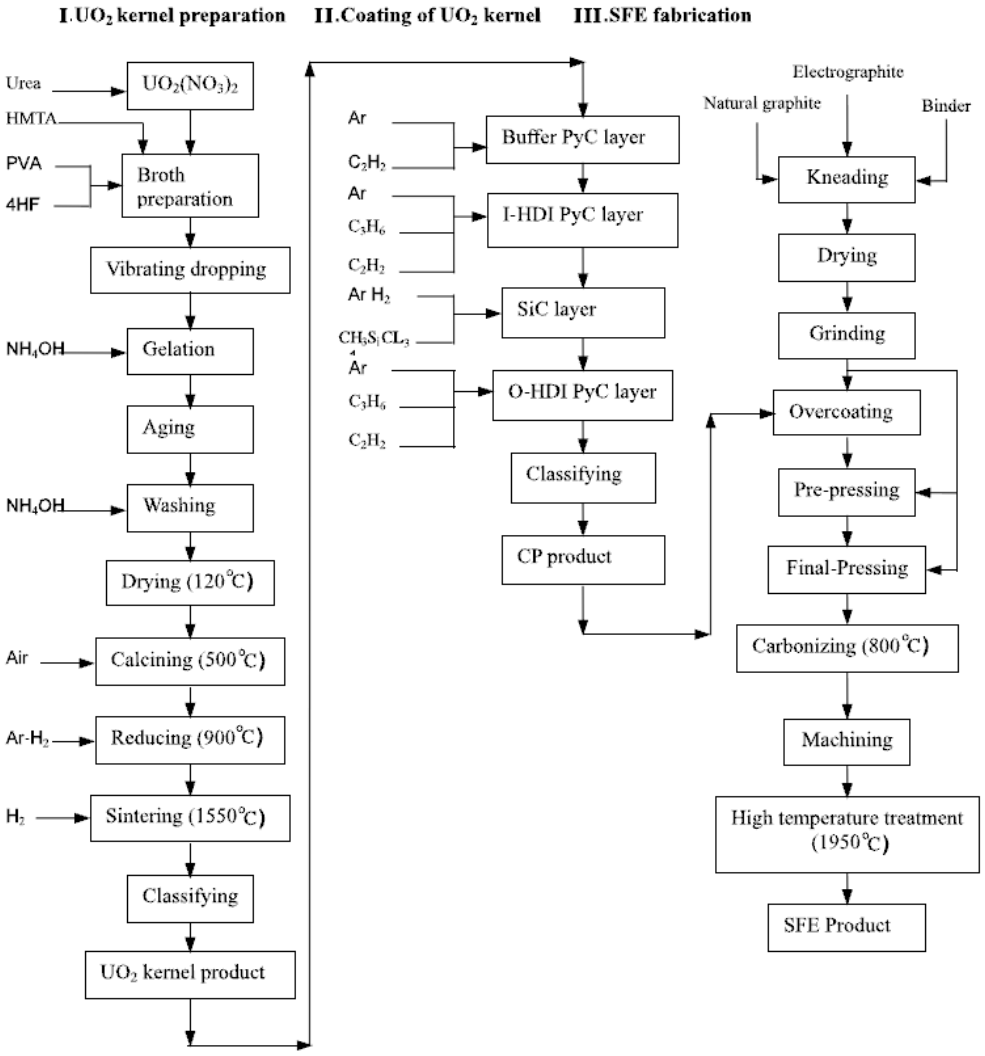

Fig. A-1. Flow chart of manufacturing process for fuel kernel, TRISO particle, and fuel pebble (taken from C. TANG, T. TANG, Y. ZHU, J. LI, and X. NI, "Design and manufacture of the fuel element for the 10 MW high temperature gas-cooled reactor," *Nucl. Eng. Des.*, **218**, 91-102 (2002).

APPENDIX B

```
 Sub ExpSim()
'
' ExpSim Macro
'

'
    Application.ScreenUpdating = False

    Dim irow As Double
    Dim iMatch As Double 'number of matches
    Dim iloop As Double 'number of pebbles
    Dim irand1 As Double 'random number 1
    Dim irand2 As Double 'random number 2
    Dim irand3 As Double 'random number 3
    Dim iRmax As Double 'max radius of pebble region where microshperes can be
    Dim iRusphere As Double 'radius of microsphere
    Dim iRes As Double 'resolution of system
    Dim iTLab As Double
    Dim iTLbc As Double
    Dim iTLac As Double
    Dim iMLqr As Double
    Dim iMLrs As Double
    Dim iMLqs As Double
    Dim iB As Double
    Dim iC As Double
    Dim ifill1 As Double
    Dim ifill2 As Double
    Dim ifill3 As Double
    Dim ifill4 As Double
    Dim ifill5 As Double
    Dim ifill6 As Double
    Dim ifill7 As Double
    Dim ifill8 As Double
    Dim ifill9 As Double

    irow = 2
    iRes = 0

Start1:

    iMatch = 0
```

```
    iloop = 1
    iRmax = 2.45
    iRusphere = 0.05
    iTLab = 3.10680203190317
    iTLbc = 2.14898950599226
    iTLac = 2.50657170668777

Start2:


        irand1 = Rnd
        irand2 = Rnd
        irand3 = Rnd

        iMLqr = irand1 * ((iRmax * 2) - (iRusphere * 2)) + (iRusphere * 2)
        iMLrs = irand2 * ((iRmax * 2) - (iRusphere * 2)) + (iRusphere * 2)
        iMLqs = irand3 * ((iRmax * 2) - (iRusphere * 2)) + (iRusphere * 2)

        ifill1 = Abs(iTLab - iMLqr)
        ifill2 = Abs(iTLab - iMLrs)
        ifill3 = Abs(iTLab - iMLqs)
        ifill4 = Abs(iTLbc - iMLqr)
        ifill5 = Abs(iTLbc - iMLrs)
        ifill6 = Abs(iTLbc - iMLqs)
        ifill7 = Abs(iTLac - iMLqr)
        ifill8 = Abs(iTLac - iMLrs)
        ifill9 = Abs(iTLac - iMLqs)

        If (ifill1 <= ifill2 And ifill1 <= ifill3) Then
           GoTo Line1

        Else: GoTo Line5

        End If
Line5:
        If (ifill2 <= ifill1 And ifill2 <= ifill3) Then
           GoTo Line2
        Else: GoTo Line6

        End If
Line6:
        If (ifill3 <= ifill2 And ifill3 <= ifill1) Then
           GoTo Line3
```

```
        Else

            ActiveWorkbook.Save

        End If

Line1:
        If (ifill5 < ifill6) Then

            If (ifill1 <= iRes And ifill5 <= iRes And ifill9 <= iRes) Then

                iMatch = iMatch + 1
                iloop = iloop + 1

            Else

                iloop = iloop + 1

            End If

        Else

            If (ifill1 <= iRes And ifill6 <= iRes And ifill8 <= iRes) Then

                iMatch = iMatch + 1
                iloop = iloop + 1

            Else

                iloop = iloop + 1

            End If

        End If

        GoTo LineLoop

Line2:
       If (ifill4 < ifill6) Then

            If (ifill2 <= iRes And ifill4 <= iRes And ifill9 <= iRes) Then

                iMatch = iMatch + 1
                iloop = iloop + 1
```

```
        Else

            iloop = iloop + 1

        End If

    Else

        If (ifill2 <= iRes And ifill6 <= iRes And ifill7 <= iRes) Then

            iMatch = iMatch + 1
            iloop = iloop + 1

        Else

            iloop = iloop + 1

        End If

    End If

    GoTo LineLoop

Line3:
    If (ifill4 < ifill5) Then

        If (ifill3 <= iRes And ifill4 <= iRes And ifill8 <= iRes) Then

            iMatch = iMatch + 1
            iloop = iloop + 1

        Else

            iloop = iloop + 1

        End If

    Else

        If (ifill3 <= iRes And ifill5 <= iRes And ifill7 <= iRes) Then

            iMatch = iMatch + 1
            iloop = iloop + 1
```

```
            Else

               iloop = iloop + 1

            End If

         End If

         GoTo LineLoop

LineLoop:

   If (iloop <= 10000000) Then
      GoTo Start2
   End If

   iB = iMatch
   iC = iRes

   Sheets("Sheet3").Select

   Range("D" & irow).Select
   ActiveCell.Value = iB
   Range("E" & irow).Select
   ActiveCell.Value = iC

   irow = irow + 1
   iRes = iRes + 0.001      'increases the resolution by 100 um.

   If (iRes <= 5) Then         'means stop when resolution reaches 5.001cm
      GoTo Start1
   End If

   Application.ScreenUpdating = True
   ActiveWorkbook.Save
   MsgBox "Done"

End Sub
```

APPENDIX C

Table C-1. Calculated values for the number of pebbles in numerical simulation up to 0.3 cm (3000 micrometers).

Number of Matches	Resolution (cm)
0	0
4	0.01
38	0.02
128	0.03
269	0.04
551	0.05
929	0.06
1482	0.07
2192	0.08
3209	0.09
4320	0.1
5767	0.11
7494	0.12
9490	0.13
12045	0.14
14577	0.15
17864	0.16
21261	0.17
25243	0.18
29812	0.19
34219	0.2
39398	0.21
44532	0.22
50020	0.23
56292	0.24
62366	0.25
68886	0.26
75584	0.27
82832	0.28
90220	0.29
98157	0.3

APPENDIX D

```
PBMR-450K Heterogeneous Pebble in core w/ 0 ZrO2 uspheres
C   Created by E. Travis Gitau
C   -----Cell Cards-----
C   TRISO Particle
1   1   -10.85   -101                u=1        imp:n=1  $Fuel Kernel
2   2   -0.980    101 -102            u=1        imp:n=1  $Porous Carbon Layer
3   2   -1.865    102 -103            u=1        imp:n=1  $IPyC Layer
4   3   -3.20     103 -104            u=1        imp:n=1  $SiC Layer
5   2   -1.865    104 -105            u=1        imp:n=1  $OPyC Layer
6   5   -1.76     105                 u=1        imp:n=1  $Graphite Matrix
C   TRISO Lattice to fill Pebble
7   0           -106 107 -108 109 -110 111  lat=1 fill=1 u=2   imp:n=1
C   Pebble
8   0            -112  fill=2 u=3 imp:n=1
9   5   -1.76       112 -113         u=3 imp:n=1          $Non-fuelled region
10  4   -0.01163211 113 19113 20113 21113 &
             22113 23113 24113 25113 26113  u=3 imp:n=1  $Helium between pebbles
C   Transform for BCC Lattice
C   Transform for fueled region
11   like 8 but trcl=(-3.464102 -3.464102 -3.464102)
12   like 8 but trcl=(-3.464102 -3.464102 3.464102)
13   like 8 but trcl=(-3.464102 3.464102 -3.464102)
14   like 8 but trcl=(-3.464102 3.464102 3.464102)
15   like 8 but trcl=(3.464102 -3.464102 -3.464102)
16   like 8 but trcl=(3.464102 -3.464102 3.464102)
17   like 8 but trcl=(3.464102 3.464102 -3.464102)
18   like 8 but trcl=(3.464102 3.464102 3.464102)
C   Transform of non-fueled region
19   like 9 but trcl=(-3.464102 -3.464102 -3.464102)
20   like 9 but trcl=(-3.464102 -3.464102 3.464102)
21   like 9 but trcl=(-3.464102 3.464102 -3.464102)
22   like 9 but trcl=(-3.464102 3.464102 3.464102)
23   like 9 but trcl=(3.464102 -3.464102 -3.464102)
24   like 9 but trcl=(3.464102 -3.464102 3.464102)
25   like 9 but trcl=(3.464102 3.464102 -3.464102)
26   like 9 but trcl=(3.464102 3.464102 3.464102)
C   Pebble Lattice to fill core
35  0        203 -204 205 -206 207 -208  lat=1 fill=3 u=4 imp:n=1
C   Core
36  0        209 -210 212 -216                fill=4     imp:n=1
C   Helium plenum above core
```

```
37  4   -0.01163211  209 -210 216 -213        imp:n=1        $Plenum
C   Reflectors
38  5   -1.76  -209 212 -213 #43             imp:n=1        $Annular reflector
39  5   -1.76   210 -211 212 -213 #44 #45 #46 imp:n=1        $Outer reflector
40  5   -1.76  -211 -212 214 #43 #46         imp:n=1        $Lower reflector
41  5   -1.76  -211 213 -215 #43 #44 #45 #46  imp:n=1        $Upper reflector
C   Outside Outer Reflector
42  0        211:-214:215 #45               imp:n=0
C   RSS Channels
43  4   -0.01163211 (-219:-220:-221:-222:-223: &
      -224:-225:-226:-227) 214 -215          imp:n=1
C   Control Channels
44  6  -2.50 (-228:-229:-230:-231:-232:-233:-234:-235: &
      -236:-237:-238:-239:-240:-241:-242:-243:-244:-245: &
      -246:-247:-248:-249:-250:-251) 217 -218  imp:n=1
45  4  -0.01163211 (-228:-229:-230:-231:-232:-233:-234:-235: &
      -236:-237:-238:-239:-240:-241:-242:-243:-244:-245: &
      -246:-247:-248:-249:-250:-251) 212 -217  imp:n=1 $Helium to fill void of control
rod
C   Helium Channels
46  4  -0.01163211  (-252:-253:-254:-255:-256:-257:-258: &
      -259:-260:-261:-262:-263:-264:-265:-266:-267:-268: &
      -269:-270:-271:-272:-273:-274:-275:-276:-277:-278: &
      -279:-280:-281:-282:-283:-284:-285:-286:-287) 214 -215 imp:n=1

C   -----Surface Cards-----
C   TRISO Particle
101   so   0.025              $Fuel Kernal D=0.05cm
102   so   0.0345             $Porous Carbon Buffer t=0.0095cm
103   so   0.0385             $IPyC t=0.004cm
104   so   0.042              $SiC t=0.0035cm
105   so   0.046              $OPyC t=0.004cm
C   TRISO Lattice
106   px   0.0817046
107   px  -0.0817046
108   py   0.0817046
109   py  -0.0817046
110   pz   0.0817046
111   pz  -0.0817046
C   Pebble
112   so   2.5                $Fuelled region of pebble
113   so   3.0                $Non-fuelled region of pebble
C   Pebble Lattice
203   px  -3.464102
```

```
204   px   3.464102
205   py  -3.464102
206   py   3.464102
207   pz  -3.464102
208   pz   3.464102
C   Reactor
209   cz  100              $Annular reflector
210   cz  185              $Fuel/Core region
211   cz  280              $Outer reflector
212   pz  -550             $Core bottom
213   pz  550              $Core top
214   pz  -645             $Upper and lower reflector bounds
215   pz  645
216   pz  433              $Where pebbles must end to equal approx. 450K
217   pz  -365             $Positions for control rods
218   pz  830
C   RSS Channels
219   c/z 0 72.6 7.7          $A clockwise
220   c/z 46.66638 55.61483 7.7  $B
221   c/z 71.49104 12.60686 7.7  $C
222   c/z 62.87344 -36.3 7.7     $D
223   c/z 24.83066 -68.2217 7.7  $E
224   c/z -24.83066 -68.217 7.7  $F
225   c/z -62.8734 -36.3 7.7     $G
226   c/z -71.497 12.60686 7.7   $H
227   c/z -46.6664 55.61483 7.7  $I
C   Control Channels
228   c/z   25.733239  195.463354  7.7   $A clockwise
229   c/z   75.446039  182.142850  7.7   $B
230   c/z  120.017316  156.409611  7.7   $C
231   c/z  156.409611  120.017316  7.7   $D
232   c/z  182.142850   75.446039  7.7   $E
233   c/z  195.463354   25.733239  7.7   $F
234   c/z  195.463354  -25.733239  7.7   $G
235   c/z  182.142850  -75.446039  7.7   $H
236   c/z  156.409611  -120.017316 7.7   $I
237   c/z  120.017316  -156.409611 7.7   $J
238   c/z   75.446039  -182.142850 7.7   $K
239   c/z   25.733239  -195.463354 7.7   $L
240   c/z  -25.733239  -195.463354 7.7   $M
241   c/z  -75.446039  -182.142850 7.7   $N
242   c/z  -120.017316 -156.409611 7.7   $O
243   c/z  -156.409611 -120.017316 7.7   $P
244   c/z  -182.142850 -75.446039  7.7   $Q
```

```
245   c/z  -195.463354 -25.733239  7.7   $R
246   c/z  -195.463354  25.733239  7.7   $S
247   c/z  -182.142850  75.446039  7.7   $T
248   c/z  -156.409611 120.017316  7.7   $U
249   c/z  -120.017316 156.409611  7.7   $V
250   c/z  -75.446039  182.142850  7.7   $W
251   c/z  -25.733239  195.463354  7.7   $X
C   Helium Channels
252   c/z   21.741000  248.500767  8.5       $A clockwise
253   c/z   64.562411  240.950197  8.5       $B
254   c/z  105.422125  226.078477  8.5       $C
255   c/z  143.078642  204.337477  8.5       $D
256   c/z  176.387787  176.387787  8.5       $E
257   c/z  204.337477  143.078642  8.5       $F
258   c/z  226.078477  105.422125  8.5       $G
259   c/z  240.950197   64.562411  8.5       $H
260   c/z  248.500767   21.741000  8.5       $I
261   c/z  248.500767  -21.741000  8.5       $J
262   c/z  240.950197  -64.562411  8.5       $K
263   c/z  226.078477  -105.422125 8.5       $L
264   c/z  204.337477  -143.078642 8.5       $M
265   c/z  176.387787  -176.387787 8.5       $N
266   c/z  143.078642  -204.337477 8.5       $O
267   c/z  105.422125  -226.078477 8.5       $P
268   c/z   64.562411  -240.950197 8.5       $Q
269   c/z   21.741000  -248.500767 8.5       $R
270   c/z  -21.741000  -248.500767 8.5       $S
271   c/z  -64.562411  -240.950197 8.5       $T
272   c/z  -105.422125 -226.078477 8.5       $U
273   c/z  -143.078642 -204.337477 8.5       $V
274   c/z  -176.387787 -176.387787 8.5       $W
275   c/z  -204.337477 -143.078642 8.5       $X
276   c/z  -226.078477 -105.422125 8.5       $Y
277   c/z  -240.950197 -64.562411  8.5       $Z
278   c/z  -248.500767 -21.741000  8.5       $AA
279   c/z  -248.500767  21.741000  8.5       $BB
280   c/z  -240.950197  64.562411  8.5       $CC
281   c/z  -226.078477 105.422125  8.5       $DD
282   c/z  -204.337477 143.078642  8.5       $EE
283   c/z  -176.387787 176.387787  8.5       $FF
284   c/z  -143.078642 204.337477  8.5       $GG
285   c/z  -105.422125 226.078477  8.5       $HH
286   c/z  -64.562411  240.950197  8.5       $II
287   c/z  -21.741000  248.500767  8.5       $JJ
```

```
C   -----Data Cards-----
C   Material Cards
m1    92235.66c -0.04964443      $Fuel Kernal-UO2-5.7 wt% U-235
      92238.66c -0.83181731      $5.7 wt % is start-up enrichment
      8016.66c  -0.11853826
m2    6000.66c   1               $Carbon for non-fuelled region
mt2   grph.01t
m3    14028.66c -0.64370         $SiC Layer
      14029.66c -0.03376
      14030.66c -0.02318
      6000.66c  -0.29936
mt3   grph.01t
m4    2003.66c  -0.00000137      $Helium density=0.01163211 g/cc
      2004.66c  -0.99999863      $          at 300K and 70 Bar
m5    6000.66c  -0.999998        $Nuclear grade graphite w/2ppm boron impurities
      5010.66c  -0.000002
mt5   grph.01t
m6    6000.66c  -0.23069795      $Control Material-B4C
      5010.66c  -0.76930205
mt6   grph.01t
C   Source Card
kcode 1000 1.0 50 750
ksrc 42.307 -105.51 -80.914
mode n
```

APPENDIX E

```
PBMR-450K Heterogeneous Pebble in core w/ 5 ZrO2 uspheres in FR
C   Created by E. Travis Gitau
C   -----Cell Cards-----
C   TRISO Particle
1   1   -10.85   -101                u=1        imp:n=1  $Fuel Kernel
2   2   -0.980    101 -102            u=1        imp:n=1  $Porous Carbon Layer
3   2   -1.865    102 -103            u=1        imp:n=1  $IPyC Layer
4   3   -3.20     103 -104            u=1        imp:n=1  $SiC Layer
5   2   -1.865    104 -105            u=1        imp:n=1  $OPyC Layer
6   5   -1.76     105                 u=1        imp:n=1  $Graphite Matrix
C   TRISO Lattice to fill Pebble
7   0           -106 107 -108 109 -110 111  lat=1 fill=1 u=2   imp:n=1
C   Pebble
8   0       -112 301  302  303  304  305  fill=2 u=3 imp:n=1
9   5   -1.76       112 -113          u=3 imp:n=1          $Non-fuelled region
10  4   -0.01163211 113 19113 20113 21113 &
              22113 23113 24113 25113 26113  u=3 imp:n=1  $Helium between pebbles
C   Transform for BCC Lattice
C   Transform for fueled region
11   like 8 but trcl=(-3.464102 -3.464102 -3.464102)
12   like 8 but trcl=(-3.464102 -3.464102 3.464102)
13   like 8 but trcl=(-3.464102 3.464102 -3.464102)
14   like 8 but trcl=(-3.464102 3.464102 3.464102)
15   like 8 but trcl=(3.464102 -3.464102 -3.464102)
16   like 8 but trcl=(3.464102 -3.464102 3.464102)
17   like 8 but trcl=(3.464102 3.464102 -3.464102)
18   like 8 but trcl=(3.464102 3.464102 3.464102)
C   Transform of non-fueled region
19   like 9 but trcl=(-3.464102 -3.464102 -3.464102)
20   like 9 but trcl=(-3.464102 -3.464102 3.464102)
21   like 9 but trcl=(-3.464102 3.464102 -3.464102)
22   like 9 but trcl=(-3.464102 3.464102 3.464102)
23   like 9 but trcl=(3.464102 -3.464102 -3.464102)
24   like 9 but trcl=(3.464102 -3.464102 3.464102)
25   like 9 but trcl=(3.464102 3.464102 -3.464102)
26   like 9 but trcl=(3.464102 3.464102 3.464102)
```

```
C   Pebble Lattice to fill core
35  0        203 -204 205 -206 207 -208  lat=1 fill=3 u=4 imp:n=1
C   Core
36  0        209 -210 212 -216               fill=4     imp:n=1
C   Helium plenum above core
37  4   -0.01163211  209 -210 216 -213        imp:n=1        $Plenum
C   Reflectors
38  5   -1.76  -209 212 -213 #43             imp:n=1        $Annular reflector
39  5   -1.76   210 -211 212 -213 #44 #45 #46 imp:n=1        $Outer reflector
40  5   -1.76  -211 -212 214 #43 #46          imp:n=1        $Lower reflector
41  5   -1.76  -211 213 -215 #43 #44 #45 #46  imp:n=1        $Upper reflector
C   Outside Outer Reflector
42  0        211:-214:215 #45               imp:n=0
C   RSS Channels
43  4   -0.01163211 (-219:-220:-221:-222:-223: &
      -224:-225:-226:-227) 214 -215          imp:n=1
C   Control Channels
44  6  -2.50 (-228:-229:-230:-231:-232:-233:-234:-235: &
      -236:-237:-238:-239:-240:-241:-242:-243:-244:-245: &
      -246:-247:-248:-249:-250:-251) 217 -218  imp:n=1
45  4  -0.01163211 (-228:-229:-230:-231:-232:-233:-234:-235: &
      -236:-237:-238:-239:-240:-241:-242:-243:-244:-245: &
      -246:-247:-248:-249:-250:-251) 212 -217  imp:n=1 $Helium to fill void of control
rod
C   Helium Channels
46  4  -0.01163211  (-252:-253:-254:-255:-256:-257:-258: &
      -259:-260:-261:-262:-263:-264:-265:-266:-267:-268: &
      -269:-270:-271:-272:-273:-274:-275:-276:-277:-278: &
      -279:-280:-281:-282:-283:-284:-285:-286:-287) 214 -215 imp:n=1
C   ZrO2-Y2O3 microspheres
47  7   -6.02  -301:-302:-303:-304:-305 u=3 imp:n=1
48   like 47 but trcl=(-3.464102 -3.464102 3.464102)
49   like 47 but trcl=(-3.464102 3.464102 -3.464102)
50   like 47 but trcl=(-3.464102 3.464102 3.464102)
51   like 47 but trcl=(3.464102 -3.464102 -3.464102)
52   like 47 but trcl=(3.464102 -3.464102 3.464102)
53   like 47 but trcl=(3.464102 3.464102 -3.464102)
54   like 47 but trcl=(3.464102 3.464102 3.464102)
```

```
55   like 47 but trcl=(-3.464102 -3.464102 -3.464102)

C   -----Surface Cards-----
C   TRISO Particle
101   so   0.025            $Fuel Kernal D=0.05cm
102   so   0.0345           $Porous Carbon Buffer t=0.0095cm
103   so   0.0385           $IPyC t=0.004cm
104   so   0.042            $SiC t=0.0035cm
105   so   0.046            $OPyC t=0.004cm
C   TRISO Lattice
106   px   0.0817046
107   px  -0.0817046
108   py   0.0817046
109   py  -0.0817046
110   pz   0.0817046
111   pz  -0.0817046
C   Pebble
112   so   2.5              $Fuelled region of pebble
113   so   3.0              $Non-fuelled region of pebble
C   Pebble Lattice
203   px  -3.464102
204   px   3.464102
205   py  -3.464102
206   py   3.464102
207   pz  -3.464102
208   pz   3.464102
C   Reactor
209   cz  100              $Annular reflector
210   cz  185              $Fuel/Core region
211   cz  280              $Outer reflector
212   pz  -550             $Core bottom
213   pz  550              $Core top
214   pz  -645             $Upper and lower reflector bounds
215   pz  645
216   pz  433              $Where pebbles must end to equal approx. 450K
217   pz  -365             $Positions for control rods
218   pz  830
C   RSS Channels
```

```
219   c/z 0 72.6 7.7            $A clockwise
220   c/z 46.66638 55.61483 7.7  $B
221   c/z 71.49104 12.60686 7.7  $C
222   c/z 62.87344 -36.3 7.7     $D
223   c/z 24.83066 -68.2217 7.7  $E
224   c/z -24.83066 -68.217 7.7  $F
225   c/z -62.8734 -36.3 7.7     $G
226   c/z -71.497 12.60686 7.7   $H
227   c/z -46.6664 55.61483 7.7  $I
C   Control Channels
228   c/z   25.733239  195.463354  7.7   $A clockwise
229   c/z   75.446039  182.142850  7.7   $B
230   c/z  120.017316  156.409611  7.7   $C
231   c/z  156.409611  120.017316  7.7   $D
232   c/z  182.142850   75.446039  7.7   $E
233   c/z  195.463354   25.733239  7.7   $F
234   c/z  195.463354  -25.733239  7.7   $G
235   c/z  182.142850  -75.446039  7.7   $H
236   c/z  156.409611  -120.017316 7.7   $I
237   c/z  120.017316  -156.409611 7.7   $J
238   c/z   75.446039  -182.142850 7.7   $K
239   c/z   25.733239  -195.463354 7.7   $L
240   c/z  -25.733239  -195.463354 7.7   $M
241   c/z  -75.446039  -182.142850 7.7   $N
242   c/z  -120.017316 -156.409611 7.7   $O
243   c/z  -156.409611 -120.017316 7.7   $P
244   c/z  -182.142850 -75.446039  7.7   $Q
245   c/z  -195.463354 -25.733239  7.7   $R
246   c/z  -195.463354  25.733239  7.7   $S
247   c/z  -182.142850  75.446039  7.7   $T
248   c/z  -156.409611 120.017316  7.7   $U
249   c/z  -120.017316 156.409611  7.7   $V
250   c/z  -75.446039  182.142850  7.7   $W
251   c/z  -25.733239  195.463354  7.7   $X
C   Helium Channels
252   c/z   21.741000  248.500767  8.5       $A clockwise
253   c/z   64.562411  240.950197  8.5       $B
254   c/z  105.422125  226.078477  8.5       $C
```

```
255   c/z  143.078642  204.337477  8.5       $D
256   c/z  176.387787  176.387787  8.5       $E
257   c/z  204.337477  143.078642  8.5       $F
258   c/z  226.078477  105.422125  8.5       $G
259   c/z  240.950197   64.562411  8.5       $H
260   c/z  248.500767   21.741000  8.5       $I
261   c/z  248.500767  -21.741000  8.5       $J
262   c/z  240.950197  -64.562411  8.5       $K
263   c/z  226.078477  -105.422125 8.5       $L
264   c/z  204.337477  -143.078642 8.5       $M
265   c/z  176.387787  -176.387787 8.5       $N
266   c/z  143.078642  -204.337477 8.5       $O
267   c/z  105.422125  -226.078477 8.5       $P
268   c/z   64.562411  -240.950197 8.5       $Q
269   c/z   21.741000  -248.500767 8.5       $R
270   c/z  -21.741000  -248.500767 8.5       $S
271   c/z  -64.562411  -240.950197 8.5       $T
272   c/z  -105.422125 -226.078477 8.5       $U
273   c/z  -143.078642 -204.337477 8.5       $V
274   c/z  -176.387787 -176.387787 8.5       $W
275   c/z  -204.337477 -143.078642 8.5       $X
276   c/z  -226.078477 -105.422125 8.5       $Y
277   c/z  -240.950197 -64.562411  8.5       $Z
278   c/z  -248.500767 -21.741000  8.5       $AA
279   c/z  -248.500767  21.741000  8.5       $BB
280   c/z  -240.950197  64.562411  8.5       $CC
281   c/z  -226.078477 105.422125  8.5       $DD
282   c/z  -204.337477 143.078642  8.5       $EE
283   c/z  -176.387787 176.387787  8.5       $FF
284   c/z  -143.078642 204.337477  8.5       $GG
285   c/z  -105.422125 226.078477  8.5       $HH
286   c/z  -64.562411  240.950197  8.5       $II
287   c/z  -21.741000  248.500767  8.5       $JJ
C   ZrO2-Y2O3 Microspheres
301   s   -0.0817046   0.0817046   1.0621598   0.05
302   s   -1.5523874   0.7353414   -1.3889782   0.05
303   s    0.7353414   -0.4085230  -1.0621598   0.05
304   s    1.0621598   1.3889782   1.7157966   0.05
```

```
305   s   -0.7353414   -1.0621598   0.0817046   0.05

C   -----Data Cards-----
C   Material Cards
m1    92235.66c -0.04964443      $Fuel Kernal-UO2-5.7 wt% U-235
      92238.66c -0.83181731      $5.7 wt % is start-up enrichment
      8016.66c  -0.11853826
m2    6000.66c   1              $Carbon for non-fuelled region
mt2   grph.01t
m3    14028.66c -0.64370         $SiC Layer
      14029.66c -0.03376
      14030.66c -0.02318
      6000.66c  -0.29936
mt3   grph.01t
m4    2003.66c  -0.00000137      $Helium density=0.01163211 g/cc
      2004.66c  -0.99999863      $          at 300K and 70 Bar
m5    6000.66c  -0.999998        $Nuclear grade graphite w/2ppm boron impurities
      5010.66c  -0.000002
mt5   grph.01t
m6    6000.66c  -0.23069795      $Control Material-B4C
      5010.66c  -0.76930205
mt6   grph.01t
m7    40090.66c -0.36415         $97%ZrO2-3%Y2O3 partially stablized
      40091.66c -0.08030
      40092.66c -0.12408
      40094.66c -0.12849
      40096.66c -0.02114
      8016.66c  -0.25823
      39089.66c -0.02363
C   Source Card
kcode 1000 1.0 50 750
ksrc 42.307 -105.51 -80.914
mode n
```

APPENDIX F

```
PBMR-450K Heterogeneous Pebble in core w/ 5 ZrO2 uspheres in NFR
C   Created by E. Travis Gitau
C   -----Cell Cards-----
C   TRISO Particle
1   1   -10.85   -101                u=1        imp:n=1  $Fuel Kernel
2   2   -0.980    101 -102            u=1        imp:n=1  $Porous Carbon Layer
3   2   -1.865    102 -103            u=1        imp:n=1  $IPyC Layer
4   3   -3.20     103 -104            u=1        imp:n=1  $SiC Layer
5   2   -1.865    104 -105            u=1        imp:n=1  $OPyC Layer
6   5   -1.76     105                 u=1        imp:n=1  $Graphite Matrix
C   TRISO Lattice to fill Pebble
7   0           -106 107 -108 109 -110 111  lat=1 fill=1 u=2 imp:n=1
C   Pebble
8   0         -112                          fill=2 u=3 imp:n=1
9   5   -1.76   112 -113  301  302  303  304  305 u=3 imp:n=1          $Non-fuelled region
10  4   -0.01163211 113 19113 20113 21113 &
            22113 23113 24113 25113 26113  u=3 imp:n=1  $Helium between pebbles
C   Transform for BCC Lattice
C   Transform for fueled region
11   like 8 but trcl=(-3.464102 -3.464102 -3.464102)
12   like 8 but trcl=(-3.464102 -3.464102 3.464102)
13   like 8 but trcl=(-3.464102 3.464102 -3.464102)
14   like 8 but trcl=(-3.464102 3.464102 3.464102)
15   like 8 but trcl=(3.464102 -3.464102 -3.464102)
16   like 8 but trcl=(3.464102 -3.464102 3.464102)
17   like 8 but trcl=(3.464102 3.464102 -3.464102)
18   like 8 but trcl=(3.464102 3.464102 3.464102)
C   Transform of non-fueled region
19   like 9 but trcl=(-3.464102 -3.464102 -3.464102)
20   like 9 but trcl=(-3.464102 -3.464102 3.464102)
21   like 9 but trcl=(-3.464102 3.464102 -3.464102)
22   like 9 but trcl=(-3.464102 3.464102 3.464102)
23   like 9 but trcl=(3.464102 -3.464102 -3.464102)
24   like 9 but trcl=(3.464102 -3.464102 3.464102)
25   like 9 but trcl=(3.464102 3.464102 -3.464102)
26   like 9 but trcl=(3.464102 3.464102 3.464102)
C   Pebble Lattice to fill core
35  0       203 -204 205 -206 207 -208  lat=1 fill=3 u=4 imp:n=1
C   Core
36  0       209 -210 212 -216              fill=4     imp:n=1
C   Helium plenum above core
```

```
37  4   -0.01163211  209 -210 216 -213        imp:n=1        $Plenum
C   Reflectors
38  5   -1.76  -209 212 -213 #43             imp:n=1        $Annular reflector
39  5   -1.76   210 -211 212 -213 #44 #45 #46 imp:n=1        $Outer reflector
40  5   -1.76  -211 -212 214 #43 #46         imp:n=1        $Lower reflector
41  5   -1.76  -211 213 -215 #43 #44 #45 #46  imp:n=1        $Upper reflector
C   Outside Outer Reflector
42  0        211:-214:215 #45               imp:n=0
C   RSS Channels
43  4   -0.01163211 (-219:-220:-221:-222:-223: &
      -224:-225:-226:-227) 214 -215          imp:n=1
C   Control Channels
44  6  -2.50 (-228:-229:-230:-231:-232:-233:-234:-235: &
      -236:-237:-238:-239:-240:-241:-242:-243:-244:-245: &
      -246:-247:-248:-249:-250:-251) 217 -218  imp:n=1
45  4  -0.01163211 (-228:-229:-230:-231:-232:-233:-234:-235: &
      -236:-237:-238:-239:-240:-241:-242:-243:-244:-245: &
      -246:-247:-248:-249:-250:-251) 212 -217  imp:n=1 $Helium to fill void of control
rod
C   Helium Channels
46  4  -0.01163211  (-252:-253:-254:-255:-256:-257:-258: &
      -259:-260:-261:-262:-263:-264:-265:-266:-267:-268: &
      -269:-270:-271:-272:-273:-274:-275:-276:-277:-278: &
      -279:-280:-281:-282:-283:-284:-285:-286:-287) 214 -215 imp:n=1
C   ZrO2-Y2O3 microspheres
47  7   -6.02  -301:-302:-303:-304:-305 u=3 imp:n=1
48   like 47 but trcl=(-3.464102 -3.464102 3.464102)
49   like 47 but trcl=(-3.464102 3.464102 -3.464102)
50   like 47 but trcl=(-3.464102 3.464102 3.464102)
51   like 47 but trcl=(3.464102 -3.464102 -3.464102)
52   like 47 but trcl=(3.464102 -3.464102 3.464102)
53   like 47 but trcl=(3.464102 3.464102 -3.464102)
54   like 47 but trcl=(3.464102 3.464102 3.464102)
55   like 47 but trcl=(-3.464102 -3.464102 -3.464102)

C   -----Surface Cards-----
C   TRISO Particle
101   so   0.025              $Fuel Kernal D=0.05cm
102   so   0.0345             $Porous Carbon Buffer t=0.0095cm
103   so   0.0385             $IPyC t=0.004cm
104   so   0.042              $SiC t=0.0035cm
105   so   0.046              $OPyC t=0.004cm
C   TRISO Lattice
106   px   0.0817046
```

```
107   px  -0.0817046
108   py   0.0817046
109   py  -0.0817046
110   pz   0.0817046
111   pz  -0.0817046
C   Pebble
112   so   2.5              $Fuelled region of pebble
113   so   3.0              $Non-fuelled region of pebble
C   Pebble Lattice
203   px  -3.464102
204   px   3.464102
205   py  -3.464102
206   py   3.464102
207   pz  -3.464102
208   pz   3.464102
C   Reactor
209   cz  100              $Annular reflector
210   cz  185              $Fuel/Core region
211   cz  280              $Outer reflector
212   pz  -550             $Core bottom
213   pz  550              $Core top
214   pz  -645             $Upper and lower reflector bounds
215   pz  645
216   pz  433              $Where pebbles must end to equal approx. 450K
217   pz  -365             $Positions for control rods
218   pz  830
C   RSS Channels
219   c/z 0 72.6 7.7           $A clockwise
220   c/z 46.66638 55.61483 7.7  $B
221   c/z 71.49104 12.60686 7.7  $C
222   c/z 62.87344 -36.3 7.7     $D
223   c/z 24.83066 -68.2217 7.7  $E
224   c/z -24.83066 -68.217 7.7  $F
225   c/z -62.8734 -36.3 7.7     $G
226   c/z -71.497 12.60686 7.7   $H
227   c/z -46.6664 55.61483 7.7  $I
C   Control Channels
228   c/z   25.733239  195.463354  7.7   $A clockwise
229   c/z   75.446039  182.142850  7.7   $B
230   c/z  120.017316  156.409611  7.7   $C
231   c/z  156.409611  120.017316  7.7   $D
232   c/z  182.142850   75.446039  7.7   $E
233   c/z  195.463354   25.733239  7.7   $F
234   c/z  195.463354  -25.733239  7.7   $G
```

```
235   c/z  182.142850  -75.446039  7.7   $H
236   c/z  156.409611  -120.017316 7.7   $I
237   c/z  120.017316  -156.409611 7.7   $J
238   c/z   75.446039  -182.142850 7.7   $K
239   c/z   25.733239  -195.463354 7.7   $L
240   c/z  -25.733239  -195.463354 7.7   $M
241   c/z  -75.446039  -182.142850 7.7   $N
242   c/z  -120.017316 -156.409611 7.7   $O
243   c/z  -156.409611 -120.017316 7.7   $P
244   c/z  -182.142850 -75.446039  7.7   $Q
245   c/z  -195.463354 -25.733239  7.7   $R
246   c/z  -195.463354  25.733239  7.7   $S
247   c/z  -182.142850  75.446039  7.7   $T
248   c/z  -156.409611 120.017316  7.7   $U
249   c/z  -120.017316 156.409611  7.7   $V
250   c/z  -75.446039  182.142850  7.7   $W
251   c/z  -25.733239  195.463354  7.7   $X
C   Helium Channels
252   c/z   21.741000  248.500767  8.5       $A clockwise
253   c/z   64.562411  240.950197  8.5       $B
254   c/z  105.422125  226.078477  8.5       $C
255   c/z  143.078642  204.337477  8.5       $D
256   c/z  176.387787  176.387787  8.5       $E
257   c/z  204.337477  143.078642  8.5       $F
258   c/z  226.078477  105.422125  8.5       $G
259   c/z  240.950197   64.562411  8.5       $H
260   c/z  248.500767   21.741000  8.5       $I
261   c/z  248.500767  -21.741000  8.5       $J
262   c/z  240.950197  -64.562411  8.5       $K
263   c/z  226.078477  -105.422125 8.5       $L
264   c/z  204.337477  -143.078642 8.5       $M
265   c/z  176.387787  -176.387787 8.5       $N
266   c/z  143.078642  -204.337477 8.5       $O
267   c/z  105.422125  -226.078477 8.5       $P
268   c/z   64.562411  -240.950197 8.5       $Q
269   c/z   21.741000  -248.500767 8.5       $R
270   c/z  -21.741000  -248.500767 8.5       $S
271   c/z  -64.562411  -240.950197 8.5       $T
272   c/z  -105.422125 -226.078477 8.5       $U
273   c/z  -143.078642 -204.337477 8.5       $V
274   c/z  -176.387787 -176.387787 8.5       $W
275   c/z  -204.337477 -143.078642 8.5       $X
276   c/z  -226.078477 -105.422125 8.5       $Y
277   c/z  -240.950197 -64.562411  8.5       $Z
```

```
278   c/z  -248.500767 -21.741000  8.5       $AA
279   c/z  -248.500767  21.741000  8.5       $BB
280   c/z  -240.950197  64.562411  8.5       $CC
281   c/z  -226.078477 105.422125  8.5       $DD
282   c/z  -204.337477 143.078642  8.5       $EE
283   c/z  -176.387787 176.387787  8.5       $FF
284   c/z  -143.078642 204.337477  8.5       $GG
285   c/z  -105.422125 226.078477  8.5       $HH
286   c/z  -64.562411  240.950197  8.5       $II
287   c/z  -21.741000  248.500767  8.5       $JJ
C   ZrO2-Y2O3 Microspheres
301   s   1.1941   1.6479   2.0716   0.05
302   s   -0.4606  1.6741   2.1660   0.05
303   s   -1.2204  0.4440   2.3693   0.05
304   s   1.8608   1.8908   -0.0422  0.05
305   s   0.9971   2.0830   1.1451   0.05

C   -----Data Cards-----
C   Material Cards
m1    92235.66c -0.04964443      $Fuel Kernal-UO2-5.7 wt% U-235
      92238.66c -0.83181731      $5.7 wt % is start-up enrichment
      8016.66c  -0.11853826
m2    6000.66c   1               $Carbon for non-fuelled region
mt2   grph.01t
m3    14028.66c -0.64370         $SiC Layer
      14029.66c -0.03376
      14030.66c -0.02318
      6000.66c  -0.29936
mt3   grph.01t
m4    2003.66c  -0.00000137      $Helium density=0.01163211 g/cc
      2004.66c  -0.99999863      $          at 300K and 70 Bar
m5    6000.66c  -0.999998        $Nuclear grade graphite w/2ppm boron impurities
      5010.66c  -0.000002
mt5   grph.01t
m6    6000.66c  -0.23069795      $Control Material-B4C
      5010.66c  -0.76930205
mt6   grph.01t
m7    40090.66c -0.36415         $97%ZrO2-3%Y2O3 partially stablized
      40091.66c -0.08030
      40092.66c -0.12408
      40094.66c -0.12849
      40096.66c -0.02114
      8016.66c  -0.25823
      39089.66c -0.02363
```

```
C   Source Card
kcode 1000 1.0 50 750
ksrc 42.307 -105.51 -80.914
mode n
```

VITA

Name: Ernest Travis Ngure Gitau

Address: Nuclear Security Science & Policy Institute
3473 TAMU
Texas A&M University
College Station, TX 77843

Email Address: travis.gitau@tamu.edu

Education: B.S., Nuclear Engineering, Missouri University of Science and Technology, 2009
M.S., Nuclear Engineering, Texas A&M University, 2011